國立交通大學

統計學研究所

博士論文

非線性隨機效應剖面資料之無母數監控方法

Nonparametric Monitoring Schemes for Nonlinear Profiles with Random Effects

研 究 生：鄭清仁

指導教授：洪志真 博士

中華民國一百零一年九月

非線性隨機效應剖面資料之無母數監控方法

Nonparametric Monitoring Schemes for Nonlinear Profiles with Random Effects

研 究 生：鄭清仁　　Student：Ching-Ren Cheng

指導教授：洪志真 博士　　Advisor：Jyh-Jen Horng Shiau

國 立 交 通 大 學

統 計 學 研 究 所

博 士 論 文

A Thesis

Submitted to Department of Statistics

College of Science

National Chiao Tung University

in partial Fulfillment of the Requirements

for the Degree of

Doctor of Philosophy

in

Statistics

September 2012

Hsinchu, Taiwan, Republic of China

中華民國一百零一年九月

非線性隨機效應剖面資料之無母數監控方法

研究生：鄭清仁　　指導教授：洪志真博士

國立交通大學統計學研究所

摘　要

隨著現代工業製程的進步，品質的特性經常是以應變量（response）與共變量（covariate）的函數關係呈現，也就是文獻裡所謂的剖面資料（profile）。因此，為了因應實際的需求，發展剖面資料的管制方法是必要的。近年來亦有多篇文獻探討該議題。此篇論文對於具隨機效應的剖面資料提供了完整的管制方法。首先，我們先考慮服從常態分配的剖面資料。為了提升管制方法的效率，我們利用主成分分析得到其主成分記分（principal component score），並利用該記分來發展管制圖。在此論文，我們對於常態分配的剖面資料分別探討在第一階段（Phase Ⅰ）和第二階段（Phase Ⅱ）的分析。在實際的應用裡，資料經常並非服從常態分配的假設。因此，在沒有假設資料分配的情況下，我們亦發展剖面資料的管制方法。為此，我們先對於多變量資料，發展無分配假設（distribution-free）的第一階段管制方法。接著，再對剖面資料發展無分配假設的第一及第二階段的管制方

法。在第一階段的分析，我們利用型一錯誤（type-I error）及型二錯誤（type-II error）來當作衡量準則。而在第二階段的分析裡，我們利用平均運行步長（average run length）來衡量。透過模擬分析，我們所發展的管制方法對於各種製程的變化都能有效地偵測，包含平均位置的位移、資料散佈的位移或是函數形狀的改變。我們亦利用真實的資料來示範我們所提出的方法的適用性及效率。

Nonparametric Monitoring Schemes for Nonlinear Profiles with Random Effects

Student: Chin-Ren Cheng Advisor: Dr. Jyh-Jen Horng Shiau

Institute of Statistics

National Chiao Tung University

Hsinchu, Taiwan

Abstract

As modern technology advances in many industrial processes, the quality characteristics are often gathered in the form of a relationship between the response variable and explanatory variable(s), which are often referred to as profiles in the literature. Therefore, developing schemes for monitoring various types of functional characteristics becomes necessary for practical use and has attracted many researchers in resent years. The purpose of this dissertation is to provide a comprehensive analysis for profiles with random effects. First, the case of the profiles following the Gaussian distribution is considered. To monitor the profiles efficiently, the principal component scores of profiles obtained from the principal component analysis are utilized to construct control charts. Both the Phase I analysis and Phase II monitoring for Gaussian profiles are discussed in this dissertation. Since the Gaussian assumption may be violated in many practical applications, we also develop a distribution-free control chart for profiles. To this end, we first develop a novel distribution-free Phase I control chart for multivariate data. Then, two distribution-free control charts for profile data are constructed for Phase I and

Phase II applications, respectively. The type-I and type-II error rates are considered as the performance measures for Phase I analysis whereas the average run length is used for Phase II analysis. Our simulation studies indicate that the proposed control charts are efficient in detecting shifts in various kinds of aspects, including the mean, dispersion, and shape of the profile. Some real data analysis are also provided to demonstrate the applicability and effectiveness of the proposed control charts.

誌　　謝

包含在中正大學的日子，我的博士班生涯終於要在第六年結束了。這六年的日子裡，不論是做研究的精神或是對於統計的知識，都得到了很大的進步。從一開始考上中正大學的博士班，完成碩士論文推廣的研究，又考過了資格考；接下來推甄上了交大，又考了一次資格考，接著從洪志真老師的指導之下拿到了博士學位。這一路雖然辛苦，但是在大家的勉勵及幫助之下也算順利。

首先第一個要感謝的當然是我的指導老師：洪志真老師。如果沒有洪老師每週耐心地和我討論問題和研究方法，我也不會如此順利的拿到學位。還有我在中正大學的指導老師：黃郁芬老師。感謝他當初啟發了我對作研究的興趣且一起共同完成了三篇論文。幸運的是：我的兩位指導老師對於學生都相當的親切也都很關心學生，也讓我在學習的過程中備感溫馨。感謝當初在中正大學另一位老師：王太和老師。雖然他現在已經轉往美國任教，我還是十分感謝他對我的幫助，不論是教學或是研究都令我非常印象深刻。感謝大陸南開大學的鄒長亮老師給予我很多幫助。另外，當然還要感謝交大和清大所有的老師，還有特地從美國回台授課的魏武雄老師和黃俊宗老師。感謝口試委員們：曾勝滄老師、黃榮臣老師、鄭少為老師以及王秀瑛老師。感謝他們對於我的論文提出的建議及改進。

感謝一起在研究室奮鬥的學長姐、同學及學弟妹。也感謝常常一起打球並且在統研盃奮戰過的所有人，讓我在課業之餘有一個抒發的管道。也感謝在中正的學長姐們，偶而大家可以一起互相勉勵。還有系辦助理：郭碧芬和劉怡君小姐。在交大這幾年也多虧了她們幫我們解決了許多行政及電腦的問題。

最後當然要感謝我的家人：老爸、老媽和姐姐們。她們所對我付出的關心和支持是無可取代的。另外還有我的女朋友玉卿，我這幾年的博士班生涯如果沒有她我也不知道自己能不能支持下去。也要感謝中正大學讓我們在嘉義相遇並相戀。

接下來當學生的日子結束了，往後的日子挑戰還更大。要能夠在社會上有立足之地，還需要大家繼續的支持及鼓勵。真誠地感謝。

清仁 2012/09

Contents

List of Tables

List of Figures

Chapter 1

Introduction

Statistical process control (SPC) has been widely used in various areas, especially in industry. One of the most important purposes in SPC is to monitor crucial quality characteristics of processes/products in order to control the process to stay in a stable state. Among SPC tools, the control chart is a proven effective process monitoring tool used to determine whether the process is in control or not.

The control chart applications are distinguished into Phase I and Phase II with distinct objectives. The objectives of the Phase I application are to bring the process to a state of statistical control and further characterize the in-control process by analyzing historical observations. The control chart would allow the user to collect in-control data by filtering out the abnormal or so-called "out-of-control" (OC) observations in the historical data set. The collected in-control (IC) data are then used to characterize the IC process with a suitable statistical model, which will be used later to construct the control chart in the Phase II application. Since the data used in Phase I analysis are gathered in the past, Phase I analysis is regarded as the retrospective analysis in the literature. Assuming that the process is in statistical control already, the Phase II application emphasizes the online process monitoring of the process characteristics. In this phase, practitioners focus on detecting as efficiently as possible the OC conditions caused by assignable causes during production. Since the data considered in this phase are coming serially

from the future on-going process procedure, Phase II analysis is also regarded as a prospective analysis. Moreover, in Phase II analysis, the necessary process parameters are usually assumed known; that is, they are already known from previous knowledge or are well estimated from the historical data after Phase I analysis.

Traditionally, the quality characteristics that control charts monitor are univariate or multivariate random variables. Nevertheless, in many situations, the quality-related characteristic of interest is not a variable or a vector but a functional relationship between the response variable and one or more explanatory variables. Under these circumstances, the monitoring focus should be on the functional characteristic of the data (referred to as the profile in the literature) instead of on the response values measured at the specific levels of the explanatory variables. In this case, the observations within a profile are often highly correlated and their ordering (as the ordering of the explanatory variables) remains unchanged over time. Moreover, the values of explanatory variables may vary from profile to profile in many situations. Therefore, although profile data look similar to multivariate data, the traditional multivariate monitoring schemes often may not be appropriate for profiles. In addition, the profiles observed from a process usually have some features in common and hence exhibit similar patterns. For some cases, the observed profiles can be well represented as a fixed (but needs to be estimated) function plus independent errors, and hence can be suitably modeled by a fixed-effect model. However, for more cases in practice, the profiles in general are of common shapes or similar patterns but still quite different individually, a situation needs to be modeled with a random-effect model or a mixed-effect model to accommodate the profile-to-profile variations. It is noted that, in the literature, the terms "random effects" and "mixed effects" sometimes are used interchangeably — a random-effect model becomes a mixed-effect model when the mean of the random-effect component is deliberately set to zero by moving the mean into the fixed-effect component.

In this dissertation, we propose some monitoring schemes for profiles with random effects. We first review related research works in the literature and some background knowledge used in this dissertation in Chapter 2. In Chapter 3, two monitoring schemes for profiles under Gaussian assumption are developed for Phase I and II applications, respectively. In practical use of SPC procedures, the distribution of the profiles is often unknown or differs from Gaussian. Before developing monitoring schemes for profile data, we first construct a novel control chart for multivariate observations without distribution assumptions for Phase I applications in Chapter 4. Then, by combining the schemes presented in Chapters 3 and 4, we develop two distribution-free monitoring schemes for profiles in retrospective and prospective analysis, respectively, in Chapter 5. Finally, the conclusion and some directions of future works are given in Chapter 6.

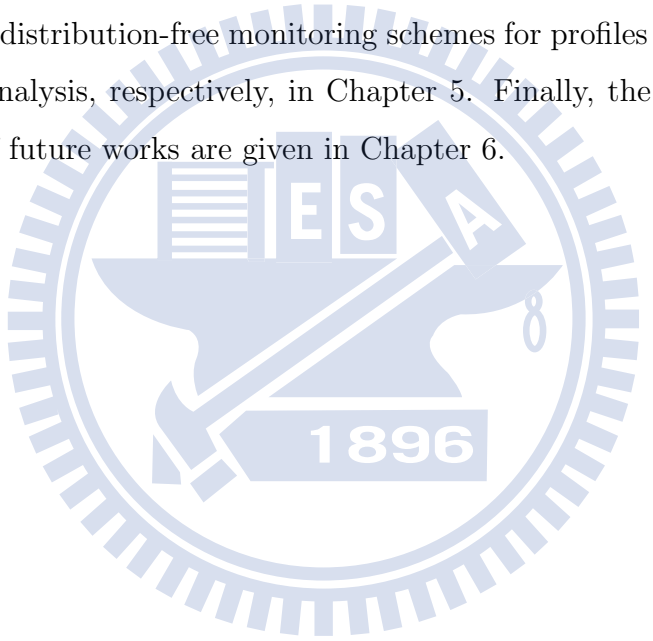

Chapter 2

Literature Review and Background

This chapter gives a literature review on related research works in process monitoring and some background knowledge of this dissertation study in Sections 2.1 and 2.2, respectively.

2.1 Literature Review

In this section, we review some previous works in the literature related to our study. For easy reference, we tabulate the reference in profile monitoring and multivariate process monitoring in Tables 2.1 and 2.2, respectively.

2.1.1 Phase II Analysis

The works on the profile monitoring started with the simplest case that the profiles are characterized by a single covariate and the functional relationship can be described by a linear regression model. Assuming that the intercept and slope in the model are known, Kang and Albin (2000) proposed two approaches to deal with the Phase II profile monitoring problem. One is the Hotelling's T^2 chart based on

the vector of the least squared estimates of the intercept and slope of the incoming profile. The other takes the residuals between the sample profile and the reference profile as a subgroup, then combines the EWMA chart on the average of the residuals and the range-chart (R-chart). The authors preferred the second approach. Kim et al. (2003) considered three EWMA control charts for monitoring the estimated intercept, slope, and variance of the linear model, respectively. To lessen the correlations among the estimators of the parameters, the centered linear model was considered in their method. Based on the same spirit with the methodology proposed by Kim et al. (2003), Saghaei et al. (2009) utilized the CUSUM chart on the estimated parameters of the simple linear model. Zou et al. (2006) proposed a likelihood ratio (LR) based control chart with a change-point model. To avoid the situation of the paucity of the reference sample, Zou et al. (2007b) developed a self-starting monitoring scheme for linear profiles. In their methodology, the residual and the variance are monitored individually via two EWMA charts, and the estimated parameters are updated immediately when a new observation arrives. Zhang et al. (2009) constructed a control chart based on the LR to monitor linear profiles. Instead of taking exponentially weighted average of the LR statistic, they sequentially update the estimates of the parameters used in the LR statistic via the EWMA scheme and monitor the corresponding values of the statistic.

In practice, the functional relationship between the response and covariate may not be linear. Kazemzadeh et al. (2009) extended the simple linear model to the polynomial model to fit the profiles. For roundness profile data, Colosimo et al. (2008) considered a spatial autoregressive regression model to account for the continuity in space of the profile, and construct a control chart to monitor the parameters in the model. Vaghefi et al. (2009) developed control charts based on the residuals of the (known) nonlinear model, and several types of metrics were considered to measure the difference between the incoming profile and the reference profile.

It sometimes happens that the profile is better characterized by several covari-

ates. Zou et al. (2007a) extended the simple linear model to the general linear model including the polynomial and multiple linear regression models for profile monitoring. Zou et al. (2008) presented a control chart that integrates the usual multivariate EWMA procedure with the generalized likelihood ratio test proposed by Fan et al. (2001).

To be more general, Eyvazian et al. (2011) considered the case of the multiple responses as profiles of multiple covariates, which is the so-called multivariate multiple profiles. They assumed the profiles can be fitted by the multivariate multiple linear regression model and proposed several multivariate control charts to monitor the parameters in the model. Zou et al. (2012a) took the multivariate multiple linear profiles into account and constructed the control chart based on the LASSO-based multivariate control chart proposed by Zou and Qiu (2009). Lee et al. (2011) dealt with the multiple profiles of one covariate in a semiconductor manufacturing process and no linear structure was assumed in their method.

2.1.2 Phase I Analysis

Kang and Albin (2000) suggested that by replacing the EWMA chart to the Shewhart chart, their proposed chart can be applied to Phase I analysis. Mahmoud and Woodall (2004) utilized the indicator variables to compare several simple linear regression lines, and considered the F-statistic to identify which of the profiles are out of control. As a generalization of simple linear profiles, Kazemzadeh et al. (2008) discussed that the Phase I monitoring scheme for polynomial profiles. Zhang and Albin (2009) used the χ^2 statistic, which is the sum of squared standardized residuals between the reference profile and the centered profile to be tested, to detect the outlying profiles. Similar to the work of Zou et al. (2006), Mahmoud et al. (2007) considered the change-point model in the Phase I monitoring for simple linear profiles.

In the case of the nonlinear model with multiple covariates, Williams et al. (2007a) and Williams et al. (2007b) constructed control charts for the parameters

in the (known) nonlinear model. Jensen et al. (2008) and Jensen and Birch (2009) considered the linear and nonlinear mixed models, respectively, to account for the profile-to-profile variation, and then a T^2-type control chart is used to monitor the parameters in the model simultaneously.

For the multiple linear regression profile case, Mahmoud (2008) pointed out that the power of the usual Hotelling's T^2 control chart would be reduced when the number of the covariates increases. The author regarded the average of the fitted values of the historical profiles as a new covariate; and with that only the simple linear regression model needs to be considered. Since outlying profiles have abnormal values of the parameters in the new model, the parameters were utilized to construct a control chart in Phase I. Parallel to Phase II (Eyvazian et al., 2011), Noorossana et al. (2010) also developed a Phase I monitoring scheme for multivariate multiple linear regression profiles.

2.1.3 Dimension Reduction Methods

In the profile data analysis, profiles are often discretized and hence can be regarded as multivariate data. Since the number of the design points (values of the covariate) is usually large, the dimension reduction techniques can be applied to profile data. Jin and Shi (2001) considered the wavelet transformation for the profile and constructed a control chart based on the corresponding coefficients to implement the monitoring scheme. Both the Phase I and II analysis were discussed in their article. Lada et al. (2002) also developed a Phase II control chart based on the wavelet coefficients. For the dimension reduction purpose, a novel minimizing criterion was considered to choose a small number of the coefficients. In the use of the wavelet transformation for profiles, Jeong et al. (2006) proposed a T^2 chart for Phase II analysis based on the coefficients for which the deviations from the reference parameters exceed a threshold. Chicken et al. (2009) considered the likelihood ratio statistic of the coefficients to construct a control chart under a change-point model.

Ding et al. (2006) considered the independent component analysis (ref. Hyvärinen et al., 2001) to the wavelet coefficients to reduce the corresponding dimensions in Phase I applications. Shiau et al. (2009) applied the principal component analysis (PCA) to profiles and proposed several control charts based on the scores of the first few effective principal components (PCs) to implement Phase I and II process monitoring.

2.1.4 Distribution-Free Methods

The literature involving distribution-free monitoring procedures for profile data is quite limited. In the development of nonparametric methods, Walker and Wright (2002) pointed out that the smoothing technique is an important tool to summarize and capture the structure of a profile. In addition, the authors used the generalized additive model to fit the profiles and then developed a method to decompose the sources of the variation of profiles; however, no monitoring schemes were provided in this paper. Febrero et al. (2008) considered the depth measure for profiles and detected the outlying cases with lower values of depth. Three types of depthes, including the Fraiman-Muniz depth (Fraiman and Muniz, 2001), h-modal depth (Cuevas et al., 2006), and random projection depth (Cuevas et al., 2007), are considered and the corresponding performances were compared. In Phase II analysis, Cheng (2009) and Wang (2009) respectively considered the simplicial depth (Liu, 1990) and the Oja depth (Zou and Serfling, 2000) to construct the r-chart, Q-chart, and DDMA-chart (Liu, 1995; Liu et al., 2004) by using the PC scores of profiles.

Zou et al. (2009) considered the change-point model integrating with the generalized likelihood ratio (GLR) testing statistic. The GLR statistic measures the difference between the generalized log-likelihood functions under IC (i.e., no change point) and OC (i.e., there exists at least a change point) conditions. Taking each of the profiles as a potential change point, the values of the GLR statistic are calculated and then the maximum value is used to determine whether the process is OC or not. Qiu and Zou (2010) constructed a nonparametric profile control chart

by using the smoothed estimates of the scaled residuals of a nonparametric regression model. The authors also presented a self-starting version of the monitoring scheme. Qiu et al. (2010) considered the nonlinear mixed effect model to describe profiles to deal with the correlation within a profile, which is a condition usually happen in practice; see Section 3.3.3.

2.1.5 Multivariate Process Monitoring

There are vast amount of papers discussing multivariate process monitoring schemes for either location or dispersion of the process, but only some recent papers are reviewed here. For more related references, see the papers described in the following and the references cited therein.

Among the multivariate monitoring schemes developed under the multivariate normal distribution, the most popular method could be the Hotelling's T^2 control chart. It is widely used for monitoring the location of the process in both Phase I and Phase II analysis. However, the Hotelling's T^2 chart is notorious for its poor power in detecting small location shifts. To get more detecting power for small shifts, Crosier (1988) and Lowry et al. (1992) proposed the multivariate CUSUM and multivariate EWMA control charts, respectively. Mason et al. (2003) pointed out that there would be some special systematic patterns rather than the random pattern in the Hotelling's T^2 chart if some specific conditions occur in the process.

Vargas (2003) and Jensen et al. (2007) proposed their T^2 control charts based on the robust estimators of the location and scatter matrix for Phase I applications. They claimed that the control chart using the minimum volume ellipsoid (MVE) or minimum covariance determinant (MCD) estimator is more powerful in detecting reasonable number of outliers than the regular Hotelling's T^2 control chart. The use of the scatter matrix estimated by successive difference was also discussed in their papers. Later, Williams et al. (2006) derived the asymptotic distribution of the T^2 statistic based on the successive-difference estimator of the scatter matrix. Zamba and Hawkins (2006) considered the change-point model for monitoring the

process mean in both Phase I and Phase II analysis. To avoid a long process of collecting in-control data, Hawkins and Maboudou-Tchao (2007) developed a self-starting EWMA procedure to monitor the process mean. Assuming only a few dimensions of the vector shift, Zou and Qiu (2009) proposed an EWMA control chart integrating the LASSO-based testing statistic.

The aforementioned methodologies focus mainly on monitoring the process mean. Nevertheless, the scatter matrix should also be monitored in real applications. For Phase II applications, Yeh et al. (2004) proposed an EWMA control chart based on the likelihood ratio test statistic for comparing the sample covariance matrix of the incoming grouped data with that of the reference sample. Yeh et al. (2005) considered the EWMA of $\boldsymbol{X}_t\boldsymbol{X}_t'$, where $\boldsymbol{X}_t$ is the observed vector at time t, as the estimator of the scatter matrix, and proposed the control charts based on the entries of the estimated scatter matrix to monitor the variability of the process. Huwang et al. (2007) considered not only the EWMA of $\boldsymbol{X}_t\boldsymbol{X}_t'$, but also the EWMA of $(\boldsymbol{X}_t - \hat{\boldsymbol{\mu}}_t)(\boldsymbol{X}_t - \hat{\boldsymbol{\mu}}_t)'$, where $\hat{\boldsymbol{\mu}}_t$ is the EWMA of $\boldsymbol{X}_t$, as the estimators of the scatter matrix. The trace of each estimated scatter matrix was utilized to construct a Shewhart-type control chart. Hawkins and Maboudou-Tchao (2008) adopted the $\boldsymbol{X}_t\boldsymbol{X}_t'$ version of the scatter matrix estimator described above and applied the Alt's likelihood ratio statistic (Alt, 1984) to monitor the process dispersion. To gain more power than the usual two-sided test on the scatter matrix, Yen and Shiau (2010) derived the likelihood ratio test statistic for testing one-sided alternative hypothesis of increasing process dispersion and developed a control chart accordingly. Yen et al. (2012) further developed an effective chart for detecting dispersion increase and decrease simultaneously by combining two one-sided charts.

Some authors developed multivariate control charts to monitor the location and dispersion of the process simultaneously. Reynolds and Cho (2006) constructed two T^2-type control charts based on the EWMA of each component of $\boldsymbol{X}_t$ and $\boldsymbol{X}_t^2$, respectively ($\boldsymbol{X}_t^2$ refers to the vector of the square of each component of

$\boldsymbol{X}_t$), then combined the two T^2 charts to monitor the mean and scatter matrix simultaneously. Maboudou-Tchao and Hawkins (2011) combined the self-starting monitoring scheme for the mean in Hawkins and Maboudou-Tchao (2007) and the EWMA procedure for the scatter matrix in Hawkins and Maboudou-Tchao (2008) for the same purpose.

The methodologies described above were all developed based on the normality assumption of the observations. However, this assumption is often violated in practice. Stoumbos and Sullivan (2002) and Testik et al. (2003) studied the robustness of the multivariate EWMA control chart. They pointed out that the multivariate EWMA chart is quite robust to normality if one choose a small weighting parameter λ. But how small λ should be depends on the distribution of the data, which is often difficult to estimate in practical applications. Therefore, distribution-free schemes for process monitoring are definitely in need.

Qiu and Hawkins (2001, 2003) constructed the CUSUM control chart based on the so-called antiranks of vectors, in which the antiranks are the indices of the order statistics. Liu (1995) proposed three control charts, r, Q, and S charts, which can be viewed as the univariate X, $\bar{X}$, and CUSUM charts applying on the depth of the multivariate data. Liu et al. (2004) constructed a nonparametric moving average (MA)-chart derived from the notation of data depth for multivariate data. The simplical depth (Liu, 1990) was considered in their methodology. Hamurkaroğlu et al. (2004) demonstrated the use of the r and Q charts under the Mahalanobis depth (Mahalanobis, 1936).

Qiu (2008) considered an approach involving the log-linear model to construct a CUSUM chart based on the Pearson's χ^2 statistic. Zou and Tsung (2011) proposed an EWMA monitoring procedure based on the spatial signs of vectors (introduced in Section 2.2.5). To incorporate the information in the multivariate data more than just the multivariate direction, Zou et al. (2012b) proposed a spatial rank-based multivariate EWMA control chart. In addition, they incorporated the self-starting procedure into the the proposed monitoring scheme. Boone and

Chakraborti (2012) considered the univariate sign and Wilcoxon sign-rank statistics for each component of the multivariate data and constructed the Hotelling's T^2-type control charts based on these distribution-free statistics to monitor the process location.

2.2 Background

Section 2.2.1 reviews several levels of model assumptions often made on distribution symmetry in the literature. Section 2.2.2 introduces the definition of spatial sign and related assumptions. Sections 2.2.3 - 2.2.5 describe some applications of spatial sign, including nonparametric hypothesis testing, robust parameter estimation, and statistical process monitoring.

2.2.1 Symmetry Property of a Distribution

Let $\boldsymbol{y}$ be a p-variate random vector that can be described by the model

$$\boldsymbol{y} = \boldsymbol{\mu} + \boldsymbol{e}, \tag{2.1}$$

where $\boldsymbol{\mu}$ is the mean vector and $\boldsymbol{e}$ is the error vector with zero mean and variance-covariance matrix $\boldsymbol{\Sigma}$. Assuming that $\boldsymbol{\Sigma}$ is positive definite, there exists a full-rank $p \times p$ matrix $\boldsymbol{\Omega}$ such that $\boldsymbol{\Sigma} = \boldsymbol{\Omega}\boldsymbol{\Omega}'$. Let $\boldsymbol{\varepsilon} = \boldsymbol{\Omega}^{-1}\boldsymbol{e}$ be the standardized error vector with zero mean and identity variance-covariance matrix. Then the model (2.1) can be re-written as

$$\boldsymbol{y} = \boldsymbol{\mu} + \boldsymbol{\Omega}\boldsymbol{\varepsilon}. \tag{2.2}$$

$\boldsymbol{\Omega}$ is often called the *transformation matrix* in the literature. Imposing various assumptions on the distribution of $\boldsymbol{\varepsilon}$ leads to various parametric or semiparametric or nonparametric models. For example, when constructing a semiparametric or nonparametric multivariate test, the symmetry assumption is often needed. The *symmetry* property of the distribution of a standardized variable $\boldsymbol{\varepsilon}$ is defined in the

sense that the distribution is invariant under certain transformations. Note that the assumption made on $\boldsymbol{\varepsilon}$ is equivalent to that made on $\boldsymbol{\Omega}^{-1}(\boldsymbol{y}-\boldsymbol{\mu})$, hence the connection of the probability density functions (pdfs) between $\boldsymbol{\varepsilon}$ and $\boldsymbol{y}$ is that

$$f_{\boldsymbol{y}}(\boldsymbol{y}) = |\boldsymbol{\Omega}|^{-1} f_{\boldsymbol{\varepsilon}}\big(\boldsymbol{\Omega}^{-1}(\boldsymbol{y}-\boldsymbol{\mu})\big),$$

where $f_{\boldsymbol{y}}$ and $f_{\boldsymbol{\varepsilon}}$ denote the pdfs of $\boldsymbol{y}$ and $\boldsymbol{\varepsilon}$, respectively. Oja (2010) provided a good review about the symmetry property with respect to various kinds of transformation. In this dissertation, we only consider the kinds of symmetry described in this section.

Definition 2.1. The random p-vector $\boldsymbol{\varepsilon}$ is called *elliptically symmetrical* (or *spherically symmetrical*) if $\boldsymbol{O\varepsilon} \sim \boldsymbol{\varepsilon}$, for all orthogonal matrices $\boldsymbol{O}$. It is called *symmetrical* (or *centrally symmetrical*) if $-\boldsymbol{\varepsilon} \sim \boldsymbol{\varepsilon}$.

Here, the symbol "$\sim$" denotes "is distributed as". Note that the elliptically symmetrical random vector is also symmetrical since the matrix $-\boldsymbol{I}_p$ is orthogonal. Thus, the following three "nested" assumptions lead to a hierarchy of symmetrical models:

(A0) $\boldsymbol{\varepsilon} \sim N_p(\boldsymbol{0}, \boldsymbol{I}_p)$;

(A1) $\boldsymbol{\varepsilon}$ is elliptically symmetrical;

(A2) $\boldsymbol{\varepsilon}$ is symmetrical.

The strongest assumption (A0) is equivalently to the usual assumption, $\boldsymbol{y} \sim N_p(\boldsymbol{\mu}, \boldsymbol{\Sigma})$, made on random samples in the literature. In many multivariate data analysis applications, such as principal component analysis (PCA), canonical correlation analysis (CCA), and factor analysis (FA), it relies on the assumption (A0) to develop good theoretical properties of the methodologies. Because the assumption (A1) or (A2) made on $\boldsymbol{\varepsilon}$ is weaker than (A0), it corresponds to a boarder class of distributions. Also, the model based on the assumption (A1) or (A2) may be regarded as a semiparametric generalization of the multivariate normal model based on (A0) in the sense that no particular distribution is assumed.

2.2.2 Concept of Spatial Sign

In the univariate case, data can be ordered and the sign of an observation indicates its direction (+1, 0 or −1) from the origin. For any univariate variable y, the following sign function

$$U(y) = \begin{cases} |y|^{-1}y, & \text{if } y \neq 0, \\ 0, & \text{if } y = 0, \end{cases}$$

gives the sign of y. Although there is no such natural ordering for multivariate data, the multivariate sign function can be defined in the same manner as

$$U(\boldsymbol{y}) = \begin{cases} ||\boldsymbol{y}||^{-1}\boldsymbol{y}, & \text{if } \boldsymbol{y} \neq \boldsymbol{0}, \\ \boldsymbol{0}, & \text{if } \boldsymbol{y} = \boldsymbol{0}, \end{cases}$$

for any multivariate vector $\boldsymbol{y}$, where $||\cdot||$ is the Euclidean norm. $U(\boldsymbol{y})$ is called the multivariate (spatial) sign vector of $\boldsymbol{y}$, and sometimes called the *direction vector*, since it only indicates the direction of the observation by mapping it on the multi-dimensional unit sphere. For illustration, Figure 2.1(a) and 2.1(b) show the scatter plots of a random sample from the bivariate standard normal distribution and the corresponding spatial sign vectors, respectively.

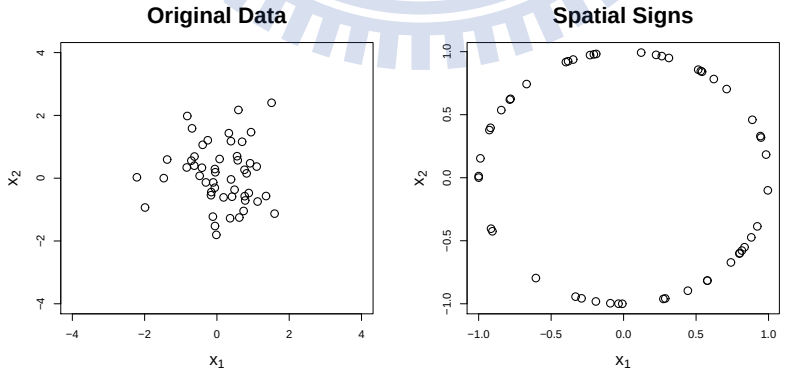

(a) (b)

Figure 2.1: The scatter plots of a random sample from $N_2(\boldsymbol{0}, \boldsymbol{I}_2)$ and the corresponding spatial sign vectors.

Consider again the model assumption issue mentioned earlier in the last section. A broader class of distribution models can be obtained if the assumptions are only made on the sign vector. Let the spatial sign vector of the random vector $\boldsymbol{\varepsilon}$ be $\boldsymbol{u} = U(\boldsymbol{\varepsilon})$. The following assumptions are then considered:

(B1) $\boldsymbol{u}$ is uniformly distributed on the multivariate unit sphere;

(B2) $\boldsymbol{u}$ is symmetrical.

The distributions of $\boldsymbol{\varepsilon}$ corresponding to the models (B1) and (B2) are named the *elliptical direction distribution* and *directionally symmetrical distribution*, respectively. Note that there is no additional assumption on the distribution of the *radius* $r = ||\boldsymbol{\varepsilon}||$. The radius r and direction $\boldsymbol{u}$ may be dependent, thus skew distributions are allowed under models (B1) and (B2). Among the models introduced so far, a hierarchy of the models is straightforward to obtain as follows.

Property 2.1. *The models (A0)-(A2) and (B1)-(B2) satisfy the following joint hierarchy*

$$\begin{array}{ccccc} (A0) & \Rightarrow & (A1) & \Rightarrow & (A2) \\ & & \Downarrow & & \Downarrow \\ & & (B1) & \Rightarrow & (B2). \end{array}$$

The symbol "⇒" denotes "implies". For the tests or monitoring schemes introduced/developed later, we focus on the distribution-free property under the family of elliptical direction distributions. For more details about the spatial sign and symmetrical distribution families, see Chapter 2 of Oja (2010).

2.2.3 Multivariate Sign Test

Consider an independent and identically distributed (i.i.d.) random sample $\{\boldsymbol{y}_1, \cdots, \boldsymbol{y}_n\}$ from $F(\boldsymbol{y} - \boldsymbol{\theta})$, where $F(\cdot)$ represents the cumulative distribution function (cdf) of a continuous p-dimensional distribution "located" at $\boldsymbol{\theta}$. Consider testing the null hypothesis $H_0 : \boldsymbol{\theta} = \boldsymbol{\theta}_0$ against the alternative hypothesis $H_1 : \boldsymbol{\theta} \neq \boldsymbol{\theta}_0$. Without

loss of generality, $\boldsymbol{\theta}_0$ is assumed zero; otherwise, simply replace $\boldsymbol{y}_i$ by $\boldsymbol{y}_i - \boldsymbol{\theta}_0$ for $i = 1, \ldots, n$. In this testing hypothesis problem, different levels of assumptions were imposed on F in the literature. For example, for $\boldsymbol{y}_i$'s from the multivariate normal distribution, the well-known Hotelling's T^2 test is a powerful test, which rejects H_0 if

$$T^2 = (n-1)\bar{\boldsymbol{y}}'\boldsymbol{S}^{-1}\bar{\boldsymbol{y}} \geq \frac{(n-1)p}{n-p} F_{p,n-p}(\alpha),$$

where $\bar{\boldsymbol{y}}$ and $\boldsymbol{S}$ are the regular sample mean and sample variance-covariance matrix of the data, respectively, and $F_{p,n-p}(\alpha)$ is the upper α quantile of the F distribution with p and $n-p$ degrees of freedom. However, stronger assumptions made on the cdf F cause more restrictions in using the test. Thus, one would like to construct a powerful test with distribution assumptions to be as weak as possible.

Recall that a test statistic $t(\cdot)$ is said to be *affine invariant* if $t(\boldsymbol{y}_1, \ldots, \boldsymbol{y}_n) = t(\boldsymbol{D}\boldsymbol{y}_1, \ldots, \boldsymbol{D}\boldsymbol{y}_n)$ for every $(\boldsymbol{y}_1, \ldots, \boldsymbol{y}_n)$ and all nonsingular $p \times p$ matrix $\boldsymbol{D}$. This property ensures that the test will stay the same under certain transformations of data, e.g., rotating data around the origin or altering the scale of measurements. Note that the Hotelling's T^2 statistic is affine invariant. However, the dependency on the normality assumption could be a serious drawback for Hotelling's T^2 test and many parametric methodologies. For example, it is hard to control the type-I error probability of the Hotelling's T^2 test at a specified level when the normal assumption is violated. To circumvent this drawback, Randles (2000) proposed a test based on the spatial sign, which provides a robust alternative for testing the hypotheses when the population distribution is unknown.

More specifically, Randles (2000) constructed an affine invariant multivariate sign test utilizing the transformation-retransformation approach proposed by Chakraborty et al. (1998) and the directional transformation proposed by Tyler (1987). The transformation-retransformation approach uses a data-determined nonsingular matrix $\boldsymbol{A}_{\boldsymbol{y}}$ based on $\boldsymbol{y}$ that has an affine-equivariance property; that is, when each $\boldsymbol{y}_i$ is transformed by a fixed nonsingular $p \times p$ matrix $\boldsymbol{D}$ into $\boldsymbol{D}\boldsymbol{y}_i$,

then the resulting matrix $\boldsymbol{A_{Dy}}$ satisfies

$$\boldsymbol{D}'\boldsymbol{A}'_{\boldsymbol{Dy}}\boldsymbol{A}_{\boldsymbol{Dy}}\boldsymbol{D} = c\boldsymbol{A}'_{\boldsymbol{y}}\boldsymbol{A}_{\boldsymbol{y}},$$

where c is a positive scalar that might depend on $\boldsymbol{D}$ and $\boldsymbol{y}_i$'s. After transforming the data by $\boldsymbol{A_y}$, the spatial sign vectors of the transformed data are

$$\boldsymbol{u}_i = U(\boldsymbol{A}_{\boldsymbol{y}}\boldsymbol{y}_i) \text{ for } i = 1, \ldots, n. \tag{2.3}$$

Following the form of the Hotelling's T^2 test, the test statistic is then constructed as a quadratic form of the spatial sign vectors,

$$Q = n\bar{\boldsymbol{u}}'\big(\mathbf{AVE}\{\boldsymbol{u}_i\boldsymbol{u}_i'\}\big)^{-1}\bar{\boldsymbol{u}}, \tag{2.4}$$

where $\mathbf{AVE}\{\boldsymbol{B}_i\} = \sum_{i=1}^{n}\boldsymbol{B}_i/n$ denotes the average of $\boldsymbol{B}_i$'s over i, in which $\boldsymbol{B}_i$ can be a vector or a matrix; and $\bar{\boldsymbol{u}} = \mathbf{AVE}\{\boldsymbol{u}_i\}$. For $\boldsymbol{A_y}$, Randles (2000) adopted the Tyler's transformation matrix (Tyler, 1987). Tyler's method is to find a data-driven scatter matrix, $\boldsymbol{S}_T$, which is a $p \times p$ symmetric positive-definite matrix with $\text{trace}(\boldsymbol{S}_T) = p$, such that

$$\mathbf{AVE}\big\{U(\boldsymbol{A}_T\boldsymbol{y}_i)U(\boldsymbol{A}_T\boldsymbol{y}_i)'\big\} = \frac{1}{p}\boldsymbol{I}_p,$$

for any $\boldsymbol{A}_T$ satisfying $\boldsymbol{A}'_T\boldsymbol{A}_T = \boldsymbol{S}_T^{-1}$. The $\boldsymbol{S}_T$ is called the *Tyler's scatter matrix* and $\boldsymbol{A}_T$ is the corresponding *Tyler's transformation matrix*.

The Tyler's scatter and transformation matrices are surprisingly easy to compute empirically as follows. The iterative procedure begins with $\boldsymbol{S} \leftarrow \boldsymbol{I}_p$ as the initial value, and then transform it to the next value via

$$\boldsymbol{S} \leftarrow p\boldsymbol{S}^{1/2}\mathbf{AVE}\{\boldsymbol{u}_i\boldsymbol{u}_i'\}\boldsymbol{S}^{1/2}. \tag{2.5}$$

Here, "$\leftarrow$" means "set to". Continue updating step given in (2.5) until $||p\mathbf{AVE}\{\boldsymbol{u}_i\boldsymbol{u}_i'\} - \boldsymbol{I}_p||$ is sufficiently small, where the matrix norm is defined as $||\boldsymbol{A}|| = \sqrt{\text{trace}(\boldsymbol{A}'\boldsymbol{A})}$. The Tyler's scatter matrix is then set as $\boldsymbol{S}_T = [p/\text{trace}(\boldsymbol{S})]\boldsymbol{S}$ and the corresponding Tyler's transformation matrix $\boldsymbol{A}_T$ is chosen such that $\boldsymbol{A}'_T\boldsymbol{A}_T = \boldsymbol{S}_T^{-1}$.

Tyler (1987) claimed that the Tyler's scatter matrix $\hat{\boldsymbol{S}}_T$ is the "most robust" estimator of the scatter matrix for elliptically symmetric distributions, and is unique if the sample is from a continuous p-dimensional distribution with $n > p(p-1)$. Replacing the $\boldsymbol{A}_{\boldsymbol{y}}$ in (2.3) by $\boldsymbol{A}_T$, the test statistic (2.4) then becomes

$$Q = np\bar{\boldsymbol{u}}'\bar{\boldsymbol{u}}, \tag{2.6}$$

and H_0 is rejected for large values of Q. Randles (2000) showed that the test statistic Q is affine invariant when $n > p(p-1)$ and is distribution-free under H_0 in the class of elliptical direction distributions. The author also illustrated that the proposed sign-based test is quite powerful under elliptically symmetrical or some skew distributions, and is well competitive to Hotelling's T^2 test and other nonparametric tests.

2.2.4 Multivariate Spatial Median

The center of the distribution under study is usually unavailable in practice and needs to be estimated from data empirically. Among many statistics, the spatial median is often recommended in the literature for describing the multivariate center due to its robustness.

Definition 2.2. Let $\{\boldsymbol{y}_1, \ldots, \boldsymbol{y}_n\}$ be a p-variate random sample of size n. The *(sample) spatial median* $\hat{\boldsymbol{\theta}}$ is defined as the minimizer of the criterion function

$$\sum_{i=1}^{n} ||\boldsymbol{y}_i - \boldsymbol{\theta}||. \tag{2.7}$$

Taking the gradient of the objective function (2.7), one sees that if $\hat{\boldsymbol{\theta}}$ solves the equation

$$\sum_{i=1}^{n} \frac{\boldsymbol{y}_i - \hat{\boldsymbol{\theta}}}{||\boldsymbol{y}_i - \hat{\boldsymbol{\theta}}||} = \sum_{i=1}^{n} U(\boldsymbol{y}_i - \hat{\boldsymbol{\theta}}) = \boldsymbol{0},$$

then $\hat{\boldsymbol{\theta}}$ is the desired spatial median. Milasevic and Ducharme (1987) showed that the spatial median is unique if the dimension of data $p > 1$. Vardi and Zhang

(2000) provided an algorithm by modifying the Weiszfeld's algorithm (Weiszfeld, 1937; Weiszfeld and Plastria, 2009) to compute the spatial median. Specifically, the algorithm takes the regular sample median for each dimension as the initial estimate of each component of $\boldsymbol{\theta}$ and then iterates the following step

$$\boldsymbol{\theta} \leftarrow \boldsymbol{\theta} + \frac{\mathbf{AVE}\{U(\boldsymbol{y}_i - \boldsymbol{\theta})\}}{\mathbf{AVE}\{||\boldsymbol{y}_i - \boldsymbol{\theta}||^{-1}\}}, \tag{2.8}$$

until convergence. This algorithm is extremely simple and converges quickly and monotonically.

There is a natural link between the spatial median and the Tyler's scatter matrix as described below. Hettmansperger and Randles (2002) proposed a procedure for estimating the spatial median $\boldsymbol{\theta}$ and Tyler's transformation matrix $\boldsymbol{A}$ simultaneously. The desired parameters $(\boldsymbol{\theta}, \boldsymbol{A})$ satisfy

$$\mathbf{AVE}\{U(\boldsymbol{A}(\boldsymbol{y}_i - \boldsymbol{\theta}))\} = \mathbf{0},$$
$$\mathbf{AVE}\{U(\boldsymbol{A}(\boldsymbol{y}_i - \boldsymbol{\theta}))U(\boldsymbol{A}(\boldsymbol{y}_i - \boldsymbol{\theta}))'\} = \frac{1}{p}\boldsymbol{I}_p,$$

and $\boldsymbol{A}'\boldsymbol{A} = \boldsymbol{S}^{-1}$. These estimators of the location and transformation matrix are called *Hettmansperger-Randles (HR) estimators*, and are very easy to compute in high dimensions. The iterations are described as follows.

1. Initially set $(\boldsymbol{\theta}, \boldsymbol{S}) \leftarrow (\tilde{\boldsymbol{\theta}}, \boldsymbol{I}_p)$, where $\tilde{\boldsymbol{\theta}}$ is composed of the p regular sample medians of the p components. Let $\boldsymbol{S}^{1/2}$ be any $p \times p$ matrix such that $\boldsymbol{S}^{1/2}\boldsymbol{S}^{1/2} = \boldsymbol{S}$.

2. Fix $\boldsymbol{S}$ and let $\boldsymbol{z}_i = \boldsymbol{S}^{-1/2}(\boldsymbol{y}_i - \boldsymbol{\theta})$, for $i = 1, \ldots, n$. Then iterate

$$\boldsymbol{\theta} \leftarrow \boldsymbol{\theta} + \frac{\mathbf{AVE}\{U(\boldsymbol{z}_i)\}}{\mathbf{AVE}\{||\boldsymbol{z}_i||^{-1}\}}$$

   until convergence.

3. Fix $\boldsymbol{\theta}$ and let $\boldsymbol{z}_i = \boldsymbol{S}^{-1/2}(\boldsymbol{y}_i - \boldsymbol{\theta})$, for $i = 1, \ldots, n$. Then iterate

$$\boldsymbol{S} \leftarrow p\boldsymbol{S}^{1/2}\mathbf{AVE}\{U(\boldsymbol{z}_i)U(\boldsymbol{z}_i)'\}\boldsymbol{S}^{1/2}$$

until $||p\mathbf{AVE}\{U(\boldsymbol{z}_i)U(\boldsymbol{z}_i)'\} - \boldsymbol{I}_p||$ is sufficiently small, and then let $\boldsymbol{S} \leftarrow [p/\text{trace}(\boldsymbol{S})]\boldsymbol{S}$.

4. Repeat steps 2 and 3 until both of $\boldsymbol{\theta}$ and $\boldsymbol{S}$ converge.

The resulting values of $\boldsymbol{\theta}$ and $\boldsymbol{S}_T$ are the estimated spatial median and the Tyler's scatter matrix. Then the corresponding Tyler's transformation matrix is an $\boldsymbol{A}_T$ such that $\boldsymbol{A}_T'\boldsymbol{A}_T = \boldsymbol{S}_T^{-1}$. Unfortunately, there is no proof so far to ensure that the HR algorithm converges, but it actually works in most of situations. The existence and uniqueness of $(\boldsymbol{\theta}, \boldsymbol{A})$ are shown by Hettmansperger and Randles (2002) for the directionally symmetrical distributions, and hence the elliptical direction distributions. They also showed that the distribution-free property holds for the elliptical direction distributions.

2.2.5 Multivariate Sign-Based Control Chart for Phase II Application

In Phase II multivariate statistical process control (MSPC), one of the main tasks is to detect the process change as quickly as possible when the process is out of control. Usually, the location parameter is one of the process characteristics of concern in practice. Let $\boldsymbol{y}_{-m_0+1}, \ldots, \boldsymbol{y}_0$ be m_0 i.i.d. historical p-variate observations and $\boldsymbol{y}_i$ be the ith future observation collected over time, for $i = 1, 2, \ldots$. Consider the following multivariate change-point model

$$\boldsymbol{y}_i \sim \begin{cases} F(\boldsymbol{y} - \boldsymbol{\theta}_0) & \text{for } i = -m_0 + 1, \ldots, 0, 1, \ldots, \tau \\ F(\boldsymbol{y} - \boldsymbol{\theta}_1) & \text{for } i = \tau + 1, \ldots, \end{cases}$$

where τ is the unknown change point and $\boldsymbol{\theta}_0 \neq \boldsymbol{\theta}_1$. Zou and Tsung (2011) proposed an MSPC methodology incorporating the multivariate sign test (Randles, 2000) and the exponentially weighted moving average (EWMA) scheme for monitoring the location parameter of online sequential observations. Their control scheme is introduced briefly as follows.

Analogous to regular monitoring schemes, the first step is to estimate the location parameter and transformation matrix (or scatter matrix) from the reference sample. For robustness, the HR estimation method introduced in the last section was also recommended in Zou and Tsung's method. Denote the estimated spatial median and Tyler's transformation matrix by $(\boldsymbol{\theta}_0, \boldsymbol{A}_0)$. The spatial sign vector of the observation $\boldsymbol{y}_i$ collected online is

$$\boldsymbol{u}_i = U(\boldsymbol{A}_0(\boldsymbol{y}_i - \boldsymbol{\theta}_0)) \text{ for } i = 1, 2, \ldots.$$

Then construct the EWMA sequence by

$$\boldsymbol{w}_i = (1 - \lambda)\boldsymbol{w}_{i-1} + \lambda \boldsymbol{u}_i,$$

where λ is a weighting parameter and $\boldsymbol{u}_0 = \boldsymbol{0}$. The proposed control chart triggers a signal if

$$Q_i = \frac{2 - \lambda}{\lambda} p \boldsymbol{w}_i' \boldsymbol{w}_i > L,$$

where $L > 0$ is a control limit chosen to achieve a specified in-control (IC) average run length (ARL).

Zou and Tsung (2011) showed that the proposed control chart is affine invariant and distribution-free in the sense that the IC ARL is the same for the class of elliptical direction distributions. The distribution-free property not only makes the monitoring scheme robust to the underlying distribution, but also provides a convenient way to determine the control limit L. More specifically, since the IC run-length distribution is the same for any continuous process with an elliptical direction distribution, L can be determined from any distribution, e.g., the standard normal distribution. The control limits for some values of p, λ, and IC ARL were tabulated in Zou and Tsung (2011). They claimed that the sign-based EWMA control chart is fast to compute with a computational time similar to the multivariate EWMA (MEWMA, Lowry et al., 1992) and more efficient in detecting process shifts, especially for small or moderate shifts when the process distribution

is heavy tailed or skewed. However, when the shift is quite large, the MEWMA chart outperforms the sign-based control chart since the sign-based control chart considers only the directions rather than the distances from the origin.

Table 2.1: Research works in profile monitoring

Distribution	Model	Phase I	Phase II
Gaussian Distribution	Simple Linear	Kang and Albin (2000) Mahmoud and Woodall (2004) Mahmoud et al. (2007) Jensen et al. (2008)	Kang and Albin (2000) Kim et al. (2003) Zou et al. (2006) Saghaei et al. (2009) Zhang et al. (2009)
	Generalized Linear	Williams et al. (2007a) Williams et al. (2007b) Kazemzadeh et al. (2008) Mahmoud (2008) Noorossana et al. (2010)	Zou et al. (2007a) Kazemzadeh et al. (2009) Eyvazian et al. (2011) Lee et al. (2011) Zou et al. (2012a)
	Nonlinear	Jensen and Birch (2009)	Colosimo et al. (2008) Vaghefi et al. (2009)
	Nonparametric	Jin and Shi (2001) Lada et al. (2002) Jeong et al. (2006) Zou et al. (2008) Chicken et al. (2009) Shiau et al. (2009) (This Dissertation)	Jin and Shi (2001) Ding et al. (2006) Shiau et al. (2009) (This Dissertation)
Distribution-Free	Nonparametric	Febrero et al. (2008) (This Dissertation)	Cheng (2009) Wang (2009) Zou et al. (2009) Qiu and Zou (2010) Qiu et al. (2010) (This Dissertation)

Table 2.2: Research works in multivariate process monitoring

Distribution	Detect shift in	Phase I	Phase II
Gaussian Distribution	Mean	Vargas (2003) Jensen et al. (2007) Zamba and Hawkins (2006)	Crosier (1988) Lowry et al. (1992) Zamba and Hawkins (2006) Hawkins and Maboudou-Tchao (2007) Zou and Qiu (2009)
	Covariance Matrix		Yeh et al. (2004) Yeh et al. (2005) Huwang et al. (2007) Hawkins and Maboudou-Tchao (2008) Yen and Shiau (2010) Yen et al. (2012)
	Mean and Covariance Matrix		Reynolds and Cho (2006) Maboudou-Tchao and Hawkins (2011)
Distribution-Free	Mean	Liu (1995) Hamurkaroğlu et al. (2004) (This Dissertation)	Qiu and Hawkins (2001) Qiu and Hawkins (2003) Liu et al. (2004) Qiu (2008) Zou and Tsung (2011) Zou et al. (2012b) Boone and Chakraborti (2012)

Chapter 3

Profile Monitoring Schemes under Gaussian Assumption

In this chapter, we consider the problem of profile monitoring when the process is from Gaussian. Equivalently, the discretized profile data are assumed from the model (A0) described in Section 2.2.1. This chapter is organized as follows. Sections 3.1 and 3.2 present the proposed process monitoring schemes for Phase I and II, respectively. Section 3.3 presents results of some simulation studies of our proposed monitoring schemes and performance comparisons between the proposed schemes and some existing methods. Section 3.4 demonstrates the applicability of the proposed control charts with a real example. Section 3.5 concludes this chapter with a brief discussion on some related issues.

3.1 Phase I Monitoring

3.1.1 Model Assumptions and Data Smoothing

Assume the observed profile data can be described by the following nonparametric regression model:

$$y_{ij} = g(x_{ij}) + f_i(x_{ij}) + \varepsilon_{ij} \text{ for } i = 1, \ldots, m, j = 1, \ldots, p_i, \tag{3.1}$$

where $g(\cdot)$ is the mean profile function, i.e., the fix-effect term, $f_i(\cdot)$ is the random-effect term of the ith profile, x_{ij} is the jth covariate value of the ith profile, and $(\varepsilon_{i1}, \ldots, \varepsilon_{ip_i})'$ is the i.i.d. random error vector with mean 0 and variance σ_ε^2. The random-effect term f_i and the errors ε_{ij} are assumed independent of each other. In this chapter, we assume f_i is distributed as $N_{p_i}(\mathbf{0}, \mathbf{\Sigma}_i)$, where $\mathbf{\Sigma}_i = [\sigma_{i,jk}]_{j,k=1,\ldots,p_i}$ and

$$\sigma_{i,jk} = E[f_i(x_{ij}) f_i(x_{ik})].$$

The collected profile data are often accompanied with noises. To filter out the noise in the raw data, smoothing profiles as a preprocess step is often adopted. Moreover, the design points of the covariate may vary from profile to profile in real applications, a situation the PCA cannot be applied directly. To cope with this situation, we can simply smooth each individual profile and obtain the values of the smoothed profile at the same set of design points, say, $\boldsymbol{x} = (x_1, \ldots, x_p)'$ for a certain p. Many popular smoothing techniques, such as kernel smoothing, local polynomial regression smoothing, smoothing splines, B-splines, and wavelets can be used and they usually make little difference for this purpose.

In this study, the local linear smoothing method (Fan and Gijbels, 1996) is adopted for simplicity. Given any x_0 in the range of the design points, the local

linear estimator for the ith profile takes the form of

$$\tilde{y}_i(x_0) = \sum_{j=1}^{p} W_j(x_0) y_{ij} \text{ for } i = 1, 2, \ldots, \tag{3.2}$$

$$W_j(x_0) = U_j(x_0) \Big/ \sum_{k=1}^{p} U_k(x_0),$$

$$U_k(x_0) = K_h(x_{ik} - x_0)[m_2(x_0) - (x_{ik} - x_0)m_1(x_0)],$$

$$m_l(x_0) = \frac{1}{n} \sum_{k=1}^{p} (x_{ik} - x_0)^l K_h(x_{ik} - x_0), \ l = 1, 2,$$

and $K_h(\cdot) = K(\cdot/h)/h$ with $K(\cdot)$ being a kernel function and h being the bandwidth. Generally, the selection of the kernel function $K(\cdot)$ is not crucial (ref. Fan and Gijbels, 1996); thus the popular Epanechnikov kernel,

$$K(u) = \frac{3}{4}(1 - u^2) I(|u| \leq 1),$$

is adopted in this study.

The local linear smoothing technique has been implemented in R, S-plus, and some other statistical softwares and is extensively used in applications. Another benefit of using the local linear smoothing is that the corresponding estimate is a linear combination of the original profile data so that its distribution can be obtained easily from the normality assumption of data. Therefore, we can simply assume the smoothed profiles are distributed as $N_p(\boldsymbol{\mu}, \boldsymbol{\Sigma})$, where $\boldsymbol{\mu}$ and $\boldsymbol{\Sigma}$ are the mean and variance-covariance matrix of the smoothed profiles, respectively.

In the use of the PCA technique, the choice of the number of effective PCs is affected by the degree of smoothness; thus the popular generalized cross-validation (GCV) method proposed by Craven and Wahba (1979) is considered in choosing the smoothing parameter, i.e., the bandwidth in our case. Without repeating smoothing, the GCV method is computationally more efficient than the ordinary cross validation (OCV) method. Moreover, it has been found that the GCV method has a tendency of less under-smoothing than the OCV method. Specifically, for a

given profile $\boldsymbol{y}$, define the GCV function as

$$\text{GCV}(h) = \frac{p\boldsymbol{y}'[\boldsymbol{I}_p - \boldsymbol{W}_h]\boldsymbol{y}}{[\text{tr}(\boldsymbol{I}_p - \boldsymbol{W}_h)]^2},$$

where $\boldsymbol{I}_p$ is the $p \times p$ identity matrix and $\boldsymbol{W}_h$ is the smoothing matrix corresponding to a certain bandwidth h. Then the desired bandwidth h is the minimizer of the GCV function. The minimization of GCV(h) with respect to h will inevitably involve trying a large number of values of h. Ramsay and Silverman (2005) introduced a greatly-speeding-up computation method by performing a preliminary generalized eigen-analysis. For more details about GCV, see Gu (2002) or Ramsay and Silverman (2005).

3.1.2 Phase I Monitoring Scheme

Let $\boldsymbol{y}$ be a profile datum following model (3.1) and $\tilde{\boldsymbol{y}}$ be the corresponding local linear smoothing estimate. To simplify notation, we suppress the "$\sim$" symbol and denote the $\boldsymbol{y}$ as a profile datum after smoothing hereafter. During Phase I, the process may not be stable yet and all the parameters necessary for monitoring must be estimated from the data on hand. In this study, we simply use the sample mean vector and sample variance-covariance matrix, denoted as $(\hat{\boldsymbol{\mu}}, \hat{\boldsymbol{\Sigma}})$, to estimate $(\boldsymbol{\mu}, \boldsymbol{\Sigma})$.

The methodologies we propose in this dissertation involves the PCA technique. In functional PCA, the eigen-functions $\nu(\cdot)$ and the corresponding eigen-values λ are defined to satisfy the equation

$$\int Q(t,s)\nu(s)ds = \lambda\nu(t),$$

where $Q(t,s)$ is the covariance function; see Ramsay and Silverman (2005). By applying the smoothing technique to profiles as a preprocessing step, we obtain smoothed profiles at a pre-determined set of design points. Thus, the regular PCA can be applied to the smoothed profiles directly. We adopt the notation of the regular PCA in what follows for simplicity. Both of the functional form and

regular form of PCA can be utilized for our purpose, but the function form is more involved in theory and in computation.

In Phase I monitoring, Shiau et al. (2009) proposed a method based on PCA and the Hotelling T^2 statistic. The method applies the eigen-analysis to $\hat{\boldsymbol{\Sigma}}$ to obtain the corresponding eigenvalue-vector pairs, denoted as $(\lambda_1, \boldsymbol{\nu}_1), \ldots, (\lambda_p, \boldsymbol{\nu}_p)$, where $\lambda_1 \geq \lambda_2 \geq \ldots \geq \lambda_p \geq 0$. The selection of the "effective" principal components (PCs) is based on the total variation explained by the chosen PCs along with the principle of parsimoniousness that we often use in variable selection. Let the number of the effective PCs be K. Consider the statistic

$$T_{0i}^2 = (\boldsymbol{s}_{0i} - \bar{\boldsymbol{s}}_0)' \boldsymbol{B}_0^{-1} (\boldsymbol{s}_{0i} - \bar{\boldsymbol{s}}_0), \tag{3.3}$$

$i = 1, ..., m$, where $\boldsymbol{s}_{0i}$ is the vector of the first K PC scores for the ith profile, $\bar{\boldsymbol{s}}_0 = \sum_{i=1}^{m} \boldsymbol{s}_{0i}/m$, and $\boldsymbol{B}_0 = \sum_{i=1}^{m} (\boldsymbol{s}_{0i} - \bar{\boldsymbol{s}}_0)(\boldsymbol{s}_{0i} - \bar{\boldsymbol{s}}_0)'/(m-1)$. A large value of the T_0^2 statistic indicates that the corresponding profile could be abnormal and perhaps should be deleted from the historical data set. Since the score vectors are distributed as multivariate normal asymptotically (Anderson, 2003), according to Tracy et al. (1992) and also Sullivan and Woodall (1996),

$$\frac{m}{(m-1)^2} T_{0i}^2 \sim Beta\left(\frac{K}{2}, \frac{m-K-1}{2}\right) \text{ approximately.}$$

Thus, for a control chart with a false-alarm rate α, the control limit can be set at the upper α quantile of the beta distribution multiply by $(m-1)^2/m$, and observations with T_{0i}^2 values exceeding the control limit are regarded as OC.

The methodology proposed by Shiau et al. (2009) has a drawback that the information on the PC $\boldsymbol{\nu}_{K+1}, \ldots, \boldsymbol{\nu}_p$ are ignored and thus the changes in the space spanned by these PCs will not be monitored. To overcome this drawback, we consider another T^2 statistic based on the remaining $p-K$ PCs defined as

$$T_{1i}^2 = (\boldsymbol{s}_{1i} - \bar{\boldsymbol{s}}_1)' \boldsymbol{B}_1^{-1} (\boldsymbol{s}_{1i} - \bar{\boldsymbol{s}}_1) \text{ for } i = 1, ...m, \tag{3.4}$$

where $\boldsymbol{s}_{1i}$ is the vector of the last $p-K$ PC scores for the ith profile, $\bar{\boldsymbol{s}}_1$ and $\boldsymbol{B}_1$ are the corresponding sample mean and sample variance-covariance matrix,

respectively. Similarly, we also have

$$\frac{m}{(m-1)^2}T_{1i}^2 \sim Beta\left(\frac{p-K}{2}\frac{m-p+K-1}{2}\right) \text{ approximately,}$$

and then the upper α quantile of the beta distribution multiply by $(m-1)^2/m$ can be used as the control limit of this chart.

To combine the information from both of the T_0^2 and T_1^2 charts, an observation is regarded as OC if any of the two charts is triggered out of control. Since both of the T^2-type charts are Shewhart-type, this control charting scheme is referred to as the Phase I combined Shewhart (CS) chart hereafter.

3.1.3 Performance Measures

In early researches about the Phase I control chart, some authors considered the signal probability, defined as the probability of observing at least one OC signal on the chart, as the measure of performance (ref. Mahmoud and Woodall, 2004; Champ and Jones, 2004; Jones-Farmer et al., 2009; Jones-Farmer and Champ, 2010). Unfortunately, using the signal probability as the performance measure, the signaled observations may include both IC and OC cases. Instead of the signal probability, we consider the type-I and type-II error rates as the measures of performance (ref. Zhang and Albin, 2009; Shiau and Sun, 2010). The type-I error rate is defined as the misjudged rate of classifying the IC observations to be OC, and the type-II error rate is the rate of treating OC cases as IC. To be more specific, suppose that there are m observations with m_{oc} OC cases. After Phase I analysis, it turns out that there are m_1 IC observations incorrectly regarded as OC and m_2 OC observations misclassified as IC. Then the type-I and type-II error rates are defined as

$$p_I = \frac{m_1}{m-m_{oc}} \text{ and } p_{II} = \frac{m_2}{m_{oc}},$$

respectively. In usual applications, the type-I error rate has to be controlled under a certain level, say, α_0. Since our proposed monitoring scheme involves combining

two Shewhart control charts, we can take the type-I error rate of each chart to be $\alpha = 1-\sqrt{1-\alpha_0}$ for the purpose of controlling the overall type-I error rate at about α_0. We remark that although the two statistics T_{0i}^2 and T_{1i}^2 are not independent theoretically, their correlation is very weak for large m.

3.2 Phase II Monitoring

3.2.1 Methodology

We now consider $\boldsymbol{y}$ as an incoming profile datum from model (3.1) after smoothing. The underlying distribution of an IC $\boldsymbol{y}$ is assumed to be a the p-dimensional multivariate normal distribution, denoted as $N_p(\boldsymbol{\mu}_0, \boldsymbol{\Sigma}_0)$. Different from the Phase I application, the parameters $(\boldsymbol{\mu}_0, \boldsymbol{\Sigma}_0)$ are either known or have been well estimated from the historical IC dataset. For each incoming profile, the main purpose is to examine if the profile follows the same mean and variance-covariance structure as $\boldsymbol{\mu}_0$ and $\boldsymbol{\Sigma}_0$. A profile has a shift either in mean or in variance-covariance matrix is regarded as an OC case.

Shiau et al. (2009) proposed a methodology based on the PC scores, which is effective when changes occur in the eigen space spanned by the effective PCs. In their methodology, the eigen-analysis is applied to $\boldsymbol{\Sigma}_0$, and the corresponding eigenvalue-vector pairs, denoted as $(\lambda_1, \boldsymbol{\nu}_1), \ldots, (\lambda_p, \boldsymbol{\nu}_p)$, where $\lambda_1 \geq \lambda_2 \geq \ldots \geq \lambda_p \geq 0$, are obtained. The selection of the effective PCs is also based on the total variation explained by the chosen PCs along with the principle of parsimoniousness. Let the number of the effective PCs be K and $\boldsymbol{P}_0 \equiv (\boldsymbol{\nu}_1, \ldots, \boldsymbol{\nu}_K)$ be the matrix of the effective PCs. Then $\boldsymbol{s} \equiv (S_1, \ldots, S_K)' = \boldsymbol{P}_0'\boldsymbol{y}$ is the vector of PC scores corresponding to the K effective PCs. By the theory of PCA, we know that $\boldsymbol{y}$ can be well approximated by $\sum_{j=1}^{K} S_j\boldsymbol{\nu}_j = \boldsymbol{P}_0\boldsymbol{s}$ if the proportion of total variation explained by the first K PCs is large enough. The T^2-type statistic proposed by

Shiau et al. (2009) is

$$T_0^2 = (\boldsymbol{y} - \boldsymbol{\mu}_0)' \boldsymbol{P}_0 \boldsymbol{\Lambda}_0^{-1} \boldsymbol{P}_0' (\boldsymbol{y} - \boldsymbol{\mu}_0), \tag{3.5}$$

where $\boldsymbol{\Lambda}_0$ =diag$[\lambda_1, \ldots, \lambda_K]$. It can be easily shown that the T_0^2 statistic follows the χ^2 distribution with degrees of freedom K, denoted as χ_K^2, under normal assumption of $\boldsymbol{y}$. A large value of the T_0^2 statistic that exceeds the upper α quantile of χ_K^2 leads to a violation of the hypothesis that the process is IC.

The efficacy of the T_0^2 chart was illustrated in Shiau et al. (2009). The authors also showed that the chart is powerful when the OC profiles can be approximated by the effective PCs as well. Unfortunately, one cannot expect this condition holds for all OC profiles. The T_0^2 chart has no power in detecting the OC profiles residing in the complementary space of the effective PCs. To cope with this problem, we propose monitoring the residual vector. Letting $\boldsymbol{P}_1 \equiv (\boldsymbol{\nu}_{K+1}, \ldots, \boldsymbol{\nu}_p)$, the residual vector is then defined as

$$\boldsymbol{e} = \boldsymbol{y} - \sum_{j=1}^{K} S_j \boldsymbol{\nu}_j = \boldsymbol{P}_1 \boldsymbol{P}_1' \boldsymbol{y}.$$

Since $\boldsymbol{y}$ follows $N_p(\boldsymbol{\mu}_0, \boldsymbol{\Sigma}_0)$, the residual vector is obviously distributed as

$$N_p\big(\boldsymbol{P}_1 \boldsymbol{P}_1' \boldsymbol{\mu}_0, \boldsymbol{P}_1 \boldsymbol{P}_1' \boldsymbol{\Sigma}_0 \boldsymbol{P}_1 \boldsymbol{P}_1'\big).$$

Let $\boldsymbol{\Lambda}_1$ =diag$[\lambda_{K+1}, \ldots, \lambda_p]$. Since $\boldsymbol{P}_1' \boldsymbol{\Sigma}_0 \boldsymbol{P}_1 = \boldsymbol{\Lambda}_1$, the variance-covariance matrix of $\boldsymbol{e}$ can be expressed as $\boldsymbol{P}_1 \boldsymbol{\Lambda}_1 \boldsymbol{P}_1'$. Therefore, analogous to the T_0^2 statistic, the charting statistic

$$T_1^2 = (\boldsymbol{y} - \boldsymbol{\mu}_0)' \boldsymbol{P}_1 \boldsymbol{\Lambda}_1^{-1} \boldsymbol{P}_1' (\boldsymbol{y} - \boldsymbol{\mu}_0) \tag{3.6}$$

is used to monitor the changes in the space spanned by $\{\boldsymbol{\nu}_{K+1}, \ldots, \boldsymbol{\nu}_p\}$. Under the normality assumption, the distribution of T_1^2 follows χ^2 distribution with degrees of freedom $p - K$, denoted as χ_{p-K}^2.

Since the p eigen-vectors form a basis of the p-dimensional space, all the OC conditions are incorporated. To monitor all the OC conditions, we combine the

information of the two T^2 statistics. Analogous to the Shewhart chart, appropriate quantiles of the χ^2_K and χ^2_{p-K} distributions are regarded as the control limits for the T_0^2 and T_1^2 charts, respectively. For the IC average run length (ARL) of the combined chart to achieve a given ARL_0, we take the false-alarm rate of each chart to be $\alpha = 1 - \sqrt{1-\alpha_0}$, where $\alpha_0 = 1/ARL_0$, the false-alarm rate corresponding to ARL_0. This chart will be referred to as the Phase II combined Shewhart (CS) chart hereafter.

It is well known that the Shewhart chart is not powerful in detecting small shifts of parameters in Phase II monitoring. To detect small shifts, an exponentially weighted moving average (EWMA) type monitoring scheme is often considered. For the ith incoming profile, the EWMA sequences based on T_0^2 and T_1^2 statistics are defined as

$$W_{0,i} = \lambda_0 T_{0,i}^2 + (1-\lambda_0) W_{0,i-1}, \tag{3.7}$$

$$W_{1,i} = \lambda_1 T_{1,i}^2 + (1-\lambda_1) W_{1,i-1}, \tag{3.8}$$

respectively, where $T_{0,i}^2$ and $T_{1,i}^2$ are the values of T_0^2 and T_1^2 statistics, respectively; and $0 < \lambda_0, \lambda_1 \leq 1$ are weighting parameters. The initial values are $W_{0,0} = E(T_{0,i}^2) = K$ and $W_{1,0} = E(T_{1,i}^2) = p - K$, since $T_{0,i}^2$ and $T_{1,i}^2$ follow χ^2_K and χ^2_{p-K} distributions, respectively, when the process is in control. Note that $\text{var}(T_{0,i}^2) = 2K$ and $\text{var}(T_{1,i}^2) = 2(p-K)$. Then, the combined EWMA chart is triggered OC if

$$W_{0,i} > L_0 \text{ or } W_{1,i} > L_1,$$

where

$$L_0 = K + \gamma_0 \sqrt{2K \frac{\lambda}{2-\lambda}\left[1-(1-\lambda)^{2i}\right]},$$

$$L_1 = p - K + \gamma_1 \sqrt{2(p-K) \frac{\lambda}{2-\lambda}\left[1-(1-\lambda)^{2i}\right]},$$

and $\gamma_0 > 0$ and $\gamma_1 > 0$ are chosen such that the combined chart achieves a prespecified IC ARL. For simplicity, the corresponding individual ARLs of the EWMA T_0^2 and T_1^2 charts are set to be equal. In this study, the term $\left[1-(1-\lambda)^{2i}\right]$ is

dropped in both of the control limits for simplification. That is, the control limits are redefined as

$$L_0 = K + \gamma_0 \sqrt{2K \frac{\lambda}{2-\lambda}}, \tag{3.9}$$

$$L_1 = p - K + \gamma_1 \sqrt{2(p-K) \frac{\lambda}{2-\lambda}}. \tag{3.10}$$

This monitoring scheme combines two EWMA charts, thus we refer to this chart as the combined EWMA (CE) chart henceforth.

Since the expressions of the T_0^2 and T_1^2 statistics involve the mean vector and variance-covariance matrix, any shift of the parameters, including location, scale, or shape, would change the magnitude of the charting statistics. Therefore, the T_0^2 and T_1^2 statistics can be utilized to monitor various kinds of shifts in process parameters. Intuitively speaking, the T_0^2 statistic is in charge of the deviations in the space spanned by the first K PCs whereas the T_1^2 statistic is in charge of the rest of the deviations.

3.2.2 Control Limit Determination and ARL Calculation

To construct a CE chart that achieves a specified ARL_0, we need to search for an appropriate control limit. Hence, finding an efficient way to calculate the ARL_0 for given trial control limits is necessary. Fortunately, the ARL_0 of the CE chart can be approximated via a two-dimensional Markov chain. Morais and Pacheco (2000) proposed a Markovian approach to calculate the ARL of the combined EWMA $\bar{X}$-$\ln S^2$ chart. For our proposed combined EWMA T^2-type chart, we imitate their method to obtain an efficient computing procedure, which is provided in the Appendix B.1. Our experience shows that the computing procedure is fairly efficient. We remark that the Markovian approach to approximating the OC ARL works only when the process change is on the mean. For other OC conditions when the variance-covariance matrix changes, or mean and variance-covariance matrix shift simultaneously, the OC ARL can only be obtained via simulations.

3.2.3 Diagnosis

When the process is out of control, diagnosing the source of process change is very important in SPC. We regard the space spanned by the first few effective PCs as the "primary space" because it contains primary variations among IC profiles. Recall that the monitoring statistics T_{0i}^2 (and W_{0i}) are designed to detect shifts within the primary space whereas T_{1i}^2 (and W_{1i}) can detect shifts within the complementary space. Thus, our proposed monitoring scheme has capability of distinguishing the OC conditions. If the shift resides in the primary space, we can further observe the pattern of scores along each of the effective PCs to pursue the source of the process shift.

In regular PCA, the effective PCs are chosen and ordered according to the proportion of the variation they explain. However, the first few PCs are not necessarily explicable. In order to make the primary PCs more meaningful, we borrow the VARIMAX rotation tool from factor analysis. Let $\boldsymbol{P}_0$ be the $p \times K$ matrix consisting of the first K PCs as defined earlier and $\boldsymbol{R}_0$ be

$$\boldsymbol{R}_0 = \boldsymbol{H}^* \boldsymbol{P}_0,$$

where $\boldsymbol{H}^*$ is the orthogonal matrix that maximizes the variance of the squared elements of each rotated PCs. In other words, $\boldsymbol{H}^*$ satisfies

$$\arg\max_{\boldsymbol{H}} \sum_{j=1}^{K} \left\{ \sum_{i=1}^{p} (\boldsymbol{H}\boldsymbol{P}_0)_{ij}^4 - \frac{1}{p} \left(\sum_{i=1}^{p} (\boldsymbol{H}\boldsymbol{P}_0)_{ij}^2 \right)^2 \right\}.$$

Maximizing the variance of the squared elements of a rotated PC can only occur if these values tend to be either relatively large or near zero; thus, the values of the elements of rotated PCs are either shrunk to zero or strongly positive (or negative). Then the rotated PCs could be utilized to diagnose where the shifts might be possibly from if an OC condition occurs in the process. The VARIMAX rotation procedure is conveniently available in the "fda" package in R software.

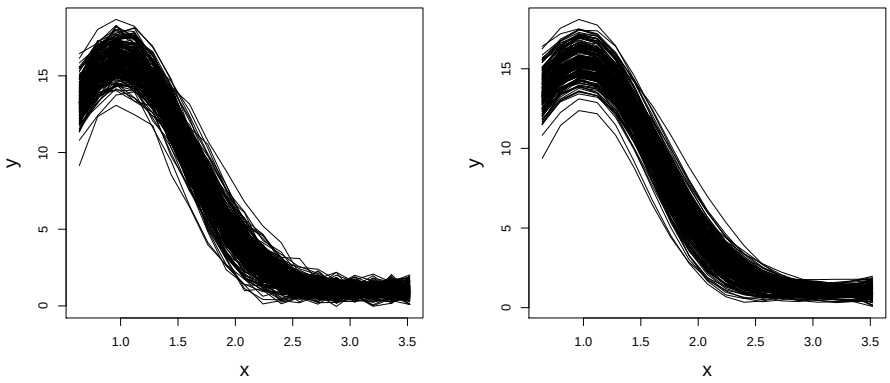

(a) (b)

Figure 3.1: (a) 200 generated profiles from the multivariate normal distribution with mean and variance-covariance matrix expressed as (3.12) and (3.13), respectively, and (b) the corresponding smoothed estimates.

3.3 Simulation Studies

In this section, we compare the performances of our proposed charts with some existing monitoring schemes. Advantages and drawbacks of these control charts are investigated. For Phase I, the performance is measured by the type-I and type-II error rates introduced in Section 3.1.3. The usual ARL is adopted as the performance measure for Phase II.

3.3.1 Model Description

An example of nonlinear profiles regarding the dissolving process of aspartame (an artificial sweetener) was first described in Kang and Albin (2000) but not studied. The quality of aspartame is characterized by the amount of aspartame dissolved per liter of water at different levels of temperature. Since there are no available aspartame data, Shiau et al. (2009) considered profiles of the following form to

imitate aspartame profiles. Consider $\boldsymbol{y} = (y_1, ..., y_p)'$ with

$$y_j = I + Me^{N(x_j-1)^2} + \varepsilon_j \text{ for } j = 1, \ldots, p, \tag{3.11}$$

where $(x_1, \ldots, x_p)'$ is a given vector of the covariate values, $I \sim N(\mu_I, \sigma_I^2)$, $M \sim N(\mu_M, \sigma_M^2)$, $N \sim N(\mu_N, \sigma_N^2)$, $\varepsilon_j \sim N(0, \sigma_\varepsilon^2)$, and all the random components are independent of each other. Unfortunately, the distribution of $\boldsymbol{y}$ in model (3.11) is too complicated and departs from the multivariate normal distribution. Instead of model (3.11), following Shiau et al. (2009), we consider the simplified case that the IC profiles are from a multivariate normal distribution with mean $\boldsymbol{\mu} = (\mu_1, \ldots, \mu_p)'$ and variance-covariance matrix $\boldsymbol{\Sigma} = [\sigma_{ij}]_{i,j=1,\ldots,p}$ as follows. For $i, j = 1, \ldots, p$,

$$\mu_j = \mu_I + \mu_M e^{\mu_N(x_j-1)^2}, \tag{3.12}$$

$$\begin{aligned}\sigma_{ij} = \sigma_I^2 + \left(\mu_M^2 + \sigma_M^2\right)\left[e^{\mu_N[(x_i-1)^2+(x_j-1)^2]+\frac{\sigma_N^2}{2}[(x_i-1)^2+(x_j-1)^2]^2}\right] \\ - \mu_M^2 e^{\mu_N[(x_i-1)^2+(x_j-1)^2]+\frac{\sigma_N^2}{2}[(x_i-1)^4+(x_j-1)^4]} + \sigma_\varepsilon^2\delta_{ij},\end{aligned} \tag{3.13}$$

where $\delta_{ij} = 1$, if $i = j$, and 0, otherwise. Note that the variance-covariance matrix $\boldsymbol{\Sigma}$ is the same as that of model (3.11). An analysis for non-Gaussian profiles from model (3.11) will be given in Chapter 5.

Let $p = 19$ and $(x_1, \ldots, x_p)$ be equally spaced and range from 0.64 to 3.52. The IC profiles are generated by setting $(\mu_I, \sigma_I) = (1, 0.2)$, $(\mu_M, \sigma_M) = (15, 1)$, $(\mu_N, \sigma_N) = (-1.5, 0.3)$, and $\sigma_\varepsilon = 0.3$. We first smooth the generated profiles by using the local linear smoother with bandwidth $h = 0.357$ (according to the GCV) as a preprocessing step before monitoring. Figure 3.1 displays 200 generated IC profiles (left panel) and the corresponding smoothed estimates (right panel). From the figures we can observe that the smoothed profiles preserve the important features while the noises at set points of temperature are successfully removed.

To assess the performance of the proposed control schemes, we consider some OC scenarios by changing the parameters $(\boldsymbol{\mu}, \boldsymbol{\Sigma})$. The magnitude of shifts in mean and/or variance-covariance matrix are listed in Table 3.1. 50 profiles generated from each of these OC models along with 200 IC profiles are shown in Figure 3.2.

Model (a) has the shift mainly from the space spanned by the effective PCs and mostly around the peak of the profiles. Model (b) simulates the case that OC profiles cannot be approximated by the effective PCs at all, a situation that the process may have lost control in an unexpected way. This kind of OC conditions potentially could be a more serious problem than OC conditions when the shift still resides in the primary space such as Model (a). The middle row of Figure 3.2 shows that the OC profiles are more wiggly than the IC ones. Model (c) illustrates the situation that the shift comprises components from both of the primary and complementary spaces. The bottom row of Figure 3.2 shows OC profiles are quite different from the IC ones. Since OC conditions may not be predicted in practice, a good monitoring scheme should have the capability of detecting situations like Model (c). We evaluate the performance of the proposed monitoring schemes via the simulated data described above.

3.3.2 Phase I Application

The simulation results for Phase I analysis are presented in this section. Since the distribution of the profile data is assumed to be multivariate normal and the design points are the same for all profiles, multivariate control charts could be utilized directly. One of the charts is the well-known Hotelling's T^2 control chart. For a sample $\{\boldsymbol{y}_1, \ldots, \boldsymbol{y}_m\}$ from a p-variate normal distribution, the Hotelling's T^2

Table 3.1: The shifts in mean and/or variance-covariance matrix of the OC models

Model	mean	variance-covariance matrix
(a)	$\delta_1 e^{\mu_N (x-1)^2}$	$\delta_2 \sum_{i=1}^{3} \lambda_i \boldsymbol{\nu}_i \boldsymbol{\nu}_i'$
(b)	$\delta_1 \sum_{i=4}^{6} \sqrt{\lambda_i} \boldsymbol{\nu}_i$	$\delta_2 \sum_{i=4}^{6} \lambda_i \boldsymbol{\nu}_i \boldsymbol{\nu}_i'$
(c)	$\delta_1 \sum_{i=1,4,5} \sqrt{\lambda_i} \boldsymbol{\nu}_i$	$\delta_2 \sum_{i=1,4,5} \lambda_i \boldsymbol{\nu}_i \boldsymbol{\nu}_i'$

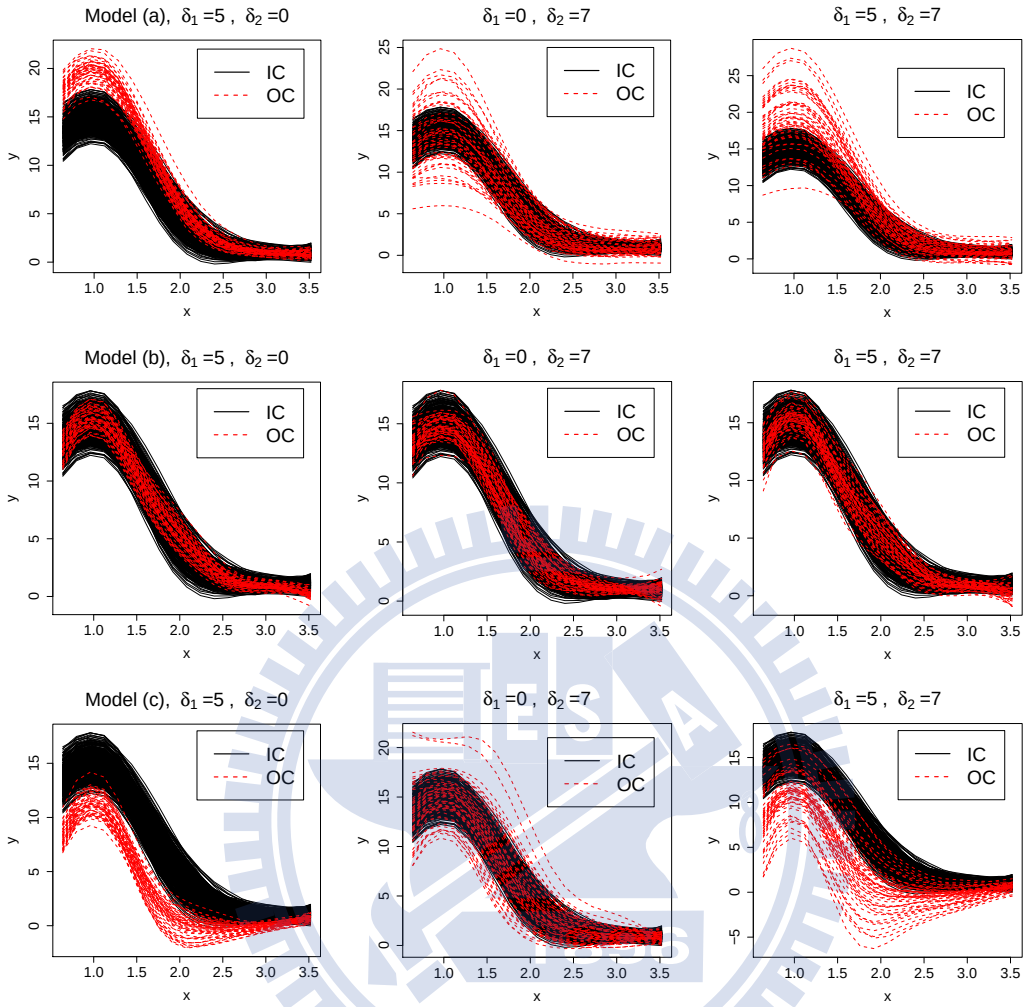

Figure 3.2: Plots of IC and OC samples from Model (a)(top row), (b)(middle row) and (c)(bottom row).

statistic is defined as

$$T_i^2 = (\boldsymbol{y}_i - \bar{\boldsymbol{y}})' \boldsymbol{B}^{-1} (\boldsymbol{y}_i - \bar{\boldsymbol{y}}) \text{ for } i = 1, \ldots, m,$$

where $\bar{\boldsymbol{y}}$ and $\boldsymbol{B}$ are the sample mean and sample variance-covariance matrix, respectively. In Phase I analysis, the T^2 statistic is approximately distributed as a beta distribution (Tracy et al., 1992), so the control limit can be conveniently set at

$$\frac{(m-1)^2}{m} \beta_{\alpha, p/2, (m-p-1)/2},$$

Table 3.2: The type-I and type-II error rates and their standard errors (in parentheses) of OC Model (a) for $\alpha = 0.05$ and $\delta_2 = 0$.

	p_I					p_{II}				
δ_1	T^2	CS(2)	CS(3)	CS(4)	CS(5)	T^2	CS(2)	CS(3)	CS(4)	CS(5)
0.625	0.0749	0.0722	0.0692	0.0706	0.0683	0.9162	**0.9095**	0.9155	0.9168	0.9210
	(.0005)	(.0005)	(.0005)	(.0005)	(.0004)	(.0013)	(.0014)	(.0013)	(.0013)	(.0013)
1.250	0.0735	0.0688	0.0677	0.0682	0.0666	0.8976	**0.8552**	0.8765	0.8869	0.8967
	(.0005)	(.0005)	(.0004)	(.0005)	(.0004)	(.0014)	(.0018)	(.0016)	(.0015)	(.0014)
1.875	0.0709	0.0645	0.0643	0.0654	0.0644	0.8711	**0.7561**	0.8082	0.8348	0.8514
	(.0005)	(.0005)	(.0004)	(.0005)	(.0004)	(.0016)	(.0024)	(.0021)	(.0019)	(.0018)
2.500	0.0704	0.0642	0.0624	0.0636	0.0629	0.8347	**0.5908**	0.6944	0.7479	0.7836
	(.0005)	(.0005)	(.0004)	(.0005)	(.0004)	(.0019)	(.0033)	(.0030)	(.0027)	(.0024)
3.125	0.0680	0.0677	0.0642	0.0639	0.0629	0.7935	**0.3343**	0.4850	0.6030	0.6827
	(.0005)	(.0005)	(.0004)	(.0005)	(.0004)	(.0023)	(.0035)	(.0041)	(.0039)	(.0035)
3.750	0.0672	0.0727	0.0687	0.0675	0.0646	0.7466	**0.1174**	0.2091	0.3313	0.4693
	(.0005)	(.0005)	(.0005)	(.0005)	(.0004)	(.0028)	(.0021)	(.0035)	(.0051)	(.0054)
4.375	0.0667	0.0759	0.0730	0.0729	0.0698	0.6885	**0.0295**	0.0557	0.0950	0.1689
	(.0005)	(.0005)	(.0005)	(.0005)	(.0005)	(.0037)	(.0009)	(.0014)	(.0024)	(.0044)
5.000	0.0669	0.0771	0.0742	0.0744	0.0727	0.6057	**0.0066**	0.0130	0.0210	0.0344
	(.0005)	(.0005)	(.0005)	(.0005)	(.0005)	(.0058)	(.0004)	(.0006)	(.0008)	(.0014)

where α is the nominal type-I error probability, and $\beta_{\alpha,a,b}$ is the upper α quantile of the beta distribution with shape parameters a and b. The observations with values of T^2 statistic larger than the control limit are considered as OC cases.

Suppose the IC profiles are from $N_p(\boldsymbol{\mu}, \boldsymbol{\Sigma})$, where $\boldsymbol{\mu}$ and $\boldsymbol{\Sigma}$ are given in (3.12) and (3.13), respectively, and the OC profiles are from the models described in Table 3.1. Various values of δ_1 and δ_2 are considered. For each scenario, a sample of 450 IC and 50 OC profiles is generated. Let the false-alarm rate $\alpha = 0.05$. The type-I and type-II error rates accompanied with their standard errors (in the parentheses) for the six OC conditions are summarized in Tables 3.2 - 3.7, respectively. Each value of error rates is obtained by averaging 1,000 replications.

Table 3.3: The type-I and type-II error rates and their standard errors (in parentheses) of OC Model (a) for $\alpha = 0.05$ and $\delta_1 = 0$.

	p_I					p_{II}				
δ_2	T^2	CS(2)	CS(3)	CS(4)	CS(5)	T^2	CS(2)	CS(3)	CS(4)	CS(5)
0.875	0.0721	0.0688	0.0668	0.0676	0.0663	0.8507	0.8045	**0.7928**	0.8082	0.8246
	(.0005)	(.0005)	(.0005)	(.0005)	(.0004)	(.0016)	(.0019)	(.0020)	(.0019)	(.0018)
1.750	0.0719	0.0691	0.0676	0.0682	0.0665	0.7812	0.7016	**0.6761**	0.7007	0.7240
	(.0005)	(.0005)	(.0004)	(.0005)	(.0005)	(.0020)	(.0022)	(.0022)	(.0023)	(.0022)
2.625	0.0713	0.0685	0.0677	0.0682	0.0664	0.7265	0.6314	**0.6014**	0.6285	0.6533
	(.0005)	(.0005)	(.0005)	(.0005)	(.0004)	(.0022)	(.0023)	(.0023)	(.0023)	(.0023)
3.500	0.0724	0.0698	0.0681	0.0681	0.0666	0.6744	0.5759	**0.5427**	0.5694	0.5951
	(.0005)	(.0005)	(.0005)	(.0005)	(.0004)	(.0024)	(.0023)	(.0024)	(.0024)	(.0024)
4.375	0.0721	0.0698	0.0686	0.0687	0.0679	0.6283	0.5312	**0.4965**	0.5220	0.5459
	(.0005)	(.0005)	(.0005)	(.0005)	(.0005)	(.0025)	(.0024)	(.0025)	(.0025)	(.0025)
5.250	0.0720	0.0698	0.0684	0.0686	0.0679	0.5913	0.4941	**0.4639**	0.4867	0.5053
	(.0005)	(.0005)	(.0005)	(.0005)	(.0004)	(.0026)	(.0024)	(.0025)	(.0025)	(.0025)
6.125	0.0721	0.0706	0.0691	0.0693	0.0676	0.5619	0.4641	**0.4320**	0.4551	0.4767
	(.0005)	(.0005)	(.0005)	(.0005)	(.0004)	(.0026)	(.0024)	(.0024)	(.0024)	(.0024)
7.000	0.0726	0.0712	0.0696	0.0698	0.0678	0.5327	0.4403	**0.4105**	0.4313	0.4526
	(.0005)	(.0005)	(.0005)	(.0005)	(.0005)	(.0026)	(.0023)	(.0023)	(.0024)	(.0024)

Consider the OC Model (a), the type-I and type-II error rates of applying the Hotelling's T^2 control chart and CS chart are given in Tables 3.2 and 3.3. The value in the parentheses of the CS chart is the number of the chosen PCs. It is noticed that the type-I error rates of both Hotelling's T^2 and CS charts are a little bit larger than the nominal value 0.05. We figure that this is mainly caused by the *iterative* procedure of removing the observations exceeding the trial control limit from the historical dataset. Note that, in each iteration, each IC observation has a certain probability to be removed, hence the false-alarm rate would accumulate and exceed the nominal value as the iteration proceeds. The large size of our simulated historical data (i.e., 500 profiles) also plays a role in accumulating the

Table 3.4: The type-I and type-II error rates and their standard errors (in parentheses) of OC Model (b) for $\alpha = 0.05$ and $\delta_2 = 0$.

	p_I					p_{II}				
δ_1	T^2	CS(2)	CS(3)	CS(4)	CS(5)	T^2	CS(2)	CS(3)	CS(4)	CS(5)
0.625	0.0736	0.0727	0.0694	0.0674	0.0670	0.9030	0.9128	0.9156	**0.9011**	0.9065
	(.0005)	(.0005)	(.0005)	(.0005)	(.0004)	(.0014)	(.0013)	(.0013)	(.0014)	(.0014)
1.250	0.0705	0.0714	0.0682	0.0634	0.0637	0.8561	0.8860	0.8871	**0.8163**	0.8337
	(.0005)	(.0005)	(.0004)	(.0004)	(.0004)	(.0018)	(.0015)	(.0015)	(.0021)	(.0020)
1.875	0.0673	0.0691	0.0657	0.0620	0.0623	0.7848	0.8490	0.8425	**0.6187**	0.6811
	(.0005)	(.0005)	(.0004)	(.0004)	(.0004)	(.0023)	(.0019)	(.0019)	(.0037)	(.0034)
2.500	0.0666	0.0686	0.0632	0.0687	0.0677	0.6867	0.8065	0.7836	**0.1924**	0.2733
	(.0005)	(.0005)	(.0004)	(.0005)	(.0005)	(.0037)	(.0024)	(.0026)	(.0035)	(.0053)
3.125	0.0686	0.0685	0.0647	0.0761	0.0749	0.4950	0.7613	0.6071	**0.0255**	0.0302
	(.0005)	(.0005)	(.0005)	(.0005)	(.0005)	(.0083)	(.0034)	(.0056)	(.0008)	(.0009)
3.750	0.0747	0.0687	0.0755	0.0763	0.0752	0.2183	0.6852	0.1199	**0.0018**	0.0020
	(.0006)	(.0005)	(.0005)	(.0005)	(.0005)	(.0099)	(.0070)	(.0067)	(.0002)	(.0002)
4.375	0.0772	0.0696	0.0780	0.0769	0.0752	0.0941	0.5971	0.0008	**0.0000**	0.0000
	(.0005)	(.0005)	(.0005)	(.0005)	(.0005)	(.0074)	(.0096)	(.0004)	(.0000)	(.0000)
5.000	0.0783	0.0705	0.0784	0.0764	0.0751	0.0523	0.5202	0.0000	**0.0000**	0.0000
	(.0005)	(.0005)	(.0005)	(.0005)	(.0005)	(.0058)	(.0109)	(.0000)	(.0000)	(.0000)

false-alarm rate, because a large sample size results in more iterations. Apart from this, the type-I error rates of both charts are steadily around 0.07 as the size of the shift increases gradually. In addition, the type-I error rates of the CS chart are similar in spite of the different number of PCs. Tables 3.4 - 3.7 present the simulation results of OC Models (b) and (c). The type-I error rates are similar to that of Model (a).

Tables A.1 - A.3 in Appendix A.1 give the proportion of the total variation explained by K PCs for $K = 1, \ldots, 4$. According to the principle of parsimoniousness in choosing K, one should choose the minimum number of the PCs for which the total variation explained has reached a prespecified satisfactory level. If we set

the satisfactory level at 95%, then for Model (a), one may select $K = 2$ for most of cases under $\delta_1 = 0$ or $\delta_2 = 0$. However, $K = 2$ does not perform the best in terms of the type-II error rates for the cases under $\delta_1 = 0$. Moreover, choosing larger K does not necessarily give a better result for type-II error rates. The reason is: if we include some additional PCs that are more than needed, the superfluous PCs would dilute the significance of the meaningful PCs in the charting statistic T_0^2; and since the chosen K usually is not large, a few superfluous PC scores would reduce the power of the T_0^2 part of the CS chart significantly. Meanwhile, taking away few of the PCs from the complementary space has a little effect to the T_1^2 statistic since the number of the "non-effective" PCs is often large. On the other hand, if we choose a K too small such that the primary space is not large enough to approximate the IC profiles well then the power of the CS chart would be reduced. Therefore, choosing an appropriate K is an important issue. Since Phase I analysis is an off-line operation, practitioners can try various values of K and inspect the OC cases detected carefully, then pick the one that gives the most reasonable results. For the example of Model (a), one may choose $K = 2$ or 3 based on the parsimoniousness principle, but can also try $K = 2$, 3 or 4 to see which one is better.

For type-II error rates, the CS chart outperforms the Hotelling's T^2 chart in most of the OC conditions regardless of the chosen K when the OC cases are generated from Model (a). That is because the charting statistic of the Hotelling's T^2 chart puts equal weights on all the design points. Therefore, it detects the shift in a particular direction less efficiently. That is, the Hotelling's T^2 chart sacrifices the detecting power to trade for a comprehensive monitoring on shifts in all dimensions. On the other hand, the CS chart puts more weights on the effective PCs thus it combines the information in a more efficient way if the shift is mainly in the primary space.

Consider the OC cases from Model (b), when the shift is in the complementary space, choosing too small K, say 2, gives the CS chart a poor ability in detecting

Table 3.5: The type-I and type-II error rates and their standard errors (in parentheses) of OC Model (b) for $\alpha = 0.05$ and $\delta_1 = 0$.

	p_I					p_{II}				
δ_2	T^2	CS(2)	CS(3)	CS(4)	CS(5)	T^2	CS(2)	CS(3)	CS(4)	CS(5)
0.875	0.0723	0.0719	0.0682	0.0665	0.0661	0.8497	0.8756	0.8769	**0.8271**	0.8361
	(.0005)	(.0005)	(.0005)	(.0005)	(.0005)	(.0016)	(.0015)	(.0015)	(.0019)	(.0018)
1.750	0.0719	0.0718	0.0686	0.0666	0.0661	0.7832	0.8207	0.8205	**0.7359**	0.7506
	(.0005)	(.0005)	(.0005)	(.0005)	(.0004)	(.0020)	(.0019)	(.0018)	(.0021)	(.0021)
2.6250	0.0714	0.0708	0.0683	0.0665	0.0663	0.7251	0.7731	0.7700	**0.6629**	0.6805
	(.0005)	(.0005)	(.0005)	(.0004)	(.0004)	(.0023)	(.0021)	(.0022)	(.0023)	(.0023)
3.500	0.0719	0.0717	0.0684	0.0664	0.0666	0.6740	0.7282	0.7257	**0.6048**	0.6212
	(.0005)	(.0005)	(.0005)	(.0005)	(.0005)	(.0024)	(.0023)	(.0024)	(.0024)	(.0024)
4.375	0.0718	0.0718	0.0686	0.0677	0.0674	0.6290	0.6862	0.6819	**0.5562**	0.5747
	(.0005)	(.0005)	(.0005)	(.0004)	(.0005)	(.0025)	(.0025)	(.0025)	(.0025)	(.0024)
5.250	0.0721	0.0712	0.0684	0.0676	0.0676	0.5931	0.6501	0.6463	**0.5247**	0.5390
	(.0005)	(.0005)	(.0005)	(.0005)	(.0005)	(.0025)	(.0024)	(.0025)	(.0025)	(.0025)
6.125	0.0721	0.0717	0.0693	0.0684	0.0675	0.5611	0.6187	0.6103	**0.4919**	0.5068
	(.0005)	(.0005)	(.0005)	(.0005)	(.0004)	(.0026)	(.0025)	(.0026)	(.0025)	(.0025)
7.000	0.0724	0.0717	0.0695	0.0686	0.0679	0.5317	0.5875	0.5798	**0.4665**	0.4819
	(.0005)	(.0005)	(.0005)	(.0005)	(.0005)	(.0026)	(.0026)	(.0027)	(.0023)	(.0024)

OC observations. However, it can be improved through choosing an appropriate K (choose $K \geq 4$ in the case of $\delta_1 = 0$ or $\delta_2 = 0$).

Consider the Model (c), the CS chart performs better than the Hotelling's T^2 chart for the mean and variance-covariance matrix shifts when choosing $K = 2 \sim 5$ and $K \geq 4$, respectively. Since the shift is in both of the primary and complementary spaces, the CS chart is quite sensitive in detecting the OC observations.

To sum up, generally, for a given type-I error rate, one can obtain a better results in terms of type-II error rate than the Hotelling's T^2 chart by using the CS chart if the number of effective PCs is selected appropriately in Phase I applications.

Table 3.6: The type-I and type-II error rates and their standard errors (in parentheses) of OC Model (c) for $\alpha = 0.05$ and $\delta_2 = 0$.

	p_I					p_{II}				
δ_1	T^2	CS(2)	CS(3)	CS(4)	CS(5)	T^2	CS(2)	CS(3)	CS(4)	CS(5)
0.625	0.0736	0.0716	0.0684	0.0675	0.0668	0.9026	0.9009	0.9084	**0.8993**	0.9055
	(.0005)	(.0005)	(.0005)	(.0005)	(.0004)	(.0014)	(.0014)	(.0014)	(.0014)	(.0014)
1.250	0.0704	0.0666	0.0655	0.0634	0.0635	0.8539	0.8303	0.8526	**0.8089**	0.8298
	(.0005)	(.0005)	(.0004)	(.0004)	(.0004)	(.0018)	(.0019)	(.0018)	(.0022)	(.0021)
1.875	0.0675	0.0620	0.0614	0.0624	0.0618	0.7836	0.7098	0.7599	**0.6023**	0.6730
	(.0005)	(.0004)	(.0004)	(.0004)	(.0004)	(.0023)	(.0027)	(.0024)	(.0040)	(.0034)
2.500	0.0669	0.0629	0.0601	0.0701	0.0683	0.6872	0.4935	0.6058	**0.1562**	0.2440
	(.0005)	(.0005)	(.0004)	(.0005)	(.0005)	(.0039)	(.0041)	(.0038)	(.0033)	(.0052)
3.125	0.0685	0.0704	0.0652	0.0761	0.0747	0.4992	0.1580	0.2886	**0.0148**	0.0197
	(.0005)	(.0005)	(.0005)	(.0005)	(.0005)	(.0080)	(.0038)	(.0054)	(.0006)	(.0007)
3.750	0.0752	0.0764	0.0742	0.0760	0.0743	0.2125	0.0103	0.0194	**0.0007**	0.0010
	(.0006)	(.0005)	(.0005)	(.0005)	(.0005)	(.0098)	(.0006)	(.0013)	(.0001)	(.0001)
4.375	0.0774	0.0775	0.0755	0.0764	0.0741	0.0928	0.0006	0.0008	**0.0000**	0.0000
	(.0005)	(.0005)	(.0005)	(.0005)	(.0005)	(.0074)	(.0001)	(.0001)	(.0000)	(.0000)
5.000	0.0783	0.0778	0.0756	0.0759	0.0742	0.0518	0.0000	0.0000	**0.0000**	0.0000
	(.0005)	(.0005)	(.0005)	(.0005)	(.0005)	(.0059)	(.0000)	(.0000)	(.0000)	(.0000)

3.3.3 Phase II Application

We now investigate the performance of the proposed CS and CE charts in Phase II applications. For comparison, the multivariate EWMA (MEWMA) chart (Lowry et al., 1992) applying to the discretized smoothed profiles is considered. Suppose that each of the incoming profiles $\boldsymbol{y}_i = (y_{i1}, \ldots, y_{ip})'$ follows $N_p(\boldsymbol{\mu}_0, \boldsymbol{\Sigma}_0)$ and $(\boldsymbol{\mu}_0, \boldsymbol{\Sigma}_0)$ are assumed known. Then the charting statistic of the MEWMA control chart is defined as

$$T^2_{M,i} = \frac{2-\lambda}{\lambda} \boldsymbol{Z}_i' \boldsymbol{\Sigma}_0^{-1} \boldsymbol{Z}_i,$$

Table 3.7: The type-I and type-II error rates and their standard errors (in parentheses) of OC Model (c) for $\alpha = 0.05$ and $\delta_1 = 0$.

	p_I					p_{II}				
δ_2	T^2	CS(2)	CS(3)	CS(4)	CS(5)	T^2	CS(2)	CS(3)	CS(4)	CS(5)
0.875	0.0721	0.0694	0.0670	0.0665	0.0662	0.8505	0.8455	0.8609	**0.8189**	0.8311
	(.0005)	(.0005)	(.0005)	(.0005)	(.0004)	(.0017)	(.0017)	(.0016)	(.0019)	(.0018)
1.750	0.0720	0.0687	0.0666	0.0671	0.0663	0.7788	0.7695	0.7915	**0.7171**	0.7348
	(.0005)	(.0005)	(.0004)	(.0005)	(.0004)	(.0021)	(.0020)	(.0019)	(.0022)	(.0021)
2.625	0.0714	0.0680	0.0660	0.0664	0.0661	0.7272	0.7148	0.7412	**0.6539**	0.6740
	(.0005)	(.0005)	(.0005)	(.0004)	(.0004)	(.0023)	(.0022)	(.0022)	(.0024)	(.0024)
3.500	0.0722	0.0689	0.0659	0.0671	0.0664	0.6746	0.6633	0.6906	**0.5905**	0.6126
	(.0005)	(.0005)	(.0004)	(.0005)	(.0005)	(.0023)	(.0023)	(.0022)	(.0024)	(.0024)
4.375	0.0720	0.0686	0.0666	0.0680	0.0673	0.6260	0.6188	0.6443	**0.5445**	0.5654
	(.0005)	(.0005)	(.0004)	(.0004)	(.0005)	(.0025)	(.0024)	(.0024)	(.0024)	(.0024)
5.250	0.0723	0.0681	0.0663	0.0678	0.0674	0.5900	0.5826	0.6110	**0.5102**	0.5287
	(.0005)	(.0005)	(.0004)	(.0005)	(.0004)	(.0026)	(.0024)	(.0025)	(.0025)	(.0025)
6.125	0.0718	0.0691	0.0667	0.0687	0.0675	0.5614	0.5529	0.5828	**0.4772**	0.4957
	(.0005)	(.0005)	(.0004)	(.0005)	(.0004)	(.0026)	(.0025)	(.0025)	(.0025)	(.0026)
7.000	0.0724	0.0692	0.0666	0.0685	0.0675	0.5333	0.5267	0.5530	**0.4529**	0.4722
	(.0005)	(.0005)	(.0005)	(.0005)	(.0005)	(.0026)	(.0025)	(.0025)	(.0024)	(.0024)

where $0 < \lambda \leq 1$ is the weighting parameter and $\boldsymbol{Z}_i$ is a vector operating in a recursive form by setting $\boldsymbol{Z}_0 = \boldsymbol{\mu}_0$, and

$$\boldsymbol{Z}_i = \lambda \boldsymbol{y}_i + (1-\lambda)\boldsymbol{Z}_{i-1} \text{ for } i = 1, 2, \ldots.$$

This chart is triggered for large values of T_M^2. Note that we drop the term $1 - (1-\lambda)^{2i}$ from the regular EWMA form of the charting statistic for simplicity. We remark that, for a fair comparison, we apply the MEWMA chart to the smoothed profile data.

Moreover, a Phase II profile monitoring scheme proposed by Qiu et al. (2010) is also included in our comparative study. The authors considered the nonparametric mixed-effect (NME) model to fit the IC profiles as follows. Considering the

same model as (3.1), the authors used the following local weighted negative log likelihood:

$$WL(a,b;s,\lambda,t)=\sum_{i=1}^{t}\sum_{j=1}^{p_i}\left[y_{ij}-a-b(x_{ij}-s)\right]^2K_h(x_{ij}-s)(1-\lambda)^{t-i}/\nu^2(x_{ij}) \tag{3.14}$$

for any point $s\in[0,1]$ and present time t, where λ is a weighting parameter; and $\nu^2(x)=\gamma(x,x)+\sigma^2$ is the variance function of the response profile at x. The function (3.14) combines the local linear kernel smoothing procedure with the EWMA scheme in time through the term $(1-\lambda)^{t-i}$. Moreover, the heteroscedasticity of the observations is also considered through $\nu^2(x_{ij})$.

In order to obtain the local linear kernel estimator of $g(s)$, the authors proposed minimizing (3.14) with respect to a and b. Then the solution can be expressed as

$$\hat{g}_{t,h,\lambda}(s)=\sum_{i=1}^{t}\sum_{j=1}^{p_i}U_{ij}^{(t,h,\lambda)}(s)y_{ij}\Big/\sum_{i=1}^{t}\sum_{j=1}^{p_i}U_{ij}^{(t,h,\lambda)}(s), \tag{3.15}$$

where

$$U_{ij}^{(t,h,\lambda)}=\frac{(1-\lambda)^{t-i}K_h(x_{ij}-s)}{\nu^2(x_{ij})}\times\left[m_2^{(t,h,\lambda)}(s)-(x_{ij}-s)m_1^{(t,h,\lambda)}(s)\right],$$

$$m_l^{(t,h,\lambda)}(s)=\sum_{i=1}^{t}(1-\lambda)^{t-i}\sum_{j=1}^{p_i}(x_{ij}-s)^lK_h(x_{ij}-s)/\nu^2(x_{ij})\text{ for }l=1,2.$$

Assume g_0 is the known population mean function based on the previous knowledge and let $\xi_{ij}=y_{ij}-g_0(x_{ij})$ for each i and j, and $\hat{\xi}_{t,h,\lambda}$ be the estimator defined as (3.15) after replacing y_{ij} by ξ_{ij}. Then, the charting statistic used for SPC is

$$T_{t,h,\lambda}=c_{t,\lambda}\int\frac{[\hat{\xi}_{t,h,\lambda}(s)]^2}{\nu^2(s)}\Gamma_1(s)ds, \tag{3.16}$$

where

$$c_{t,\lambda} = a_{t,\lambda}^2 / b_{t,\lambda},$$
$$a_{t,\lambda} = \sum_{i=1}^{t} (1-\lambda)^{t-i} p_i,$$
$$b_{t,\lambda} = \sum_{i=1}^{t} (1-\lambda)^{2(t-i)} p_i,$$

and Γ_1 is some prespecified probability density function.

In practical use, the discretized version of the testing statistical quantity

$$T_{t,h,\lambda} \approx \frac{c_{t,\lambda}}{n_0} \sum_{k=1}^{n_0} \frac{[\hat{\xi}_{t,h,\lambda}(s_k)]^2}{\nu^2(s_k)},$$

where $\{s_k, k = 1, \ldots, n_0\}$ are n_0 i.i.d. random variates generated from the p.d.f. Γ_1. An OC signal is triggered when the value of $T_{t,h,\lambda}$ exceeds the control limit. The control limit is searched for by the resampling algorithm presented in the paper. This chart is referred to as the mixed-effects nonparametric profile control (MENPC) chart hereafter.

Without imposing any distribution assumptions on the model, the methodology of MENPC scheme is distribution-free. We include the MENPC chart in our comparative study because it incorporates the within-profile correlation as what we study in this dissertation, a situation seldom considered in the literature. Note that the estimation obtained from the equation (3.15) incorporates both smoothing and EWMA schemes, thus the MENPC chart is directly applied to the raw profile data in the following simulation studies.

Consider again the example that the IC profiles are from $N_p(\boldsymbol{\mu}, \boldsymbol{\Sigma})$, in which $\boldsymbol{\mu}$ and $\boldsymbol{\Sigma}$ are given in (3.12) and (3.13), respectively. Let $\boldsymbol{S}$ be the local linear smoother, in which the bandwidth $h = 0.357$ is chosen by the GCV method. Then the variance-covariance matrix of the smoothed IC profile is $\boldsymbol{S}\boldsymbol{\Sigma}\boldsymbol{S}'$. Denote $\boldsymbol{\Sigma}_0 = \boldsymbol{S}\boldsymbol{\Sigma}\boldsymbol{S}'$. Apply the eigen-decomposition to $\boldsymbol{\Sigma}_0$ to obtain the corresponding eigenvalues and eigenvectors, $(\lambda_1, \boldsymbol{\nu}_1), \ldots, (\lambda_p, \boldsymbol{\nu}_p)$. It is found that the first three eigenvectors explain 97.32% of the total variation, so we choose $K = 3$ in the CS

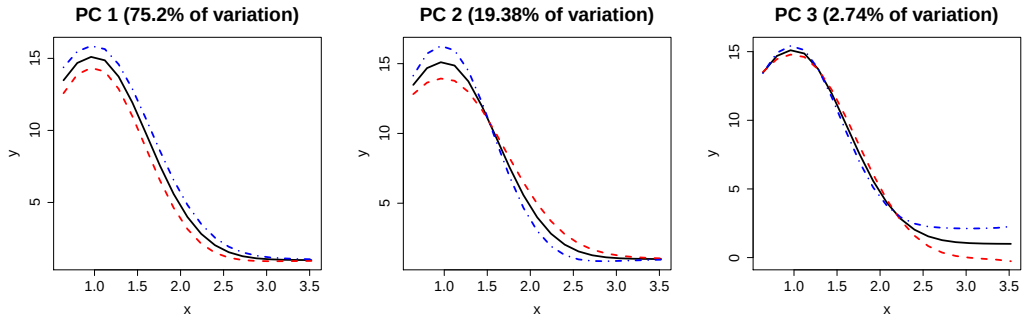

Figure 3.3: The effect-visualizing plots of the first three PCs, $\boldsymbol{\mu}_0 \pm 3\boldsymbol{\nu}_r, r = 1, 2, 3$.

and CE control charts. To visualize the effects of the PCs, Ramsay and Silverman (2005) proposed a technique that plots $\boldsymbol{\mu} \pm c\boldsymbol{\nu}_r$, where c is a suitable multiple. Figure 3.3 presents the plots of the first three PCs. From the plots, we can observe that 75.2% of the total variation are in the vertical level shifts among profiles (excluding the tail area), which is captured by the first PC; the second PC (19.38%) explains mainly the various declining rates among the profiles, and the third PC (2.74%) captures the variation in the area after $x = 2.24$.

The performance of control charts in Phase II applications are usually evaluated through the ARL. For a good control chart, not only the IC ARL, denoted as ARL_0, should be controlled at a nominal value, one would like to have the OC ARL as small as possible meaning that an OC signal needs to be flagged as soon as possible when the process is out of control.

In this simulation study, the ARL_0 is set at 370. Then the control limits of the CS chart are chosen as $\chi^2_{3,\alpha'}$ and $\chi^2_{16,\alpha'}$ for T_0^2 and T_1^2 statistics, respectively, where $\alpha' = 1 - \sqrt{1 - 1/370}$. In order to compare the performance of the charts involving EWMA, the weight parameter λ is set at 0.2. For the control limits of the CE chart, the Markovian approach (see Section 3.2.2) is applied to calculate the IC ARL and used to tune the control limits such that the IC ARL of the CE chart achieves 370. To get this, the parameters γ_0 and γ_1 in equations (3.9) and (3.10) are then chosen to be 3.783 and 3.25, respectively, for which the IC ARLs of T_0^2 and T_1^2 EWMA chart are 735. The control limits of the MEWMA and MENPC

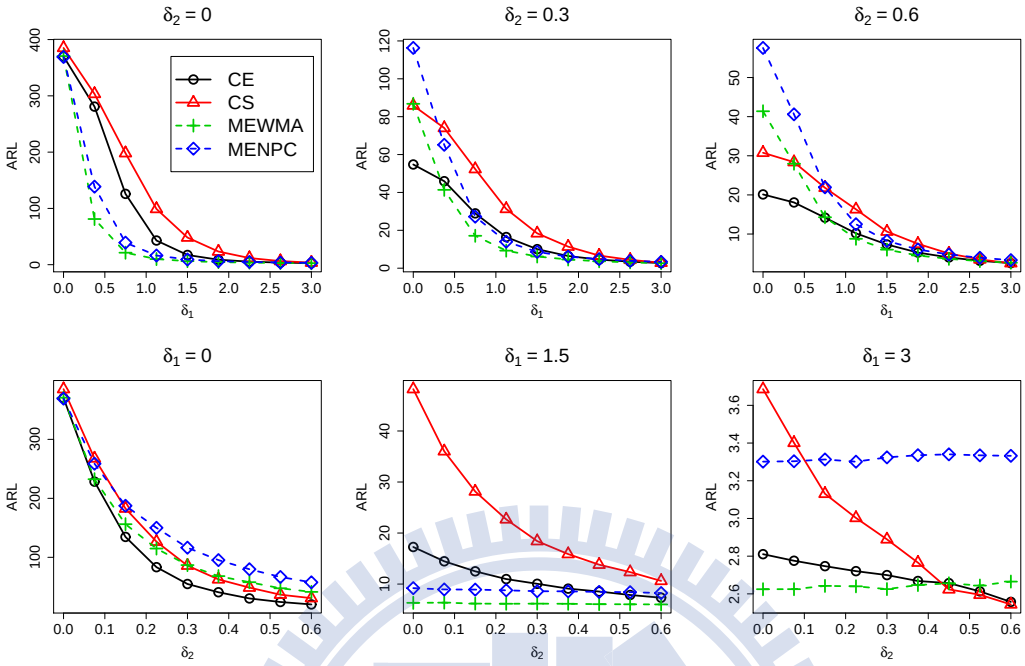

Figure 3.4: ARL comparison among the CE, CS, MEWMA, and MENPC charts under Model (a) for given δ_2 (top row) and δ_1 (bottom row).

charts are chosen to be 29.915 and 85.678, respectively, by simulations. All the ARL values reported in this section are averages of 10,000 replications. Moreover, as suggested by Hawkins and Olwell (1998), we focus on the steady-state OC ARL of a chart, and assume that shifts occur right after time point $t = 30$. When computing the OC ARL, any signals occur before 30 will be ignored.

Comparing the performances between the CS and CE charts first. The CE chart outperforms the CS chart in most of the OC conditions except some extreme OC conditions (e.g. given $\delta_1 = 3$ in Models (b) and (c)). It matches our intuition because the Shewhart-type control charts are less efficient than their EWMA versions for small to moderate shifts of process parameters but would be more powerful for large shifts.

Consider OC Model (a), the plots of ARLs for given δ_1 or δ_2 (size of the mean or variance-covariance shift) are shown in Figure 3.4. We can observe that the MEWMA chart performs quite well in most of cases. The CE chart is efficient in

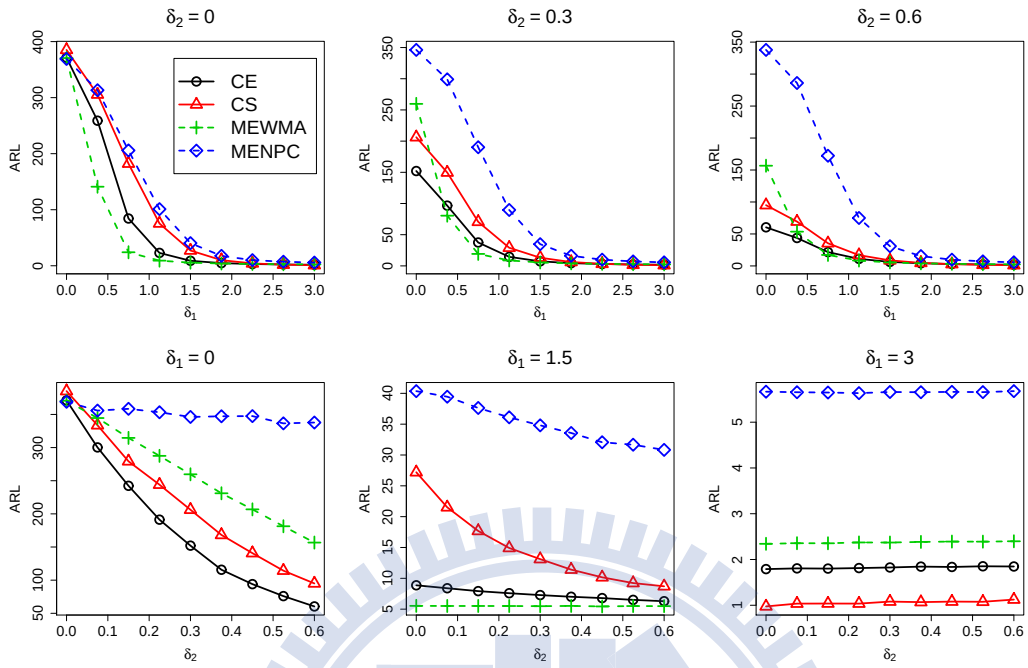

Figure 3.5: ARL comparison among the CE, CS, MEWMA, and MENPC charts under Model (b) for given δ_2 (top row) and δ_1 (bottom row).

detecting shifts in the variance-covariance matrix ($\delta_2 \neq 0$) and performs the best when the shift is only on the variance-covariance matrix ($\delta_1 = 0$, $\delta_2 \neq 0$). The CE chart is not as efficient as the MEWMA chart for moderate to large shifts on mean when δ_2 is given (see upper panel in Figure 3.4) since the shift is in the primary space and only the T_0^2 part of the charting statistics works in this case. However, when the shift size gets large, especially in the variance-covariance matrix, the CE chart outperforms the MEWMA chart. Although the MENPC chart is a distribution-free method, it is quite comparative with the others for most cases, especially in the case that only the mean shifts but not the variance-covariance matrix (i.e., $\delta_1 \neq 0$, $\delta_2 = 0$). However, the charting statistic of MENPC considers only the variance of profiles at the design points instead of the whole covariance structure, so it is not such sensitive even for large shifts in the variance-covariance matrix.

Figure 3.5 shows the values of ARL under OC Model (b). The performance

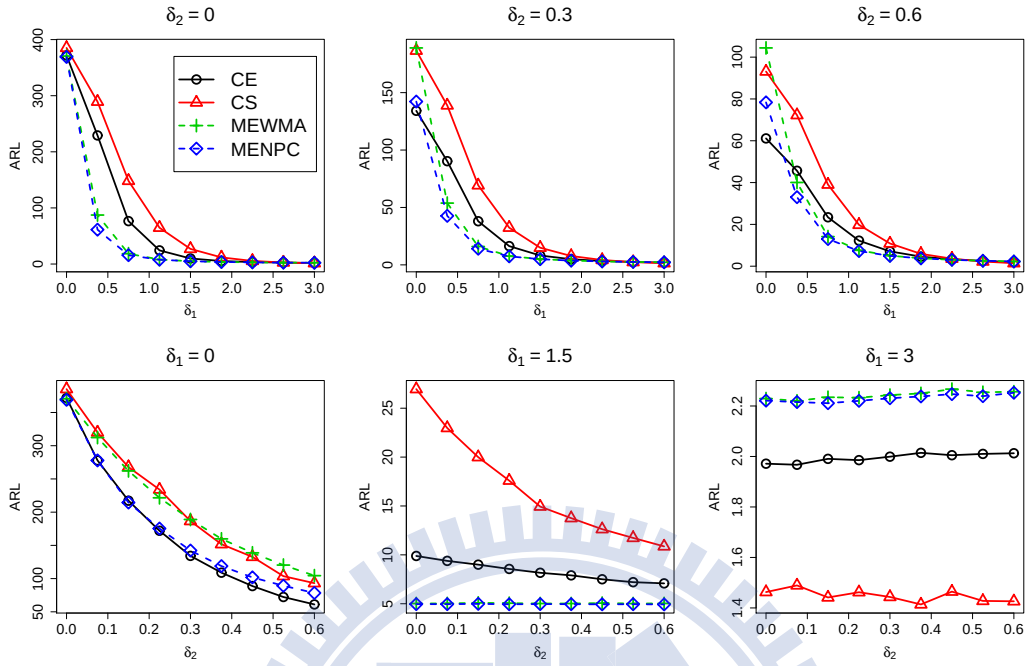

Figure 3.6: ARL comparison among the CE, CS, MEWMA, and MENPC charts under Model (c) for given δ_2 (top row) and δ_1 (bottom row).

of the MEWMA chart outperforms the others in many cases. However, the CE chart is better than the MEWMA chart if the shift occurs only on the variance-covariance matrix. When the mean and variance-covariance matrix shift at the same time, the performances of the MEWMA and CE charts are comparative. However, under extreme cases when both the mean and variance-covariance matrix shift severely, the CE chart is more efficient in detecting OC observations. The MENPC chart is not competitive in this case, especially in detecting shifts in the variance-covariance matrix. This may be due to the facts that the MENPC chart ignores the covariance of profiles in the charting statistic and the shifts in the complementary space mainly effect the covariance structure but the variance of profiles. The CS chart is the best among the four methods under the extreme OC condition (given $\delta_1 = 3$).

Model (c) is the case when the shift is in both of the primary and complementary spaces, and Figure 3.6 presents the ARL performances of the four methods

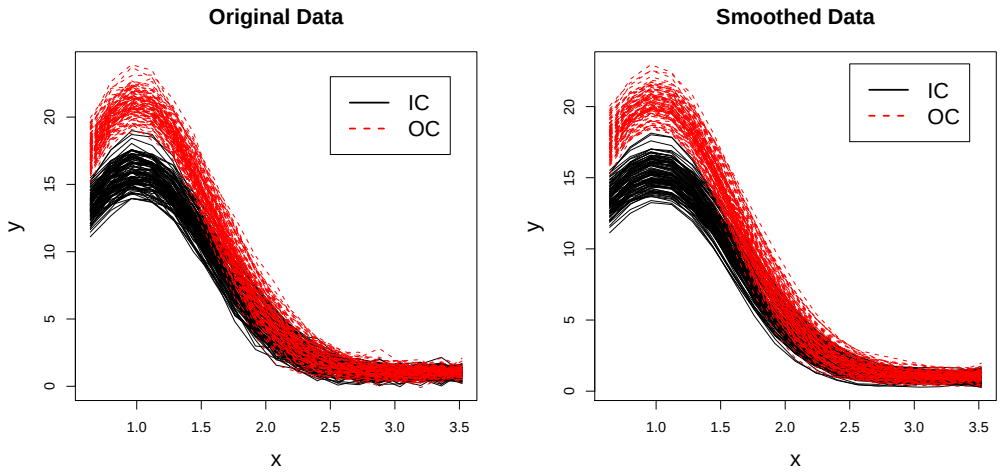

Figure 3.7: (a) Plots of the IC and OC profiles from Model (a) before (left panel) and after (right panel) smoothing.

under comparison. The results are similar to that of Model (a), but the MENPC chart is more comparable with the others. It is noted from the plot given $\delta_1 = 3$ that the CS chart becomes the most powerful one if a severe change occurs in the process; the performances of the MENPC and MEWMA charts are similar but the worst; and the CE chart performs in between.

Next, we demonstrate how the OC conditions might be diagnosed. As an example, first generate 100 IC profiles from a multivariate normal distribution with parameters $(\boldsymbol{\mu}, \boldsymbol{\Sigma})$ as in (3.12) and (3.13) and then 100 OC profiles from Model (a) with $\delta_1 = 5$ and $\delta_2 = 0$. That is, the OC condition is the scale change in the mean function. The scale change has effects on all three PCs, but the extent could be different. Figure 3.7 shows the plots of these profiles before and after smoothing. We can clearly observe that the differences between the IC and OC profiles are mostly at the first 2/3 of the profiles; in particular, the peak of the OC profiles is much higher than the IC ones.

To diagnose the OC conditions, the PC scores are explored and presented in Figure 3.8(a). The magnitude of the first two PC scores enlarges dramatically after the 100th profile, but not the third one. Therefore, it is difficult to reveal the OC

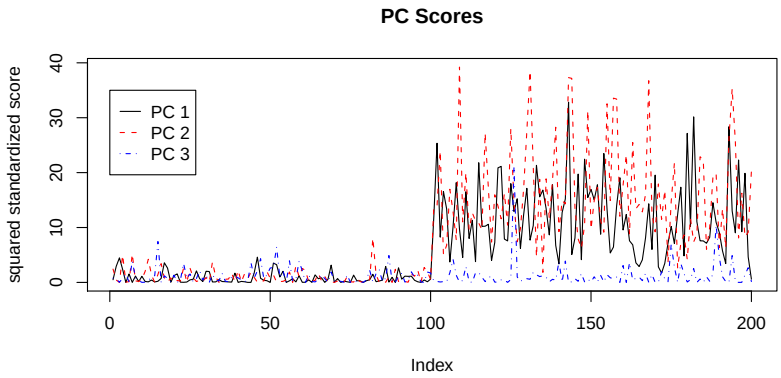

(a)

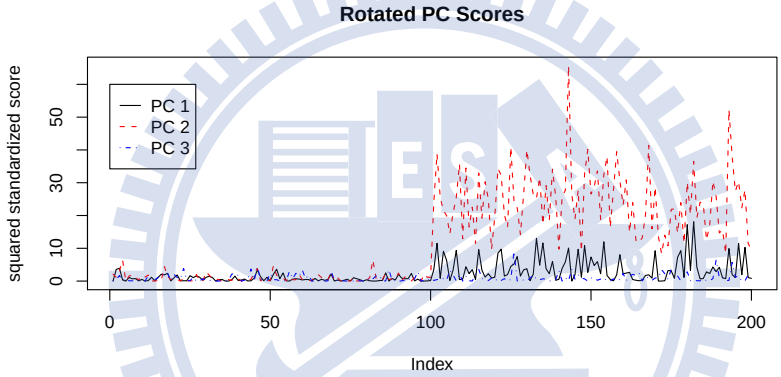

(b)

Figure 3.8: (a) The scores of the first three PCs and (b) the scores of the first three rotated PCs by VARIMAX rotation.

condition from the pattern of the regular PCs.

Denote $\boldsymbol{\nu}_1^*, \ldots, \boldsymbol{\nu}_p^*$ the rotated PCs (RPCs) found through the VARIMAX rotation of the IC profiles. Figure 3.9 shows the effect-visualizing plots of the first three RPCs after rotating. It is clearly seen that each of the three RPCs is in charge of the variation in about 1/3 of the region — the first part by the second RPC, the second part by the first RPC, and the third part by the third RPC. Figure 3.8(b) shows the RPC scores of the same 100 IC profiles and the 100 OC ones. Now, the patterns for the RPCs differentiate the effects of the three PCs

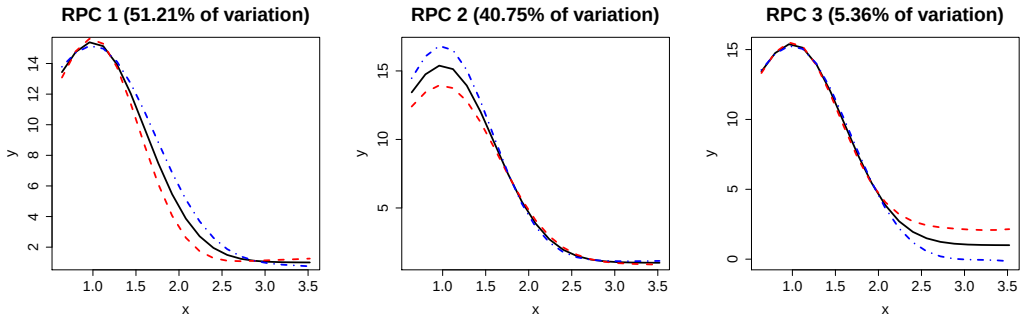

Figure 3.9: The effect-visualizing plots of the first three rotated PCs, $\boldsymbol{\mu}_0 \pm 3\boldsymbol{\nu}_r^*, r = 1, 2, 3$.

on the scale change. The second RPC scores enlarge drastically after the 100th profile, indicating that the primary change in the OC profiles is on the first part of the profile, the peak area. The VARIMAX rotation provides a great aid for practitioners to search for the assignable causes when an OC signal flags. In this case, the RPCs provide more information than the original PCs in seeking the assignable causes for the OC profiles. However, for cases, the original PCs may be more helpful than the RPCs sometimes. Thus, both the original PC and the RPC scores can be considered as diagnostic aids for OC observations.

If there are OC conditions that can not be explained by the first few effective PCs or rotated PCs (e.g., Model (b)), no unusual patterns will be observed from the first few PC scores. In those cases, it indicates that the process may already be seriously changed and the profiles are no longer suitably fitted by the effective PCs.

3.4 Real Data Application

In this section, we demonstrate our proposed monitoring schemes with a real data set. A manufacturing process of aluminum electrolytic capacitors (AEC's), which was first described in Qiu et al. (2010), is a process that transforms raw materials, such as anode and cathode aluminum foil, guiding pin, electrolyte sheet, plastic cover, aluminum shell, and plastic tube, into AEC's that are appropriate for use

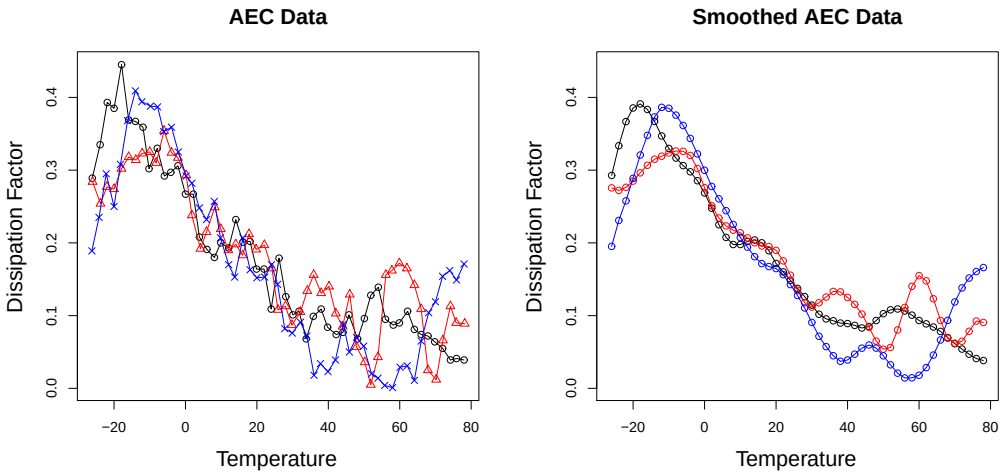

(a) (b)

Figure 3.10: The original and the smoothed profiles of the three of the AEC data.

in low-leakage circuits and are well adapted to a wide range of environmental temperatures. The whole manufacturing process consists of multiple operations, e.g., clenching, rolling, soaking, etc., and a careful quality monitoring is required before packing. The dissipation factor (DF), which is measured automatically by an electronic device, is regarded as an important characteristic in monitoring the quality of AEC's. However, the DF is affected significantly by the temperature of the environment and hence the profile of the DF as a function of temperature is a characteristic of interest regarding the quality of the AEC. To monitor the adaptability, the sampled AEC's are put in a container in which the temperature can be controlled. The temperature in the container is gradually increased from $-26°$F to $78°$F and recorded by a sensor. In this process, the measurements of DF and the corresponding temperature are taken at 53 equally-spaced time points for a total of 144 AEC profiles. Note that the actual temperature measured in a container at each time point is fluctuant but around its nominal level at each observation time. Therefore, the temperature records are different from profile to profile although the differences are small.

To cope with the non-consistent temperature recording problem and filter out

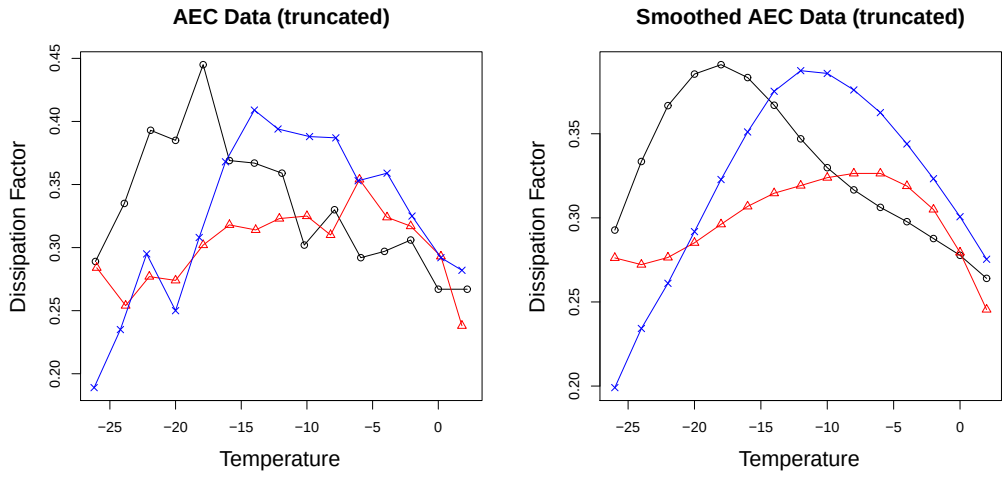

(a) (b)

Figure 3.11: The first 15 records of the three profiles and their corresponding smoothing estimates.

the noise as well, the local linear smoothing technique is applied to the data before analysis. Figure 3.10 depicts three AEC profiles and their smoothing estimates (using bandwidth $h = 6.54$ from GCV). According to the Q-Q plots of data at each set point, neither the original nor the smoothed 144 AEC profiles with 53 set points follow the multivariate normal distribution. To overcome this problem, we choose only a segment of the AEC profiles to alleviate the effect of non-normality. According to the Q-Q plots for each of the first 15 set points (not shown here) and the p-value (about 0.085) of the multivariate normality test proposed by Mardia (1970), the evidences are not strong enough to reject the normality. Therefore, the 144 profiles with 15 set points are used to demonstrate our proposed methodology. Three of the original and smoothed profiles after truncation are shown in Figure 3.11.

Qiu et al. (2010) regarded the first 96 profiles as the training data in Phase I analysis and the rest as testing data in Phase II analysis. To use the CS chart in Phase I analysis, we apply PCA to the sample covariance matrix of the first 96 smoothed profiles, which leads to choose $K = 3$ because the first three PCs

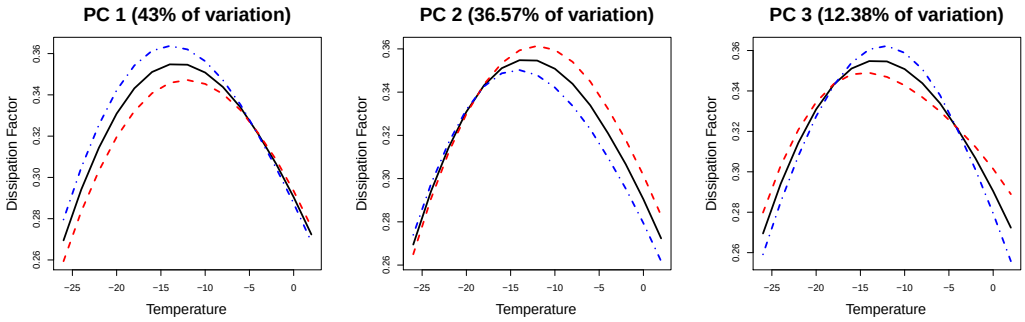

Figure 3.12: The effect-visualizing plots of the first three PCs, $\boldsymbol{\mu}_0 \pm 3\boldsymbol{\nu}_r, r = 1, 2, 3$.

explain 91.96% of the total variation. As a result, none of the profiles is regarded as an OC profile by our proposed CS chart for Phase I application. Thus all the 96 profiles are used to estimate the mean and covariance matrix for Phase II.

Let $\boldsymbol{\mu}_0$ and $\boldsymbol{\Sigma}_0$ be the sample mean vector and sample variance-covariance matrix of the 96 IC profiles (after smoothing). The effect-visualizing plots are also used to interpret the effect of the three PCs and shown in Figure 3.12. From these plots, we observe that the mean curve is mound-shaped; the first two PCs explain the variation from the temperature less than $-5°$ and greater than $-18°$, respectively; and the two crosses at temperatures $-18°$ and $-4°$ on the plot for the third PC indicate that the third PC explains the variation of the profiles in the rate of declining from the top.

Next, the rest of the 48 AEC profiles are used to demonstrate our proposed Phase II monitoring scheme. By setting $\lambda = 0.2$, the values of the T^2-type and EWMA-type statistics corresponding to T_0^2 and T_1^2 are shown in Figure 3.13. Set the ARL_0 at 200. Then the control limits in the CS chart is $\chi^2_{3,\alpha'}$ and $\chi^2_{12,\alpha'}$ for T_0^2 and T_1^2 charts, respectively, where $\alpha' = 1 - \sqrt{1 - 0.005}$. The parameters γ_0 and γ_1 in equations (3.9) and (3.10) are chosen to be 3.38 and 3.004, respectively, and the control limits of CE charts are then $L_0 = 5.76$ and $L_1 = 16.91$. From Figure 3.13(a), based on the T_0^2 statistic, the Shewhart chart detects only the 139th profile, whereas the EWMA chart regards the profiles from 114th to 125th and 139th to 144th as OC cases. For the T_1^2-based charts, Figure 3.13(b) shows

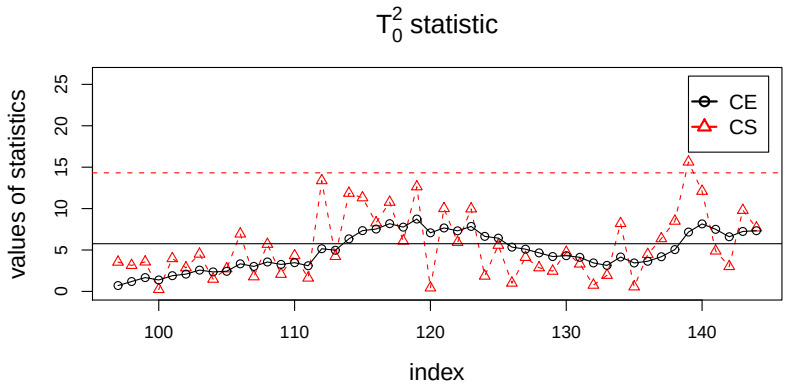

(a)

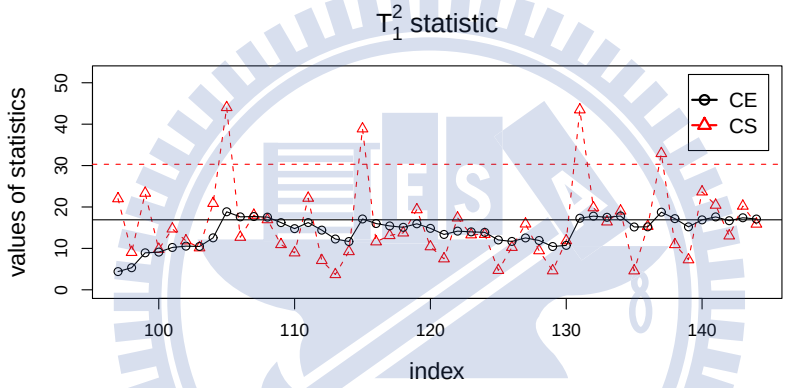

(b)

Figure 3.13: The values of the charting statistics based on T_0^2 (panel (a)) and T_1^2 (panel (b)) for the AEC data.

that the results of the two charts are fairly consistent — the 105th, 115th, 131st, and 137th profiles are detected by the Shewhart chart and a little bit more by the EWMA chart. The OC cases considered by the CS (CE) chart is the union of the OC cases claimed by the two Shewhart (EWMA) charts based on the T_0^2 and T_1^2 statistics.

Figure 3.14 shows the effect-visualizing plots with respect to the first three RPCs. From these plots, the three RPCs explain the variation in the front, middle, and end areas (with some overlaps) of the profiles, respectively. To search for the

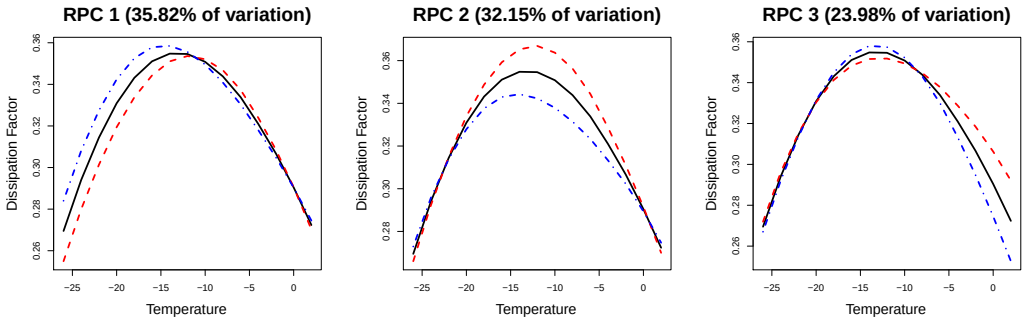

Figure 3.14: The visualized plots of the first three rotated PCs, $\boldsymbol{\mu}_0 \pm 3\boldsymbol{\nu}_r^*, r = 1, 2, 3$.

source of the process shift, one can examine the scores of the primary PCs or the RPCs for each OC case detected by the T_0^2-based charts. The plots of the scores of the first three original PCs as well as the RPCs are shown in Figure 3.15. For each OC-flagged profile, at least one of the scores is abnormally large. For example, the 115th profile, detected by both T_0^2 and T_1^2 of the CE chart and only T_1^2 of the CS chart, has a large value on the second PC score indicating the shift could be in the last 2/3 part of the profile and may be quite different from the general pattern of the IC profiles; the 139th profile, detected by both T_0^2 of the CS and CE charts, has an unusually large value on the score of the first original PC as well as the first RPC, exhibiting a pattern quite different from others at the front part of the profile; the 140th profile has a large score value on the second RPC, indicating that the change affects mainly on the middle 2/3 of the profile and it may have an unusually high or low peak. Note that a large score value appears on the first PC at point 112, but it was not signaled by either the CS or CE chart. A closer look shows that the T_0^2 statistics on both CS and CE charts are very close to the control limits. In addition, the EWMA chart exhibits an increasing trend beginning at the 112nd profile. It indicates that some OC conditions may have occurred in the process at or before the 112nd but not signaled until the 114th profile. The aforementioned OC profiles are shown in Figure 3.16 and their patterns match what we observe from the PC or RPC scores.

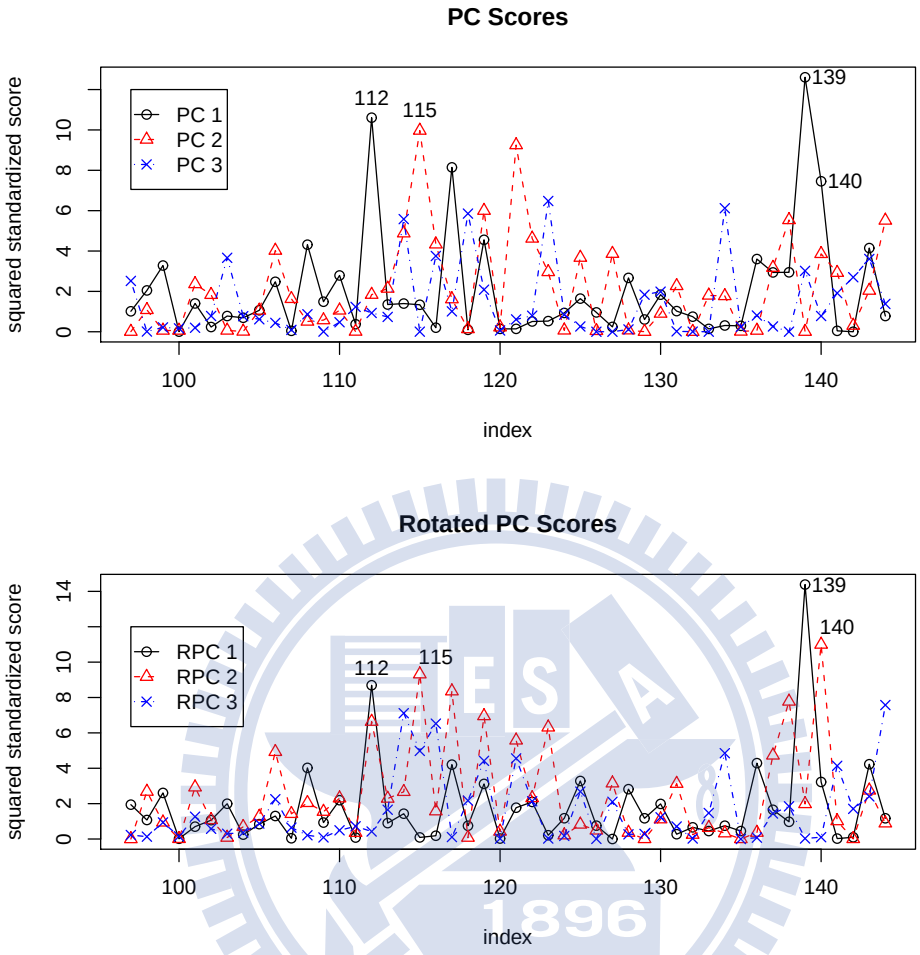

Figure 3.15: The scores of the first three rotated PCs for the AEC data.

3.5 Conclusions

In this chapter, we present a comprehensive monitoring procedure incorporating the Phase I and Phase II for profiles under Gaussian assumption. Each profile is projected onto the eigen-vectors of the variance-covariance matrix, and then two T^2-type statistics, T_0^2 and T_1^2, are used to monitor the profile. Intuitively speaking, the T_0^2 statistic is in charge of the component in the primary space that explains the most of the variation in the IC profiles, whereas the T_1^2 statistic is used to monitor the residuals. An OC signal triggered by the T_0^2 part of the control chart indicates

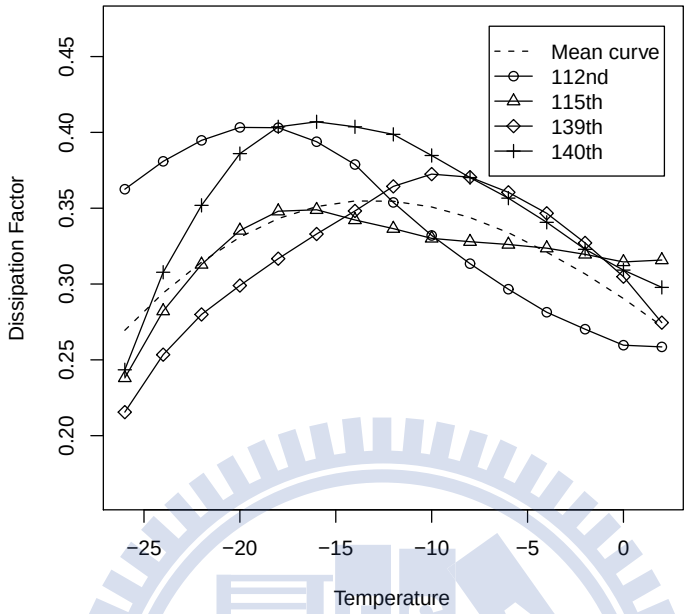

Figure 3.16: The 112nd, 115th, 139th, 140th AEC profile and the mean curve.

that the OC condition occurs in the space spanned by the first few effective PCs, whereas triggered by the T_1^2 part indicates that the OC condition occurs in an unexpected way, a more serious problem in the process. A profile is regarded as an OC case when any of the two T^2 charts signals. In order to monitor both kinds of shifts simultaneously, we consider combining the two Shewhart control charts based on the T_0^2 and T_1^2 statistics in Phase I analysis. In Phase II, in addition to the combined Shewhart chart, a combined EWMA-type control chart is also considered to enhance the power of monitoring small to moderate changes in process parameters. Some numerical studies show that our proposed charts are powerful in detecting shifts in the mean or variance-covariance matrix and perform quite well when compared with some existing monitoring schemes. In the real case study, we use a segment of the AEC data to demonstrate our proposed methods and show that the monitoring schemes can be easily implemented. Moreover, in Phase II applications, exploring the original and rotated PC scores provides an

intuitive and meaningful diagnosis on OC conditions.

The profile monitoring tools presented in this chapter are developed based on the normality assumption, which may not hold in many applications. In the next two chapters, we will develop distribution-free monitoring schemes for multivariate data and profiles, respectively.

Chapter 4

A Distribution-Free Multivariate Control Chart for Phase I Applications

In Phase I analysis, one of the most important goals is to detect and remove the OC cases from the historical data, and then the parameters needed in Phase II monitoring can be well estimated from a "clean" reference sample. To this end, it is common to connect the OC-cases-detection problem with hypothesis testing on process parameters. Since the process often is not stable yet and an OC case may arise anytime during Phase I, the Shewhart control chart is often advised instead of the EWMA chart; see Mahmoud and Woodall (2004) and Montgomery (2009).

In this chapter, we only focus on detecting observations with a significant mean shift for a multivariate process. To be free of the distribution assumption, the multivariate sign test described in Section 2.2.3 is considered to develop a robust monitoring scheme. The organization of this chapter is as follows. In Section 4.1, we elaborate our distribution-free Phase I control chart for multivariate data. A performance comparison between our proposed and some traditional methods via simulations is presented in Section 4.2. Moreover, a real-case application is

illustrated in Section 4.3. Finally, conclusions are given in Section 4.4.

4.1 Methodology

4.1.1 A Multivariate Sign-Based Control Chart

Let $\{\boldsymbol{y}_{ik}, i = 1, \ldots, m, k = 1, \ldots, n\}$ be an i.i.d. random sample consisting of m subgroups, each of size n, with a continuous p-dimensional distribution function $F(\boldsymbol{y} - \boldsymbol{\theta}_0)$, where $\boldsymbol{\theta}_0$ is the IC location parameter. An OC case is an observation having the same distribution function F but with a different location parameter; that is, $F(\boldsymbol{y}-\boldsymbol{\theta}_1)$, where $\boldsymbol{\theta}_1 \neq \boldsymbol{\theta}_0$. Analogous to the multivariate sign-based EWMA control chart proposed by Zou and Tsung (2011), we estimate the multivariate spatial median and the Tyler's transformation matrix $(\boldsymbol{\theta}, \boldsymbol{A})$ by the HR estimators, which are the solutions of the following two equations (ref. Section 2.2.4):

$$\frac{1}{mn}\sum_{i=1}^{m}\sum_{k=1}^{n} U(\boldsymbol{A}(\boldsymbol{y}_{ik} - \boldsymbol{\theta})) = \boldsymbol{0}, \tag{4.1}$$

$$\frac{1}{mn}\sum_{i=1}^{m}\sum_{k=1}^{n} U(\boldsymbol{A}(\boldsymbol{y}_{ik} - \boldsymbol{\theta}))U(\boldsymbol{A}(\boldsymbol{y}_{ik} - \boldsymbol{\theta}))' = \frac{1}{p}\boldsymbol{I}_p. \tag{4.2}$$

Denote the estimated $(\boldsymbol{\theta}, \boldsymbol{A})$ by $(\hat{\boldsymbol{\theta}}, \hat{\boldsymbol{A}})$. The corresponding sign vector of each $\boldsymbol{y}_{ik}$ is

$$\boldsymbol{u}_{ik} = U(\hat{\boldsymbol{A}}(\boldsymbol{y}_{ik} - \hat{\boldsymbol{\theta}})).$$

Then, for $i = 1, \ldots, m$, let the charting statistic be

$$Q_i = np\bar{\boldsymbol{u}}_i'\bar{\boldsymbol{u}}_i,$$

where $\bar{\boldsymbol{u}}_i = \sum_{k=1}^{n} \boldsymbol{u}_{ik}/n$. A large value of Q_i could indicate an OC signal. This chart will be referred to as the multivariate sign Shewhart (MSS) chart hereafter. The following propositions can be obtained from Randles (2000) directly.

Proposition 4.1. The statistic Q is affine invariant when $n > p(p-1)$.

Proposition 4.2. The MSS chart is distribution-free such that the type-I error rate is the same for the class of elliptical direction distributions.

Proposition 4.3. If the underlying distribution of $\boldsymbol{y}_{ik}$ is directionally symmetric about the origin, then

$$Q_i \xrightarrow{d} \chi^2_p,$$

as $n \to \infty$.

Proposition 4.1 is appealing because it ensures that the performance of the MSS chart is free of the coodinate system. The type-I error rate in Proposition 4.2 means the probability of misclassifying an IC observation as an OC case. This proposition assists us to determine the control limit of our control chart and will be discussed in the next section. Finally, Proposition 4.3 shows the limiting distribution of the Q statistic.

4.1.2 Control Limit Determination

Although Proposition 4.3 gives the asymptotic distribution of the charting statistic Q, in practice, it is impossible to have a subgroup size large enough for it to be useful in constructing a control chart. The rational subgroup concept means that the subgroup should be selected such that if assignable causes occur, the chance for differences due to these assignable cases between subgroups will be maximized, while the chance for differences within a subgroup will be minimized. However, too large a subgroup size increases the chance for assignable causes to occur within a subgroup. The subgroup size is usually fairly small, about 3 to 6. Under such circumstances, the $100(1-\alpha)\%$ percentile of χ^2_p distribution cannot be considered as the control limit for the MSS chart. On the other hand, the distribution-free property stated in Proposition 4.2 ensures that the type-I error rate remains the same for all the elliptical direction distributions. Thus, the control limit of the MSS chart can be obtained by simulating samples from a known elliptical direction

distribution. The following procedure finds the control limits by simulating samples from the standard multivariate normal distribution:

1. Set the dimension p, subgroup size n, and type-I error probability α.
2. Generate $n \times B$ samples from $N_p(\mathbf{0}, \boldsymbol{I}_p)$ for a large B.
3. Calculate the corresponding Q statistic values for each of the B subgroups.
4. Take the sample upper α quantile from the B values of Q.

The tables in Appendix A.2 list the control limits of the MSS chart for α values equal to 0.1, 0.05, 0.025, and 0.01 with various combinations of p and n by setting $B = 50,000$. The desired control limits can be easily computed by a simple computer program.

4.1.3 One-at-a-Time Procedure

One goal for Phase I analysis is to detect and remove the OC observations to obtain a reference sample of all IC observations. One would like both of the type-I and type-II error rates of a control chart to be as small as possible. Unfortunately, similar to the hypothesis testing, reducing the type-I error rate usually results in increasing the type-II error rate and vice versa. Thus, common practice is to control the type-I error rate within a preset tolerable level and then try to make the type-II errors as less frequent as possible. In SPC terminology, to construct a good control chart, one should control the false-alarm rate under a level that practitioners can bear first and then enhance the detecting power of the control chart as much as possible. Recall that the Phase I monitoring scheme is an iterative procedure: at each iteration, establish a trial control limit(s) using the current historical data set; check if any of the current data would exceed the control limit(s); if there are any, remove them all and re-establish the control limit(s) with the rest of the data; repeat the iteration until no more OC cases found; then the remaining observations are regarded as the IC samples. In our empirical experiments, by using this

conventional Phase I procedure described above, IC observations are excessively misjudged as OC; as a result, the type-I error rate cannot be held under the preset level. Shiau and Sun (2010) introduced a new strategy of Phase I procedure: instead of removing all the signaled OC observations, only the observation with the most extreme value of the charting statistic is removed at each iteration; and then like the conventional procedure, the process keeps going until all the observations left are within the control limits. This procedure is referred to as the "one-at-a-time" (OAAT) procedure. Using the $\bar{X}$-chart as a demonstration, Shiau and Sun (2010) showed that the OAAT procedure can reduce greatly the false alarm rate of a control chart when compared with the conventional procedure. We will later compare the performances between the conventional and OAAT procedures when used in our proposed control chart via simulation studies.

4.2 A Comparative Simulation Study

To evaluate the performance of the proposed MSS chart, we conduct a simulation study to compare it with some existing multivariate control charts, including the Hotelling's T^2, T^2_{MVE}, and T^2_{MCD} charts.

In Phase I applications, the traditional Hotelling's T^2 control chart is also powerful and widely used in practice. When the Hotelling's T^2 control chart is applied to a historical data set consisting of m subgroups, each of size n, the sample mean and sample variance-covariance matrix are first calculated for each subgroup individually; denoted them as $\bar{\boldsymbol{y}}_i$ and $\boldsymbol{S}_i$, $i = 1, \ldots, m$. Then the charting statistic of the Hotelling's T^2 control chart is defined as

$$T_i^2 = n(\bar{\boldsymbol{y}}_i - \bar{\bar{\boldsymbol{y}}})' \bar{\boldsymbol{S}}^{-1} (\bar{\boldsymbol{y}}_i - \bar{\bar{\boldsymbol{y}}}),$$

where $\bar{\bar{\boldsymbol{y}}} = \mathbf{AVE}\{\bar{\boldsymbol{y}}_i\}$ and $\bar{\boldsymbol{S}} = \mathbf{AVE}\{\boldsymbol{S}_i\}$. Preset the tolerable false alarm rate at α. A subgroup would be regarded as OC if

$$T_i^2 > \frac{p(m-1)(n-1)}{mn-m-p+1} F_{p,mn-m-p+1}(\alpha), \tag{4.3}$$

where $F_{p,mn-m-p+1}(\alpha)$ is the upper α quantile of the F distribution with degrees of freedom p and $mn - m - p + 1$.

However, since the Hotelling's T^2 chart is developed under normality assumption, the type-I error rate may not be controlled at the nominal level if it is used to monitor a non-gaussian process. In addition, the estimators used in Hotelling's T^2 statistic, the sample mean and sample variance-covariance matrix, would be severely affected by OC cases. To be more robust, Jensen et al. (2007) considered two high breakdown estimation methods, the MVE and MCD methods, in constructing their control charts.

The MVE and MCD methods, which were first proposed by Rousseeuw (1984), provide robust estimators for the location and scatter matrix of data with a high breakdown point. The breakdown point refers to the minimum proportion of the OC observations that would contaminate the estimator severe enough that it becomes meaningless (Rousseeuw and Leroy, 1987). That is, the breakdown point is the percentage of "bad" data that would "break down" the estimator to a state that it is no longer meaningful. Here, the "good" and "bad" data are referred to the majority and minority of the data, respectively. Therefore, the highest breakdown point would be 50%. A high breakdown estimator for the location or dispersion can be obtained by using suitably selected the "good" observations from the data set, say, by the MVE or MCD method.

The MVE procedure seeks the ellipsoid with the minimum volume that contains the subset of at least a certain number, say h, of data points. Then the location estimator is defined as the geometrical center of the ellipsoid and the scatter estimator is the ellipsoid itself multiplied by an appropriate constant for consistency. The size of the chosen subset h is sometimes called the "halfset" since it is usually selected to be more than half of the data points. The MCD method considers the subset for which the covariance matrix has the minimum determinant. The idea of MCD is intuitive: since a small value of determinant leads to small eigenvalues and hence suggests that the data are near linearly dependent; and a near linear

dependency of data makes similar observations to cluster and hence forms a group of data suitable for estimating parameters. Then the MCD estimators correspond to the sample mean and sample variance-covariance matrix of a specific halfset. To achieve the highest breakdown point in both of the estimators, the subset size h is often selected to be $(m+p+1)/2$ (Lopuhaa and Rousseeuw, 1991). The ideas of the MVE and MCD procedures are quite simple, but the computation can be very difficult because the number of possible subsets with size h increases vastly in m and p. For example, for a sample with $m = 20$ and $p = 3$, $h = (20+3+1)/2 = 12$ and there are total $C_{12}^{20} = 125,970$ possible subsets to be considered. To overcome this difficulty, Rousseeuw and Leroy (1987) proposed an algorithm to approximate the MVE estimator and Rousseeuw and van Driessen (1999) proposed the so-called FAST-MCD algorithm for the MCD estimator. Both algorithms are widely used for finding MVE and MCD estimators, and have been implemented in statistical softwares, such as S-plus and SAS, etc.

Jensen et al. (2007) incorporated the ideas of MVE and MCD estimators with the SPC in Phase I monitoring. For each profile $\boldsymbol{y}_i$, the authors defined the "robust T^2 statistics" analogous to the Hotelling's T^2 statistic as

$$T^2_{MVE,i} = (\boldsymbol{y}_i - \hat{\boldsymbol{y}}_{MVE})' \boldsymbol{S}^{-1}_{MVE} (\boldsymbol{y}_i - \hat{\boldsymbol{y}}_{MVE}),$$
$$T^2_{MCD,i} = (\boldsymbol{y}_i - \hat{\boldsymbol{y}}_{MCD})' \boldsymbol{S}^{-1}_{MCD} (\boldsymbol{y}_i - \hat{\boldsymbol{y}}_{MCD}),$$

where $(\hat{\boldsymbol{y}}_{MVE}, \boldsymbol{S}_{MVE})$ and $(\hat{\boldsymbol{y}}_{MCD}, \boldsymbol{S}_{MCD})$ denote the MVE and MCD estimators, respectively, for the mean and variance-covariance matrix. Note that the T^2_{MVE} and T^2_{MCD} control charts are individual charts. The normality of the observations was assumed in their methodology, thus the control limits of the T^2_{MVE} and T^2_{MCD} control charts can be found via simulation. Jensen et al. (2007) considered the signal probability, the probability of at least one observation being detected by the control chart, as the performance measure. Thus, for a historical data set, it only needs to check whether the maximum value of the charting statistics exceeds the control limit or not. To control the signal probability at 5%, one can generate a

large number of data sets, say M, with size m from the p-variate standard normal distribution, record the maximum value of the charting statistics for each of the M data sets, then use the 95% percentile of the M maximum values as the control limit.

For the performance measures in our Phase I studies, we prefer the type-I and type-II error rates (ref. Section 3.1.3) to the signal probability. Using the control limits listed in Jensen et al. (2007) results in a smaller type-I error rate than the nominal α value. Therefore, for a fair comparison between the control charts, the control limits used in what follows are selected such that the T^2_{MVE} and T^2_{MCD} charts would achieve the nominal type-I error rate under normal assumption. In addition, the T^2_{MVE} and T^2_{MCD} charts were developed for individual observations whereas the MSS chart is for subgroups. Thus, we apply the T^2_{MVE} and T^2_{MCD} charts on the mean vectors of each subgroup.

To compare the robustness and power between the candidates, we consider p-variate random vectors from the following models:

(a) multivariate normal distribution, denoted as $N_p(\mathbf{0}, \mathbf{\Sigma})$,

(b) multivariate t distribution with degrees of freedom ν, denoted as $t_p(\nu)$,

(c) multivariate Gamma distribution with shape parameter ξ and scale parameter 1, denoted as $\text{Gam}_p(\xi)$.

The same definitions of multivariate t and Gamma distributions in Stoumbos and Sullivan (2002) are followed and briefly described as follows. Let $\boldsymbol{x} \sim N_p(\mathbf{0}, \mathbf{\Sigma})$, $R \sim \chi^2_\nu$ and $\boldsymbol{x}$ and R are independent. Then the multivariate t random vector is defined as $\boldsymbol{x}/\sqrt{R/\nu}$. The multivariate Gamma random vector has the form of diagonal$\{\boldsymbol{X'X}\}/2$, where $\boldsymbol{X}$ is a $\xi \times p$ data matrix with each of the ξ rows following $N_p(\mathbf{0}, \mathbf{\Sigma})$ and diagonal$\{\cdot\}$ denotes the vector of the diagonal elements of a matrix. Note that the shape parameter ξ in the multivariate Gamma distribution should be an integer. The multivariate t and multivariate Gamma distributions

Table 4.1: The p_I and p_{II} and their standard errors (in parentheses) for Model (a).

	p_I				p_{II}			
δ	MSS	T^2	T^2_{MVE}	T^2_{MCD}	MSS	T^2	T^2_{MVE}	T^2_{MCD}
0.000	0.0509	0.0531	0.0497	0.0496	-	-	-	-
	(.0003)	(.0008)	(.0011)	(.0016)	-	-	-	-
0.375	0.0514	0.0547	0.0472	0.0482	0.9173	0.9011	0.9154	0.9170
	(.0003)	(.0008)	(.0011)	(.0018)	(.0013)	(.0030)	(.0030)	(.0035)
0.750	0.0523	0.0564	0.0425	0.0445	0.7971	0.7011	0.7840	0.7997
	(.0003)	(.0008)	(.0010)	(.0017)	(.0018)	(.0050)	(.0052)	(.0057)
1.125	0.0551	0.0610	0.0420	0.0450	0.5620	0.3586	0.5297	0.5411
	(.0003)	(.0008)	(.0010)	(.0016)	(.0024)	(.0054)	(.0068)	(.0074)
1.500	0.0585	0.0657	0.0466	0.0534	0.2757	0.1039	0.2392	0.2510
	(.0003)	(.0009)	(.0011)	(.0020)	(.0021)	(.0033)	(.0051)	(.0055)
1.875	0.0606	0.0733	0.0491	0.0578	0.0934	0.0151	0.1151	0.1197
	(.0004)	(.0009)	(.0011)	(.0021)	(.0014)	(.0013)	(.0021)	(.0023)
2.250	0.0627	0.0783	0.0477	0.0590	0.0209	0.0008	0.0917	0.0907
	(.0004)	(.0009)	(.0011)	(.0021)	(.0007)	(.0003)	(.0011)	(.0011)
2.625	0.0636	0.0888	0.0490	0.0582	0.0039	0.0001	0.0869	0.0854
	(.0004)	(.0010)	(.0011)	(.0021)	(.0003)	(.0001)	(.0011)	(.0011)
3.000	0.0639	0.0976	0.0493	0.0577	0.0006	0.0000	0.0819	0.0827
	(.0004)	(.0010)	(.0012)	(.0020)	(.0001)	(.0000)	(.0012)	(.0012)

represent the heavy-tailed and skewed distributions, respectively. More details on the multivariate t and multivariate gamma distributions can be found in the appendix of Stoumbos and Sullivan (2002). In the following simulation studies, the variance-covariance matrix used in Models (a) - (c) is set as $\mathbf{\Sigma} = [\sigma_{ij}]$, where $\sigma_{ij} = 0.5^{|i-j|}$, $i, j = 1, \ldots, p$, and $\nu = \xi = 3$.

Let $\alpha = 0.05$ and dimension $p = 3$. Each data set consists of 90 IC and 10 OC subgroups, each of size $n = 5$. The OC observations are generated from the same models as the IC ones except that the first component is shifted by δ, i.e., $\boldsymbol{y}_i + \delta \boldsymbol{e}_1$, where $\boldsymbol{e}_1 = (1, 0, \ldots, 0)'$. As for the control limits, select 7.3357 for the MSS chart

Table 4.2: The p_I and p_{II} and their standard errors (in parentheses) for Model (b).

	p_I				p_{II}(modified)			
δ	MSS	T^2	T^2_{MVE}	T^2_{MCD}	MSS	T^2	T^2_{MVE}	T^2_{MCD}
0.000	0.0510	0.1170	0.1444	0.1481	-	-	-	-
	(.0003)	(.0012)	(.0018)	(.0027)	-	-	-	-
0.375	0.0511	0.1149	0.1399	0.1420	0.9228	0.9457	0.9439	0.9465
	(.0003)	(.0013)	(.0017)	(.0025)	(.0012)	(.0023)	(.0023)	(.0023)
0.750	0.0528	0.1195	0.1356	0.1332	0.8261	0.9201	0.9298	0.9333
	(.0003)	(.0012)	(.0018)	(.0023)	(.0018)	(.0028)	(.0027)	(.0027)
1.125	0.0537	0.1180	0.1296	0.1284	0.6619	0.8708	0.8971	0.9001
	(.0003)	(.0012)	(.0017)	(.0023)	(.0023)	(.0035)	(.0036)	(.0037)
1.500	0.0558	0.1172	0.1301	0.1355	0.4630	0.7424	0.8216	0.8196
	(.0003)	(.0012)	(.0017)	(.0027)	(.0025)	(.0051)	(.0053)	(.0056)
1.875	0.0588	0.1189	0.1349	0.1453	0.2882	0.5192	0.6447	0.6357
	(.0003)	(.0012)	(.0017)	(.0028)	(.0023)	(.0064)	(.0076)	(.0075)
2.250	0.0606	0.1199	0.1393	0.1512	0.1755	0.2659	0.4052	0.4155
	(.0003)	(.0012)	(.0018)	(.0029)	(.0018)	(.0058)	(.0077)	(.0076)
2.625	0.0610	0.1176	0.1420	0.1532	0.1086	0.1035	0.2245	0.2345
	(.0004)	(.0012)	(.0018)	(.0029)	(.0015)	(.0039)	(.0051)	(.0054)
3.000	0.0622	0.1229	0.1409	0.1535	0.0677	0.0309	0.1369	0.1441
	(.0004)	(.0012)	(.0018)	(.0029)	(.0011)	(.0020)	(.0027)	(.0029)

from Table A.4 in the Appendix A.2, 7.8202 for the Hotelling's T^2 control chart from the control limit in (4.3), and 9.4961 and 12.25 for the T^2_{MVE} and T^2_{MCD} charts obtained via simulation, respectively. The listed type-I and type-II error rates are obtained with 1,000 replications.

The conventional Phase I procedure is considered first because the OAAT procedure is more time-consuming, especially for the MVE- and MCD-based methodologies. The type-I and type-II error rates and their standard errors (in parentheses) for OC Models (a) - (c) are summarized in Tables 4.1 - 4.3, respectively.

Look at the type-I error rates first. Under Model (a), the misclassification

Table 4.3: The p_I and p_{II} and their standard errors (in parentheses) for Model (c).

	p_I				p_{II}(modified)			
δ	MSS	T^2	T^2_{MVE}	T^2_{MCD}	MSS	T^2	T^2_{MVE}	T^2_{MCD}
0.000	0.0506	0.0768	0.2902	0.1092	-	-	-	-
	(.0003)	(.0010)	(.0029)	(.0024)	-	-	-	-
0.375	0.0505	0.0751	0.2613	0.1049	0.9264	0.9254	0.9286	0.9343
	(.0003)	(.0010)	(.0029)	(.0024)	(.0011)	(.0027)	(.0030)	(.0028)
0.750	0.0516	0.0768	0.2827	0.0981	0.8312	0.8580	0.7124	0.8986
	(.0003)	(.0010)	(.0030)	(.0022)	(.0017)	(.0037)	(.0079)	(.0036)
1.125	0.0531	0.0765	0.2846	0.0969	0.6173	0.7179	0.2373	0.8179
	(.0003)	(.0010)	(.0031)	(.0023)	(.0026)	(.0052)	(.0071)	(.0055)
1.500	0.0565	0.0781	0.2809	0.1017	0.2978	0.4870	0.0939	0.6516
	(.0003)	(.0010)	(.0030)	(.0025)	(.0027)	(.0060)	(.0013)	(.0073)
1.875	0.0593	0.0804	0.2843	0.1102	0.0789	0.2170	0.0889	0.4144
	(.0003)	(.0011)	(.0031)	(.0026)	(.0014)	(.0051)	(.0010)	(.0078)
2.250	0.0607	0.0843	0.2836	0.1185	0.0141	0.0450	0.0851	0.2142
	(.0004)	(.0011)	(.0030)	(.0028)	(.0006)	(.0024)	(.0011)	(.0053)
2.625	0.0621	0.0844	0.2829	0.1205	0.0023	0.0033	0.0823	0.1170
	(.0004)	(.0011)	(.0030)	(.0029)	(.0002)	(.0006)	(.0012)	(.0026)
3.000	0.0623	0.0888	0.2851	0.1190	0.0003	0.0000	0.0775	0.0931
	(.0004)	(.0011)	(.0030)	(.0028)	(.0001)	(.0000)	(.0013)	(.0014)

rate can be roughly held at the nominal value 0.05 for all the four control charts under comparison when the process is in control. However, when the shift size, δ, increases for the OC samples, a clear increasing trend in the type-I error rate is observed for the Hotelling's T^2 control chart. The reason is that the parameter estimation used in the Hotelling's T^2 control chart gets poorer as the OC state further departs from the IC state. If robust estimators of parameters are utilized, as in the T^2_{MVE} and T^2_{MCD} charts, the increasing pattern is greatly alleviated. The proposed MSS chart also exhibits an slightly increasing trend but much milder. Note that the MSS chart behaves about the same for all the three models, which

Table 4.4: The p_I and their standard errors (in parentheses) of the MSS chart and Hotelling's T^2 control chart when using the OAAT procedure.

	MSS			T^2		
δ	(a)	(b)	(c)	(a)	(b)	(c)
0.000	0.0486	0.0483	0.0478	0.0501	0.1157	0.0789
	(.0007)	(.0007)	(.0007)	(.0007)	(.0012)	(.0010)
0.375	0.0487	0.0493	0.0478	0.0524	0.1136	0.0744
	(.0007)	(.0007)	(.0007)	(.0008)	(.0013)	(.0010)
0.750	0.0485	0.0503	0.0490	0.0523	0.1179	0.0760
	(.0007)	(.0007)	(.0007)	(.0008)	(.0012)	(.0010)
1.125	0.0479	0.0499	0.0499	0.0523	0.1155	0.0752
	(.0007)	(.0007)	(.0007)	(.0007)	(.0012)	(.0010)
1.500	0.0485	0.0498	0.0483	0.0498	0.1143	0.0754
	(.0007)	(.0007)	(.0007)	(.0008)	(.0012)	(.0010)
1.875	0.0496	0.0484	0.0461	0.0501	0.1146	0.0750
	(.0007)	(.0007)	(.0007)	(.0008)	(.0012)	(.0011)
2.250	0.0496	0.0490	0.0475	0.0487	0.1143	0.0774
	(.0007)	(.0007)	(.0007)	(.0008)	(.0012)	(.0011)
2.625	0.0500	0.0481	0.0475	0.0503	0.1114	0.0744
	(.0007)	(.0007)	(.0007)	(.0008)	(.0012)	(.0010)
3.000	0.0478	0.0485	0.0468	0.0509	0.1157	0.0766
	(.0007)	(.0007)	(.0007)	(.0008)	(.0012)	(.0011)

demonstrates the distribution-free property. In contrast, since the other three charts are constructed relying on the normality assumption, they perform poorly for the non-Gaussian Models (b) and (c). In summary, the results indicate that the MSS chart is not only distribution-free but also more robust to the magnitude of the shift in OC observations than the other three control charts. We will see later that the problem of the increasing pattern observed in the type-I error rates can be solved by implementing the OAAT procedure.

The larger-than-normal values of the type-I error rate indicate that the corre-

sponding control limits of control charts are too low for monitoring. To obtain a fair comparison among control charts in terms of the type-II error rate, we adjust the control limits to achieve the specified type-I error rate 0.05 when $\delta = 0$. Under Model (b), the control limits of the Hotelling's T^2, T^2_{MVE}, and T^2_{MCD} charts are tuned, respectively, to 11.88, 16.95, and 20.93, and to 9.35, 31.25, and 16.99 under Model (c). Consider the type-II error rate under Gaussian Model (a), the Hotelling's T^2 performs the best among the four control charts. When the model assumption holds, the Hotelling's T^2 control chart is quite powerful in detecting outliers comparing with the methodologies based on the robust tools. In addition, the T^2_{MVE} and T^2_{MCD} charts outperform the MSS chart under small shifts of outliers, e.g., $\delta \leq 1.5$. On the other hand, the performances in the type-II error rate under Models (b) and (c) are quite different from Model (a): the MSS chart performs the best for most of the OC conditions except for some large shifts under the multivariate t and Gamma distributions. Reasons for this phenomenon are: (i) the detecting power of the MSS chart outperforms the other three control charts for small to moderate shifts beacuse of its distribution-free property and (ii) since the charting statistic of the MSS chart incorporates only the direction of observations but not the magnitude, it is comparatively less sensitive in detecting large shifts of outliers than other three charts. Note that the type-II error rates are not available when $\delta = 0$ since no OC cases are generated in the data.

We now compare the performance between the MSS chart and Hotelling's T^2 control chart by using the OAAT procedure instead of the conventional procedure. The resulting type-I and type-II error rates are shown in Tables 4.4 and 4.5, respectively. The type-I error rates of the MSS chart are quite stably controlled around 0.05 under various models and shift sizes of outliers. The type-I error rates of the Hotelling's T^2 control chart are somewhat stable as the shift size of outliers increases; but they are still higher than 0.05 under non-Gaussian models. Moreover, the type-II error rates are nearly the same as that of the conventional Phase I procedure. To sum up, for the proposed MSS chart, the simulation results

Table 4.5: The p_{II} and their standard errors (in parentheses) of the MSS chart and Hotelling's T^2 control chart when using the OAAT procedure.

	MSS			T^2		
δ	(a)	(b)	(c)	(a)	(b)	(c)
0.375	0.9157	0.9262	0.9290	0.9054	0.9422	0.9224
	(.0028)	(.0025)	(.0026)	(.0030)	(.0024)	(.0027)
0.750	0.7962	0.8401	0.8378	0.7017	0.9145	0.8510
	(.0041)	(.0038)	(.0041)	(.0051)	(.0028)	(.0038)
1.125	0.5552	0.6732	0.6281	0.3533	0.8616	0.7051
	(.0056)	(.0049)	(.0056)	(.0055)	(.0036)	(.0053)
1.500	0.2924	0.4697	0.3034	0.0984	0.7191	0.4739
	(.0049)	(.0053)	(.0059)	(.0032)	(.0053)	(.0060)
1.875	0.0949	0.3069	0.0867	0.0139	0.4891	0.2001
	(.0030)	(.0049)	(.0035)	(.0012)	(.0063)	(.0049)
2.250	0.0227	0.1810	0.0165	0.0008	0.2426	0.0399
	(.0015)	(.0041)	(.0014)	(.0003)	(.0056)	(.0022)
2.625	0.0046	0.1145	0.0040	0.0001	0.0926	0.0024
	(.0007)	(.0033)	(.0006)	(.0001)	(.0037)	(.0005)
3.000	0.0005	0.0694	0.0004	0.0000	0.0263	0.0000
	(.0002)	(.0026)	(.0002)	(.0000)	(.0017)	(.0000)

indicate that, when the OAAT procedure is utilized, the misclassification rate of the IC observations can be controlled around the nominal level, while the detecting power stays almost the same as that of the conventional procedure. Since there is not much difference between the type-II error rates of the OAAT and conventional procedures, the comparisons with the T^2_{MVE} and T^2_{MCD} charts are omitted here. Naturally, it takes more CPU time for the OAAT procedure than the conventional one. However, the longer computing time is no more a concern because (i) Phase I analysis is an off-line process and (ii) it is still acceptable. Thus, we recommend the OAAT procedure for Phase I applications.

4.3 A Real Data Application

In this section, we demonstrate a real data application of our proposed Phase I monitoring scheme. Consider a real dataset from a white wine production process, which is publicly available in the UC Irvine Machine Learning Repository (ref. http://archive.ics.uci.edu/ml/datasets/Wine+Quality). This dataset consists of 4898 observations with 12 variables collected from May 2004 to February 2007. Due to privacy and logistic issues, the data contain only the physicochemical and sensory variables. The variables involving confidential information, e.g., the grape types, wine brand, and wine selling price, etc., are not included. The data are contained at the official certification entity, an inter-professional organization with the goal of improving the quality and marking of Portuguese Vinho Verde wine. For each observation, variables of physicochemical measurements include fixed acidity, volatile acidity, citric acid, residual sugar, chlorides, free sulfur dioxide, total sulfur dioxide, density, pH, sulphates, and alcohol (denoted by $x_1, \ldots, x_{11}$), and one categorical variable, the quality graded by experts, ranging from 0 (the worst) to 10 (the best). There are much more normal wines (say, levels 5-7) than the excellent (level$\geq$ 8) or poor (level$\leq$ 4) ones. For more detail of this dataset, see Cortez et al. (2009).

Considering the quality control issue of this wine production process, we first focus on the wines of level 7 with size 880. Figure 4.1 shows the scatter plots between variables citric acid (x_3), residual sugar (x_4), and density (x_8) and the corresponding normal Q-Q plots. We can observe that the joint distributions of each pair of the three variables are far from bivariate normal, and the Q-Q plots indicate all three variables are not normally distributed. Moreover, the p-value of Mardia's multivariate normality test (Mardia, 1970) is quite close to zero, also showing the violation of the normality assumption. All the evidences indicate that the multivariate normality assumption is invalid for this data set. In addition, some scatter plots exhibit patterns between variables and the covariance matrix of the

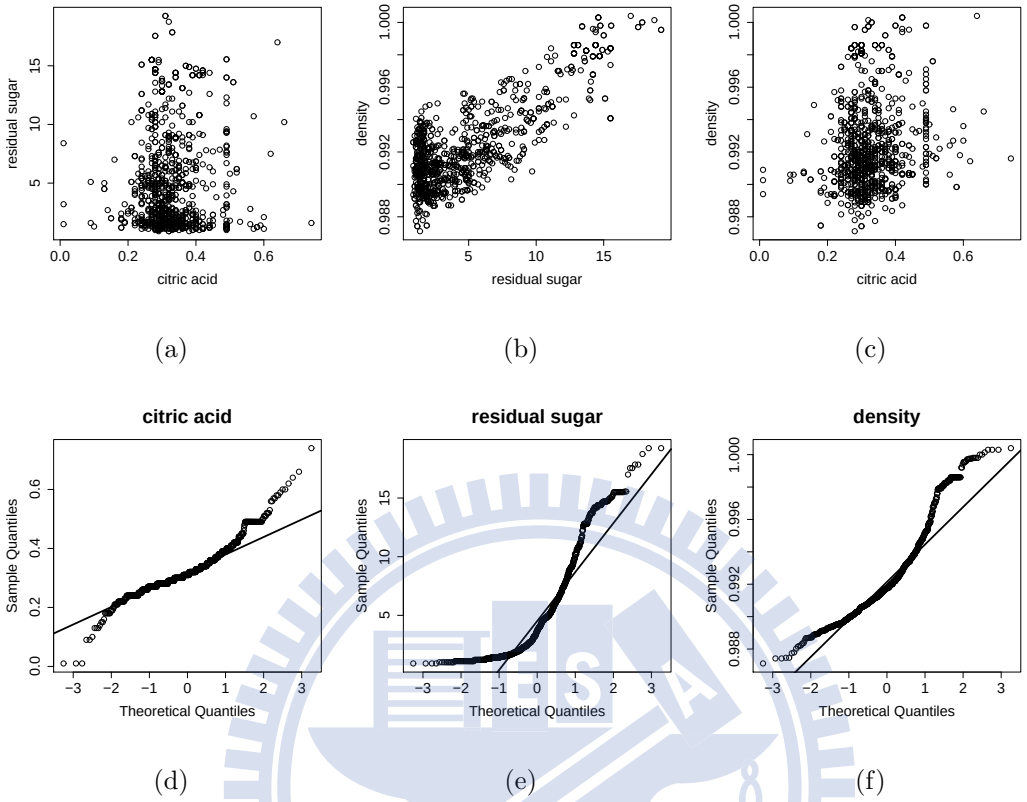

Figure 4.1: (a) - (c) are the scatter plots between variables citric acid (x_3), residual sugar (x_4), and density (x_8); (d) - (f) are the corresponding normal Q-Q plots.

data (not shown here) contains many large entries. This suggests that there exist considerable relationships between variables, thus it is inappropriate to monitor each of the variables individually.

Next, we use the level 7 wines to demonstrate our proposed MSS control chart for Phase I applications. Since the MSS chart is designed for grouped data, we group the measurements of the white wine production process in subgroups. We choose a small subgroup size, $n = 5$, to prevent the effect of outliers from diminishing in the subgroup. Then, there are $m = 880/5 = 176$ subgroups to be monitored. Setting $\alpha = 0.01$, the control limit of the MSS chart is chosen to be 22.4674 from Table A.4. By using the recommended OAAT procedure, it turns out that 66 subgroups are regarded as outliers, i.e., 550 observations are preserved

Table 4.6: The type-I and type-II error rates from mixing the level 7 and level 6 wines.

	p_I			p_{II}		
index	MSS	T^2	T^2(mod)	MSS	T^2	T^2(mod)
1	0.0000	0.2364	0.0182	0.6	0.0	0.7
2	0.0000	0.2000	0.0091	0.4	0.2	0.6
3	0.0091	0.2182	0.0091	0.6	0.3	0.7
4	0.0091	0.2091	0.0091	0.6	0.3	0.7
5	0.0000	0.2091	0.0091	0.9	0.5	1.0
6	0.0000	0.2364	0.0091	0.3	0.0	0.8
7	0.0000	0.2364	0.0091	0.3	0.0	0.6
8	0.0000	0.2091	0.0091	0.6	0.2	0.7
9	0.0000	0.2545	0.0091	0.4	0.2	0.5

after our Phase I analysis. Note that there might be some IC observations within the signaled OC subgroups. It is worth to note that lots of the wines were detected as OC even they were all classified to level 7 by experts. This could be caused by the fact that the level classification by experts is very subjective, and the human taste perception usually is not consistent over time.

To compare with the Hotelling's T^2 control chart, we mix the 550 IC observations with some OC ones — wines from other levels. Recall that the Hotelling's T^2 chart has an excessive type-I error rate if the underlying distribution of the data is not Gaussian. Thus, in addition to the regular Hotelling's T^2 control chart, we also include the T^2 chart with the control limit adjusted to achieve the type-I error rate at about 1% for a fair comparison. Regard the preserved 550 level 7 wines as IC, and 50 wines from level 6 (or 5) as OC. Since there are 2198 and 1457 observations classified as level 6 and 5, respectively, we can choose different sets of OC wines as replications. The OAAT procedure is adopted for both of the control charts. The results of 9 replications for mixing with levels 6 and 5 are listed in

Table 4.7: The type-I and type-II error rates for mixing the level 7 and level 5 wines.

	p_I			p_{II}		
index	MSS	T^2	T^2(mod)	MSS	T^2	T^2(mod)
1	0.0000	0.2364	0.0182	0.7	0.1	0.5
2	0.0000	0.2091	0.0091	0.5	0.1	0.4
3	0.0000	0.2091	0.0091	0.8	0.4	0.9
4	0.0091	0.2364	0.0182	0.6	0.1	0.7
5	0.0000	0.2364	0.0182	0.3	0.0	0.5
6	0.0000	0.2364	0.0091	0.5	0.1	0.5
7	0.0000	0.2364	0.0091	0.4	0.0	0.7
8	0.0000	0.2364	0.0091	0.3	0.0	0.6
9	0.0000	0.2364	0.0273	0.1	0.0	0.5

Tables 4.6 and 4.7, respectively. The type-I error rates of the MSS chart are under the nominal level 0.01 in all of the replications, but that of the regular Hotelling's T^2 are much larger than 0.01. After tuning the control limit of the Hotelling's T^2 control chart to achieve the type-I error rate around 0.01, the type-II error rates of the MSS chart outperforms the T^2 chart in both of the OC conditions for the most of the replications. Comparing with the level 6 wines, the level 5 wines are more different from the IC ones (the level 7 wines) physicochemically. In other words, the outlying condition is more severe. As explained earlier, the MSS chart is sometimes less sensitive than the modified Hotelling's T^2 control chart when the outlying condition is severe; and the results in Table 4.7 also demonstrate this phenomenon. Similar results are obtained when the size of OC wines is increased to 20 subgroups and are summarized in Appendix A.4.

4.4 Conclusions

In this chapter, we construct a distribution-free Phase I monitoring scheme for multivariate observations with subgroups. By using the spatial median and the Tyler's scatter estimator, the observations are transformed to a charting statistic based on the spatial sign vectors. Then an observation with the statistic exceeding the control limit is regarded as an OC case. Through simulation studies, we demonstrate that our proposed MSS chart is indeed distribution-free such that the type-I error rate can be controlled at the specified value for non-Gaussian distributions. In addition, the chart is also robust to the extent of outlying in terms of the type-I error rate. Moreover, the MSS chart is quite powerful in detecting outliers in the data. Comparing with the existing monitoring schemes, the Hotelling's T^2, T^2_{MVE}, and T^2_{MCD} charts, the MSS chart is more robust and powerful in most of the OC conditions (after adjusting the T^2 control charts to achieve the nominal type-I error rate). However, since the charting statistic of the MSS chart considers only the multivariate direction of an observation, it carries less information on the magnitude of the outlying conditions. Thus, the MSS chart is less sensitive than the traditional Hotelling's T^2 control chart for extreme outliers.

When implementing conventional Phase I monitoring schemes, the signaled observations would be all removed and then the process parameters would be re-estimated. This detecting procedure will continue until all the remaining observations are regarded as IC. However, there are excessive IC observations got misclassified by using the conventional procedure, especially when the data contain some extreme outliers. Instead of deleting all the signaled observations, the OAAT procedure proposed by Shiau and Sun (2010) removes only the observation with the largest value of the charting statistic to diminish the problem with the type-I error rate. It is shown by simulation that the control charts implemented with the OAAT procedure are able to control the type-I error rate at the nominal level. Thus, we recommend adopting the OAAT procedure in Phase I analysis.

The profile monitoring is the major theme of this dissertation, and it is worthwhile to develop a distribution-free control chart for profiles as well. Although the discretized profile can be viewed as a special kind of multivariate data, there are intrinsic differences between profiles and multivariate observations. For example, the design points of profiles are often different from profile to profile, but not for multivariate data. In addition, since the dimension of a discretized profile is often fairly large, it could be very time-consuming if the control chart developed for multivariate data is used directly. The efficiency of a control chart is of great concern in Phase II on-line monitoring. In the next chapter, we will focus on constructing monitoring schemes for profiles with no distribution assumptions for both Phase I and Phase II applications.

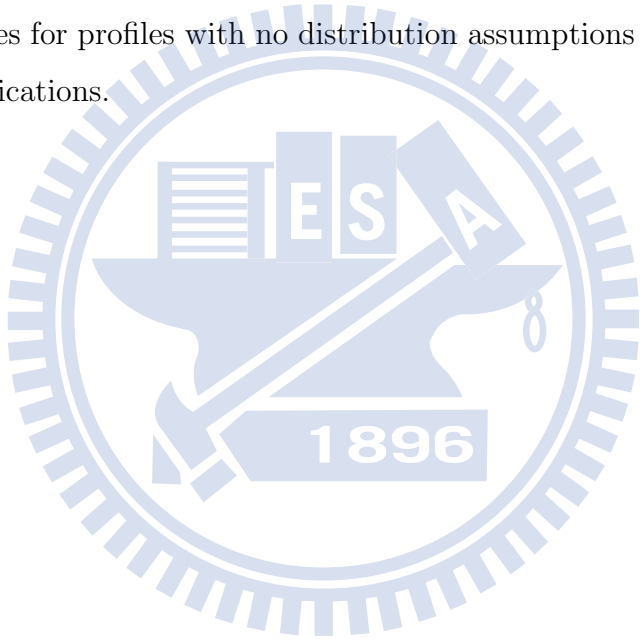

Chapter 5

Distribution-Free Profile Monitoring Schemes

In this chapter, instead of assuming a specific distribution for profile data as in Chapter 3, no distributional assumptions are impose on profiles. We combine the ideas of PCA and distribution-free multivariate data monitoring methodologies to construct a new control chart for profile monitoring. The sections of this chapter are organized as follows. Our proposed schemes for Phase I and II profile monitoring are elaborated in Section 5.1 and 5.2, respectively. In Section 5.3, results of simulation studies of the proposed methods and a performance comparison with existing methods are presented. A real-data application is demonstrated in Section 5.4. A short conclusion is given in the last section of this chapter.

5.1 Phase I Monitoring

5.1.1 Methodology

We now consider the model of the form (3.1) with no assumptions imposed on the distribution of the random-effect term. That is, for the ith profiles, $i = 1, \ldots, m$,

the profile data can be written as

$$y_{ij} = g(x_{ij}) + f_i(x_{ij}) + \varepsilon_{ij} \text{ for } j = 1, \ldots, p,$$

where $g(\cdot)$ and $f_i(\cdot)$ are the fixed-effect and random-effect terms, respectively, x_{ij} denotes the value of the covariate for the jth observation and $(\varepsilon_{i1}, \ldots, \varepsilon_{ip})'$ is the i.i.d. random error vector with mean 0 and variance σ_ε^2. The random-effect term f_i and the errors ε_{ij} are assumed independent of each other and f_i is assumed a zero-mean process. The case of univariate covariate is considered here.

To filter out the noise in a profile, a smoothing technique is applied to profile data before monitoring. Suppose that there are m subgroups of profiles with subgroup size n in the historical data set. To simplify notation, denote the n profiles of the ith subgroup *after* smoothing by $(\boldsymbol{y}_{i1}, \ldots \boldsymbol{y}_{in})$, $i = 1, \ldots, m$. In Phase I analysis, it is common to obtain the parameters used for monitoring by averaging the estimates from each of the subgroups. For example, the estimated mean and variance-covariance matrix used in the Hotelling's T^2 chart are obtained by first calculating the sample mean and sample variance-covariance matrix from each of the m subgroups, denoted by $(\hat{\boldsymbol{\mu}}_1, \ldots, \hat{\boldsymbol{\mu}}_m)$ and $(\hat{\boldsymbol{\Sigma}}_1, \ldots, \hat{\boldsymbol{\Sigma}}_m)$, respectively. Then the estimated mean and variance-covariance matrix are:

$$\hat{\boldsymbol{\mu}} = \frac{1}{m} \sum_{i=1}^{m} \hat{\boldsymbol{\mu}}_i,$$

$$\hat{\boldsymbol{\Sigma}} = \frac{1}{m} \sum_{i=1}^{m} \hat{\boldsymbol{\Sigma}}_i.$$

In this method, one should note that the subgroup size must be larger than the number of the design points in a profile for the sample variance-covariance matrix of a subgroup to be non-singular. However, the number of design points are usually large in practice in order to keep important features of profiles. Thus, we recommend that the sample mean and sample variance-covariance matrix of the whole data set are taken directly to be the estimators of the mean and scatter

matrix; that is,

$$\hat{\boldsymbol{\mu}} = \frac{1}{mn}\sum_{i=1}^{m}\sum_{k=1}^{n}\boldsymbol{y}_{ik}, \tag{5.1}$$

$$\hat{\boldsymbol{\Sigma}} = \frac{1}{mn-1}\sum_{i=1}^{m}\sum_{k=1}^{n}(\boldsymbol{y}_{ik}-\hat{\boldsymbol{\mu}})(\boldsymbol{y}_{ik}-\hat{\boldsymbol{\mu}})'. \tag{5.2}$$

Applying the eigen-analysis to $\hat{\boldsymbol{\Sigma}}$, the corresponding eigenvalue-vector pairs are obtained and denoted as $(\lambda_1, \boldsymbol{\nu}_1), \ldots, (\lambda_p, \boldsymbol{\nu}_p)$, where $\lambda_1 \geq \lambda_2 \geq \ldots \geq \lambda_p \geq 0$. Let the number of the effective PCs be K and the two T^2-type statistics be

$$T^2_{0,ik} = (\boldsymbol{s}_{0,ik} - \bar{\boldsymbol{s}}_0)'\boldsymbol{B}_0^{-1}(\boldsymbol{s}_{0,ik} - \bar{\boldsymbol{s}}_0), \tag{5.3}$$

$$T^2_{1,ik} = (\boldsymbol{s}_{1,ik} - \bar{\boldsymbol{s}}_1)'\boldsymbol{B}_1^{-1}(\boldsymbol{s}_{1,ik} - \bar{\boldsymbol{s}}_1), \tag{5.4}$$

where $\boldsymbol{s}_{0,ik}$ and $\boldsymbol{s}_{1,ik}$ are the vectors of the first K and last $p-K$ PC scores for the kth observed profile in the ith subgroup, respectively, $i = 1, \ldots, m$, $k = 1, \ldots, n$, $(\bar{\boldsymbol{s}}_0, \boldsymbol{B}_0)$ and $(\bar{\boldsymbol{s}}_1, \boldsymbol{B}_1)$ are the corresponding sample mean vectors and sample variance-covariance matrices of $\boldsymbol{s}_{0,ik}$'s and $\boldsymbol{s}_{1,ik}$'s, respectively. Note that the statistics $T^2_{0,ik}$ and $T^2_{1,ik}$ may not be uncorrelated because the squares of two uncorrelated random variables may be correlated.

Since no distribution assumptions are imposed on the profiles, the theoretical distribution of (T_0^2, T_1^2) is unavailable. Thus, the distribution-free Phase I monitoring scheme introduced in Section 4.1 is applied to the vector of the two T^2 statistics, $(T_0^2, T_1^2)'$. The monitoring procedure with respect to $(T_0^2, T_1^2)'$ is basically the same as that described in Section 4.1. We elaborate the steps of profile monitoring as follows. For a profile data set consisting of m subgroups with subgroup size n,

1. Estimate the mean and variance-covariance matrix, $(\hat{\boldsymbol{\mu}}, \hat{\boldsymbol{\Sigma}})$, of the smoothed profiles according to (5.1) and (5.2). Then apply the eigen-decomposition to $\hat{\boldsymbol{\Sigma}}$ to obtain the corresponding eigenvalues and eigenvectors, $(\lambda_1, \boldsymbol{\nu}_1), \ldots, (\lambda_p, \boldsymbol{\nu}_p)$.

2. Compute the vector of the T^2 statistics $\boldsymbol{T}_{ik} = (T^2_{0,ik}, T^2_{1,ik})'$ as in equations (5.3) and (5.4) for $i = 1, \ldots, m$ and $k = 1, \ldots, n$.

3. Estimate the spatial median and Tyler's transformation matrix $(\boldsymbol{\theta}_T, \boldsymbol{A}_T)$ by solving

$$\frac{1}{mn}\sum_{i=1}^{m}\sum_{k=1}^{n} U(\boldsymbol{A}_T(\boldsymbol{T}_{ik} - \boldsymbol{\theta}_T)) = \mathbf{0}, \tag{5.5}$$

$$\frac{1}{mn}\sum_{i=1}^{m}\sum_{k=1}^{n} U(\boldsymbol{A}_T(\boldsymbol{T}_{ik} - \boldsymbol{\theta}_T))U(\boldsymbol{A}_T(\boldsymbol{T}_{ik} - \boldsymbol{\theta}_T))' = \frac{1}{2}\boldsymbol{I}_2. \tag{5.6}$$

4. Calculate the spatial sign vector for each of the $m \times n$ observations as

$$\boldsymbol{u}_{ik} = U(\boldsymbol{A}_T(\boldsymbol{T}_{ik} - \boldsymbol{\theta}_T)) \text{ for } i = 1, \ldots, m, k = 1, \ldots, n.$$

5. Then the charting statistic is defined as

$$Q_i = 2n\bar{\boldsymbol{u}}_i'\bar{\boldsymbol{u}}_i,$$

where $\bar{\boldsymbol{u}}_i = \sum_{k=1}^{n} \boldsymbol{u}_{ik}/n$. The observations with $Q_i > L_{\alpha,n,2}$ are regarded as OC cases, where $L_{\alpha,n,2}$ is the control limit for the specific n and type-I error rate α.

6. (For the conventional procedure) If there are any OC cases detected, delete them and go back to step 1. This process goes on until all the remaining observations are within the control limit.

6′ (For the OAAT procedure) Among the detected OC cases, delete the observation with the largest value of Q statistic, and then go back to step 1. This process goes on until all the remaining observations are within the control limit.

The control limit used in the 5th step is available in Appendix A.2. This scores-based multivariate sign Shewhart chart is referred to as the SMSS chart hereafter.

The information from all design points is extracted and separated into two T^2-type statistics, $(T_0^2, T_1^2)'$. Any type of changes in profiles, including location, dispersion, or shape, would cause the location shift of the vector $(T_0^2, T_1^2)'$, and then

an alarm may be signaled by the SMSS chart. Although there is no proof to ensure that the distribution of the vector $(T_0^2, T_1^2)'$ follows the elliptical direction distribution, the spatial-sign-based control chart performs quite robust to the distribution of the profile data empirically. As a result, the SMSS chart works in detecting outliers and performs comparatively with conventional Phase I monitoring methods. We will show that via simulations in Section 5.3.

5.2 Phase II Monitoring

5.2.1 Methodology

Consider again the data from model (3.1) with no distribution assumptions on the random-effect term. We first construct a control chart for monitoring individual profiles for Phase II monitoring. The chart can be modified easily for the data with subgroups as shown later. As most of Phase II studies, the mean vector and variance-covariance matrix of the profiles are assumed known or have been well estimated from the reference sample. Suppose the mean vector and variance-covariance matrix of the smoothed profiles are given as $(\boldsymbol{\mu}_0, \boldsymbol{\Sigma}_0)'$. The eigen-analysis is then applied to $\boldsymbol{\Sigma}_0$ and the corresponding eigenvalues and eigenvectors, $(\lambda_1, \boldsymbol{\nu}_1), \ldots, (\lambda_p, \boldsymbol{\nu}_p)$, where $\lambda_1 \geq \lambda_2 \geq \ldots \geq \lambda_p \geq 0$, are obtained. Choose K to be the number of effective PCs. Then the following two T^2-type statistics of $\boldsymbol{y}_t$, the incoming smoothed profile at time t, are considered as:

$$T_{0t}^2 = (\boldsymbol{y}_t - \boldsymbol{\mu}_0)' \boldsymbol{P}_0 \boldsymbol{\Lambda}_0^{-1} \boldsymbol{P}_0' (\boldsymbol{y}_t - \boldsymbol{\mu}_0), \tag{5.7}$$

$$T_{1t}^2 = (\boldsymbol{y}_t - \boldsymbol{\mu}_0)' \boldsymbol{P}_1 \boldsymbol{\Lambda}_1^{-1} \boldsymbol{P}_1' (\boldsymbol{y}_t - \boldsymbol{\mu}_0), \tag{5.8}$$

where $\boldsymbol{P}_0$ and $\boldsymbol{P}_1$ are the matrices consisting of the first K and the last $p-K$ eigenvectors, respectively. Treat $(T_{0t}^2, T_{1t}^2)'$ as a two-dimensional vector $\boldsymbol{T}_t$, and similar to the Phase I method described in Section 5.1, we apply some nonparametric or distribution-free monitoring procedures to $\boldsymbol{T}_t$. The multivariate sign EWMA

control chart proposed by Zou and Tsung (2011) and introduced in Section 2.2.5 is considered to monitor the vectors $\boldsymbol{T}_t$. The monitoring procedure for nonlinear profiles is given as follows. Note that we need a set of historical data to estimate the spatial median and Tyler's transformation matrix $(\boldsymbol{\theta}_T, \boldsymbol{A}_T)$.

1. Apply the eigen-decomposition to $\boldsymbol{\Sigma}_0$ to obtain the corresponding eigenvalues and eigenvectors, $(\lambda_1, \boldsymbol{\nu}_1), \ldots, (\lambda_p, \boldsymbol{\nu}_p)$. For the historical data set $\{\boldsymbol{y}_1, \ldots, \boldsymbol{y}_m\}$, compute the corresponding T^2 vectors $\{\boldsymbol{T}_1, \ldots, \boldsymbol{T}_m\}$ according to equations (5.7) and (5.8).

2. Estimate the spatial median and Tyler's transformation matrix $(\boldsymbol{\theta}_T, \boldsymbol{A}_T)$ by solving

$$\frac{1}{m}\sum_{i=1}^{m} U(\boldsymbol{A}_T(\boldsymbol{T}_i - \boldsymbol{\theta}_T)) = \boldsymbol{0}, \tag{5.9}$$

$$\frac{1}{m}\sum_{i=1}^{m} U(\boldsymbol{A}_T(\boldsymbol{T}_i - \boldsymbol{\theta}_T))U(\boldsymbol{A}_T(\boldsymbol{T}_i - \boldsymbol{\theta}_T))' = \frac{1}{2}\boldsymbol{I}_2. \tag{5.10}$$

3. For an incoming profile $\boldsymbol{y}_t$, calculate the corresponding T^2 vector, $\boldsymbol{T}_t$, and the spatial sign vector as

$$\boldsymbol{u}_t = U(\boldsymbol{A}_T(\boldsymbol{T}_t - \boldsymbol{\theta}_T)).$$

4. Define the EWMA sequence as

$$\boldsymbol{w}_t = (1-\lambda)\boldsymbol{w}_{t-1} + \lambda \boldsymbol{u}_t,$$

where λ is a weighted parameter and the initial vector being $\boldsymbol{0}$. Then the proposed control chart triggers a signal if

$$Q_t = \frac{2(2-\lambda)}{\lambda}\boldsymbol{w}_t'\boldsymbol{w}_t > L,$$

where $L > 0$ is the control limit to achieve the prespecified IC ARL.

It is straightforward to modify the above control chart for data in subgroups as follows. For a data set with m subgroups with subgroup size n, say, $\{\boldsymbol{y}_{i1}, \ldots, \boldsymbol{y}_{in}\}$

for $i = 1, \ldots, m$, modify the constraints (5.9) and (5.10) in the 2nd step to the form of equations (5.5) and (5.6). For an incoming subgroup $\{\boldsymbol{y}_{t1}, \ldots, \boldsymbol{y}_{tn}\}$, the sign vector in the 3rd step is replaced by

$$\boldsymbol{u}_t = \frac{1}{n} \sum_{k=1}^{n} U(\boldsymbol{A}_T(\boldsymbol{T}_{tk} - \boldsymbol{\theta}_T)),$$

where $\boldsymbol{T}_{tk}$ is the vector of the T^2 statistics obtained from the kth profile of the incoming subgroup, $k = 1, \ldots, n$. Finally, the 4th step can be followed directly.

The control limits for some specific values of IC ARL and λ can be found in Appendix A.3. Control limits for more values of λ and dimension p are available in Table 1 of Zou and Tsung (2011). Since this EWMA control chart is based on the spatial sign of the T^2 statistics of the PC scores, we refer to it as the score-based multivariate spatial-sign EWMA (SMSE) chart hereafter.

The proposed control chart in Zou and Tsung (2011) is distribution-free for distributions under the elliptical direction family. Unfortunately, as mentioned earlier, the theoretical distribution of the charting statistic is very difficult to obtain analytically. Nevertheless, the spatial-sign-based EWMA control chart is quite robust to the distribution of the multivariate variable; consequently our proposed control chart is also robust to the distribution so that the IC ARL can be controlled at the specified value, say, 200 or 370, when the underlying distribution is unknown. Moreover, it is also quite effective to signal an alarm if an OC condition occurs in the process. In addition, if a profile changes in any aspects, the change will reflect as a location shift of the $\boldsymbol{T}$ vector to trigger the alarm. We will see that via simulation in the following section.

5.3 Simulation Studies

5.3.1 Phase I Applications

First, we consider simulated profiles that imitate the dissolving process of aspartame under different levels of temperature, an example of profiles first described

in Kang and Albin (2000). Instead of generating profiles from multivariate normal distribution as we did in Section 3.3.1, the IC aspartame profiles are directly generated from equation (3.11). That is,

$$\boldsymbol{y} = I + Me^{N(\boldsymbol{x}-1)^2} + \boldsymbol{\varepsilon},$$

where all the random components I, M, N, and $\boldsymbol{\varepsilon}$ are independently generated from normal distributions. The same settings of the parameters of the random components as before are followed, i.e., $(\mu_I, \sigma_I) = (1, 0.2)$, $(\mu_M, \sigma_M) = (15, 1)$, $(\mu_N, \sigma_N) = (-1.5, 0.3)$, and $\sigma_\varepsilon = 0.3$. Let $p = 20$, $\boldsymbol{x} = (x_1, \ldots, x_p)'$ are equally spaced ranging from 0.64 to 3.68. Choosing $h = 0.48$, 200 generated aspartame profiles and the corresponding smoothed estimators by using the local linear smoother are shown in Figure 5.1. Note that the pattern of the generated aspatame profiles is quite similar to the profiles generated from the multivariate normal distribution as in Section 3.3.1. The OC profiles considered are generated from the following models:

(a) $I \sim N(\mu_I + \delta\sigma_I, \sigma_I^2)$;

(b) $M \sim N(\mu_M + \delta\sigma_I, \sigma_M^2)$;

(c) $I \sim N(\mu_I, (\delta^*\sigma_I)^2)$;

(d) $M \sim N(\mu_M, (\delta^*\sigma_M)^2)$;

(e) $\boldsymbol{y} \sim \delta(\boldsymbol{y} - \boldsymbol{\mu}) + \boldsymbol{\mu}$.

The first four OC models simulate the situations that one of the parameters of the random components is shifted by an amount quantified by δ, while Model (e) considers the case that the variance-covariance matrix of the profile data $\boldsymbol{y}$ is multiplied by a constant and the mean vector stays unchanged. Since there exists no distribution-free methodology for profile monitoring in the literature, we consider the method developed under parametric model for comparison. In this simulation study, the discretized profiles are considered and the design points of all

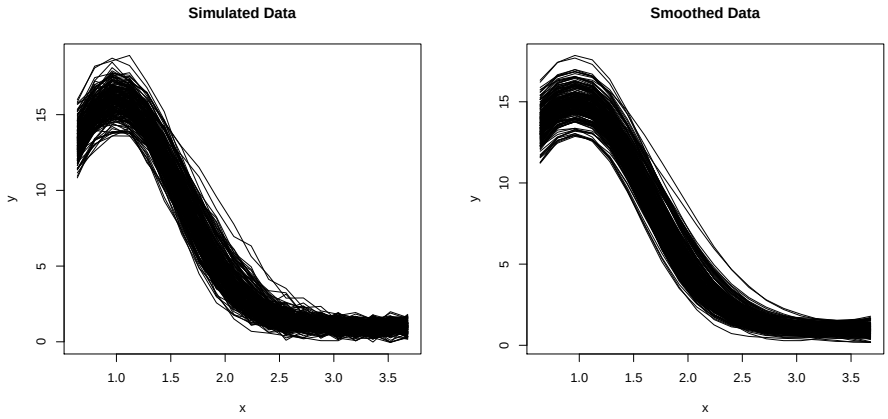

(a) (b)

Figure 5.1: (a) 200 generated aspartame profiles and (b) the corresponding smoothing estimates.

the profiles are the same, thus we can simply treat the profiles as multivariate data. Here, the Hotelling's T^2 control chart introduced in Section 4.2 is also considered. The performances of the control charts are also measured via the type-I and type-II error rates introduced in Section 3.1.3. The error rates reported in what follows are the average of 1,000 replications.

In Phase I applications, the reference sample is usually mixed with both IC and OC observations. To simulate the historical data set in Phase I, 500 subgroups of profiles with subgroup size 10 (i.e., $m = 500$ and $n = 10$) are generated, and among them there are 450 IC and 50 OC cases. We first compare the type-I error rates of the SMSS chart between using the conventional procedure and the OAAT procedure for each of the five OC conditions. Choosing $\alpha = 0.05$, the control limit of the SMSS chart is then 5.8551 (from Table A.4 in Appendix A.2 with $n = 10$ and $p = 2$). The shift size of the parameters $\delta = 0(0.6)3$ in Models (a) and (b), $\delta^* = 1(0.4)3$ in Models (c) and (d). We choose the number of effective PCs $K = 3$ for demonstration. The results are summarized in Table 5.1. From the table, we can see that the type-I error rate is increasing in the shift size when the conventional procedure is used for all the OC models. In contract, for the

Table 5.1: The type-I error rates of the SMSS chart by using the conventional and OAAT detecting procedures.

		Conventional				OAAT			
δ	δ^*	(a)	(b)	(c)	(d)	(a)	(b)	(c)	(d)
0.6	1.4	0.0505	0.0508	0.0507	0.0511	0.0491	0.0494	0.0492	0.0495
1.2	1.8	0.0514	0.0520	0.0524	0.0527	0.0500	0.0504	0.0504	0.0507
1.8	2.2	0.0529	0.0531	0.0571	0.0544	0.0507	0.0505	0.0506	0.0508
2.4	2.6	0.0569	0.0540	0.0649	0.0557	0.0499	0.0500	0.0493	0.0503
3.0	3.0	0.0638	0.0554	0.0695	0.0580	0.0492	0.0500	0.0492	0.0500

OAAT procedure, the error rate is quite robust to the shift size and stays around 0.05 stably. To ensure the type-I error rate to be controlled at a nominal level, we adopt the OAAT procedure in what follows.

We next compare the performances between the SMSS chart and the Hotelling's T^2 chart. It is well known that the type-I error rate is hard to control at the prespecified value when a parametric control chart is applied on processes with distributions different from the assumption. Therefore, for a fair comparison, we adjust the control limit of the Hotelling's T^2 chart to achieve the specified type-I error rate, say, $\alpha = 0.05$ in this case. Tables 5.2 - 5.6 tabulate the simulation results including the type-I and type-II error rates and their standard errors for OC Models (a) - (e), respectively. The columns labeled "T^2(mod)" indicate the results of the Hotelling's T^2 chart after modifying the control limit to achieve the nominal false-alarm error rate $\alpha = 0.05$. The columns "S" indicate the results of the SMSS chart and the numbers in the parentheses are the number of the effective PCs used in T_0^2 statistic. The type-II error rates are unavailable and labeled "-" in the tables when $\delta = 0$, since there are no OC profiles in the data.

The results for Models (a) and (b) (Tables 5.2 and 5.3) are similar since both models are related to the mean shift. The type-I error rates of the Hotelling's T^2 chart are stably around 0.053, slightly exceeding the nominal value 0.05. This is

Table 5.2: The type-I and type-II error rates and their standard errors (in parentheses) of OC Model (a) for $\alpha = 0.05$

	p_I					p_{II}				
δ	T^2	S(2)	S(3)	S(4)	S(5)	T^2(mod)	S(2)	S(3)	S(4)	S(5)
0.0	0.053	0.049	0.049	0.049	0.049	-	-	-	-	-
	(.0003)	(.0003)	(.0003)	(.0003)	(.0003)	-	-	-	-	-
0.6	0.0530	0.0489	0.0491	0.0493	0.0491	0.9074	0.9505	**0.9499**	0.9494	0.9505
	(.0003)	(.0003)	(.0003)	(.0003)	(.0003)	(.0014)	(.0010)	(.0009)	(.0010)	(.0010)
1.2	0.0523	0.0497	0.0500	0.0502	0.0497	0.6881	0.9479	**0.9239**	0.9299	0.9338
	(.0003)	(.0003)	(.0003)	(.0003)	(.0003)	(.0024)	(.0010)	(.0012)	(.0011)	(.0012)
1.8	0.0529	0.0494	0.0507	0.0504	0.0502	0.2035	0.9312	**0.7972**	0.8324	0.8604
	(.0003)	(.0003)	(.0003)	(.0003)	(.0003)	(.0022)	(.0012)	(.0021)	(.0019)	(.0017)
2.4	0.0529	0.0497	0.0499	0.0505	0.0502	0.0113	0.8969	**0.4186**	0.5429	0.6361
	(.0003)	(.0003)	(.0003)	(.0003)	(.0003)	(.0005)	(.0015)	(.0033)	(.0034)	(.0031)
3.0	0.0532	0.0499	0.0492	0.0492	0.0496	0.0001	0.8372	**0.0574**	0.1047	0.1754
	(.0003)	(.0003)	(.0003)	(.0003)	(.0003)	(.0001)	(.0020)	(.0013)	(.0019)	(.0027)

the effect of violating the normality assumption; however, the deviation is fairly small. On the other hand, the type-I error rates are well controlled around 0.05 for the SMSS chart despite of the shift size in mean. To obtain a fair comparison for the type-II error rates, we adjust the control limit of the T^2 chart to achieve 0.05 for the type-I error rate. The type-II error rates of the modified Hotelling's T^2 chart are slightly larger than that of the regular (unmodified) T^2 chart but the modified T^2 chart still outperforms the SMSS chart. This is because the T^2 statistics of the generated profiles do not depart much from the distribution it would have followed when the normality assumption holds. As it is well known, a parametric method usually is more efficient than a nonparametric method when the assumed parametric model is correct. Thus the Hotelling's T^2 chart has better performance than the SMSS chart in these models.

Table 5.3: The type-I and type-II error rates and their standard errors (in parentheses) of OC Model (b) for $\alpha = 0.05$

	p_I					p_{II}				
δ	T^2	S(2)	S(3)	S(4)	S(5)	T^2(mod)	S(2)	S(3)	S(4)	S(5)
0.0	0.053	0.049	0.049	0.049	0.049	-	-	-	-	-
	(.0003)	(.0003)	(.0003)	(.0003)	(.0003)	-	-	-	-	-
0.6	0.0533	0.0491	0.0492	0.0494	0.0493	0.8877	**0.9414**	0.9446	0.9461	0.9465
	(.0003)	(.0003)	(.0003)	(.0003)	(.0003)	(.0015)	(.0011)	(.0010)	(.0010)	(.0010)
1.2	0.0525	0.0506	0.0504	0.0505	0.0500	0.5343	**0.8179**	0.8570	0.8794	0.8950
	(.0003)	(.0003)	(.0003)	(.0003)	(.0003)	(.0027)	(.0020)	(.0016)	(.0015)	(.0015)
1.8	0.0531	0.0502	0.0506	0.0506	0.0506	0.0538	**0.3392**	0.4832	0.5917	0.6721
	(.0003)	(.0003)	(.0003)	(.0003)	(.0003)	(.0011)	(.0028)	(.0030)	(.0030)	(.0027)
2.4	0.0529	0.0493	0.0493	0.0499	0.0497	0.0005	**0.0272**	0.0583	0.1071	0.1718
	(.0003)	(.0003)	(.0003)	(.0003)	(.0003)	(.0001)	(.0008)	(.0012)	(.0018)	(.0025)
3.0	0.0532	0.0490	0.0492	0.0490	0.0492	0.0000	**0.0006**	0.0024	0.0052	0.0101
	(.0003)	(.0003)	(.0003)	(.0003)	(.0003)	(.0000)	(.0001)	(.0002)	(.0003)	(.0005)

The ability of detecting outliers of the SMSS chart comes from the change of the directions of the spatial signs of the T_0^2 and T_1^2 statistics. For example, the shift in the mean of I indicates the vertical shift in the profiles, which enlarges both the T_0^2 and T_1^2 statistics; thus, the corresponding spatial sign vectors cluster around the upper side of the unit circle (see Figure 5.2(a)). On the other hand, the change in the mean of M affects mainly the T_0^2 statistic hence the corresponding spatial sign vectors are closer to the right side of the unit circle (see Figure 5.2(b)). The clustering of the spatial sign vectors enlarges the value of the Q statistic and hence the SMSS chart has the ability to detect outliers.

Both Models (c) and (d) indicate the variance-covariance structure is changed in the process, so the results are analogous as summarized in Tables 5.4 and 5.5. The type-I error rates for both of the regular and modified Hotelling's T^2 charts are decreasing in δ^*. Since the shift in the variance of the random component I or M

Table 5.4: The type-I and type-II error rates and their standard errors (in parentheses) of OC Model (c) for $\alpha = 0.05$

	p_I					p_{II}				
δ^*	T^2	S(2)	S(3)	S(4)	S(5)	T^2(mod)	S(2)	S(3)	S(4)	S(5)
1.0	0.053	0.049	0.049	0.049	0.049	-	-	-	-	-
	(.0003)	(.0003)	(.0003)	(.0003)	(.0003)	-	-	-	-	-
1.4	0.0521	0.0488	0.0494	0.0493	0.0493	0.9406	0.9463	**0.9310**	0.9346	0.9377
	(.0003)	(.0003)	(.0003)	(.0003)	(.0003)	(.0011)	(.0010)	(.0011)	(.0011)	(.0011)
1.8	0.0501	0.0498	0.0504	0.0503	0.0498	0.9217	0.9379	**0.8729**	0.8898	0.9008
	(.0003)	(.0003)	(.0003)	(.0003)	(.0003)	(.0012)	(.0011)	(.0015)	(.0014)	(.0013)
2.2	0.0494	0.0495	0.0505	0.0505	0.0503	0.8993	0.9159	**0.7859**	0.8164	0.8354
	(.0003)	(.0003)	(.0003)	(.0003)	(.0003)	(.0014)	(.0013)	(.0019)	(.0018)	(.0017)
2.6	0.0482	0.0498	0.0500	0.0505	0.0500	0.8744	0.8864	**0.6857**	0.7265	0.7612
	(.0003)	(.0003)	(.0003)	(.0003)	(.0003)	(.0015)	(.0015)	(.0024)	(.0022)	(.0022)
3.0	0.0474	0.0497	0.0500	0.0499	0.0503	0.8523	0.8598	**0.5861**	0.6352	0.6784
	(.0003)	(.0003)	(.0003)	(.0003)	(.0003)	(.0017)	(.0017)	(.0023)	(.0023)	(.0023)

leads to a change in the variance-covariance structure of the profiles (see equation (3.13)), consequently it changes the estimate of the eigen-vectors. As a result, the type-I error rates cannot be controlled at a specified level. Moreover, when the reference sample is contaminated by the outliers with large dispersion, the scatter matrix would be "inflated" when estimated by the sample variance-covariance matrix. More severe outlying condition makes most IC profiles to have smaller T^2 statistic values to signal an alarm, hence the type-I error rate is decreased. In contrast, the performance of the SMSS chart in type-I error is still quite robust to the magnitude of the shift in the variance of I or M. On the other hand, the type-II error rates indicate that the SMSS chart is more powerful than the T^2 chart in detecting outliers. Since the variation in I or M is incorporated in the first few PCs, the change in the variance leads to the change in the T_0^2 statistic and hence the directions of the corresponding spatial sign vectors are more concentrated to

Table 5.5: The type-I and type-II error rates and their standard errors (in parentheses) of OC Model (d) for $\alpha = 0.05$

	p_I					p_{II}				
δ^*	T^2	S(2)	S(3)	S(4)	S(5)	T^2(mod)	S(2)	S(3)	S(4)	S(5)
1.0	0.053	0.049	0.049	0.049	0.049	-	-	-	-	-
	(.0003)	(.0003)	(.0003)	(.0003)	(.0003)	-	-	-	-	-
1.4	0.0545	0.0494	0.0495	0.0495	0.0494	0.9360	**0.9038**	0.9153	0.9228	0.9266
	(.0003)	(.0003)	(.0003)	(.0003)	(.0003)	(.0011)	(.0014)	(.0012)	(.0012)	(.0012)
1.8	0.0519	0.0504	0.0507	0.0504	0.0502	0.9095	**0.7919**	0.8304	0.8530	0.8681
	(.0003)	(.0003)	(.0003)	(.0003)	(.0003)	(.0013)	(.0019)	(.0017)	(.0016)	(.0015)
2.2	0.0503	0.0505	0.0508	0.0507	0.0504	0.8799	**0.6483**	0.7095	0.7425	0.7744
	(.0003)	(.0003)	(.0003)	(.0003)	(.0003)	(.0015)	(.0023)	(.0022)	(.0021)	(.0020)
2.6	0.0480	0.0499	0.0503	0.0506	0.0502	0.8487	**0.5199**	0.5884	0.6391	0.6777
	(.0003)	(.0003)	(.0003)	(.0003)	(.0003)	(.0017)	(.0025)	(.0025)	(.0025)	(.0023)
3.0	0.0468	0.0497	0.0500	0.0498	0.0505	0.8211	**0.3995**	0.4723	0.5305	0.5743
	(.0003)	(.0003)	(.0003)	(.0003)	(.0003)	(.0020)	(.0026)	(.0025)	(.0026)	(.0026)

the right (see Figure 5.2(c) and (d)). However, the clustering patterns of Models (c) or (d) are not as obvious as that of Models (a) or (b), thus the powers are actually lower than that in Models (a) and (b).

Consider the OC Model (e), which indicates that the variance at each of the design points dilates or shrinks and the covariance structure is unchanged. It is equivalent to changing the eigen-values of the variance-covariance matrix but not affecting the corresponding eigen-vectors. The results are summarized in Table 5.6. When $\delta > 1$, which indicates the dilation of process dispersion, the type-I error rates of the Hotelling's T^2 chart are roughly controlled at a certain level but not quite stable. In the case that the dispersion of the outliers shrinks, the type-I error rate of the T^2 chart increases as the level of shrinkage increases. This is because that the smaller dispersion of the outliers makes their T^2 statistics smaller and hence it is harder to detect them, whereas IC profiles have relatively larger T^2

Table 5.6: The type-I and type-II error rates and their standard errors (in parentheses) of OC Model (e) for $\alpha = 0.05$

	p_I					p_{II}				
δ	T^2	S(2)	S(3)	S(4)	S(5)	T^2(mod)	S(2)	S(3)	S(4)	S(5)
0.500	0.0953	0.0493	0.0491	0.0495	0.0495	1.0000	0.0000	**0.0000**	0.0000	0.0000
	(.0005)	(.0003)	(.0003)	(.0003)	(.0003)	(.0000)	(.0000)	(.0000)	(.0000)	(.0000)
0.625	0.0854	0.0494	0.0497	0.0496	0.0495	0.9998	0.0000	**0.0000**	0.0000	0.0000
	(.0004)	(.0003)	(.0003)	(.0003)	(.0003)	(.0001)	(.0000)	(.0000)	(.0000)	(.0000)
0.750	0.0739	0.0497	0.0497	0.0497	0.0493	0.9993	0.0057	**0.0055**	0.0057	0.0055
	(.0004)	(.0003)	(.0003)	(.0003)	(.0003)	(.0001)	(.0003)	(.0003)	(.0003)	(.0003)
0.875	0.0634	0.0501	0.0503	0.0501	0.0504	0.9938	0.5399	**0.5404**	0.5392	0.5397
	(.0004)	(.0003)	(.0003)	(.0003)	(.0003)	(.0004)	(.0025)	(.0025)	(.0025)	(.0025)
1.000	0.053	0.049	0.049	0.049	0.049	-	-	-	-	-
	(.0003)	(.0003)	(.0003)	(.0003)	(.0003)	-	-	-	-	-
1.143	0.0446	0.0498	0.0502	0.0502	0.0501	0.7982	0.6039	**0.6021**	0.6008	0.5999
	(.0003)	(.0003)	(.0003)	(.0003)	(.0003)	(.0019)	(.0024)	(.0024)	(.0025)	(.0024)
1.333	0.0407	0.0496	0.0498	0.0498	0.0494	0.4595	0.0362	**0.0355**	0.0356	0.0350
	(.0003)	(.0003)	(.0003)	(.0003)	(.0003)	(.0025)	(.0008)	(.0008)	(.0008)	(.0008)
1.600	0.0466	0.0494	0.0497	0.0496	0.0495	0.1128	0.0001	**0.0001**	0.0002	0.0002
	(.0003)	(.0003)	(.0003)	(.0003)	(.0003)	(.0015)	(.0000)	(.0001)	(.0001)	(.0001)
2.000	0.0519	0.0493	0.0491	0.0495	0.0493	0.0090	0.0000	**0.0000**	0.0000	0.0000
	(.0003)	(.0003)	(.0003)	(.0003)	(.0003)	(.0004)	(.0000)	(.0000)	(.0000)	(.0000)

statistics and hence easier to be misclassified. On the other hand, our proposed SMSS chart is quite robust to the change in dispersion in term of the type-I error rate. For the type-II error rate, the Hotelling's T^2 chart is able to detect outliers only in the dilation case but is almost useless in the shrinkage case. On the contrary, the SMSS chart is very powerful in detecting outliers whether the dispersion dilates or shrinks. Since both the dilatation and shrinkage of the dispersion lead to changes in the values of the T_0^2 and T_1^2 statistics, especially the T_1^2 statistic, the directions of the corresponding spatial sign vectors change and tend to concentrate

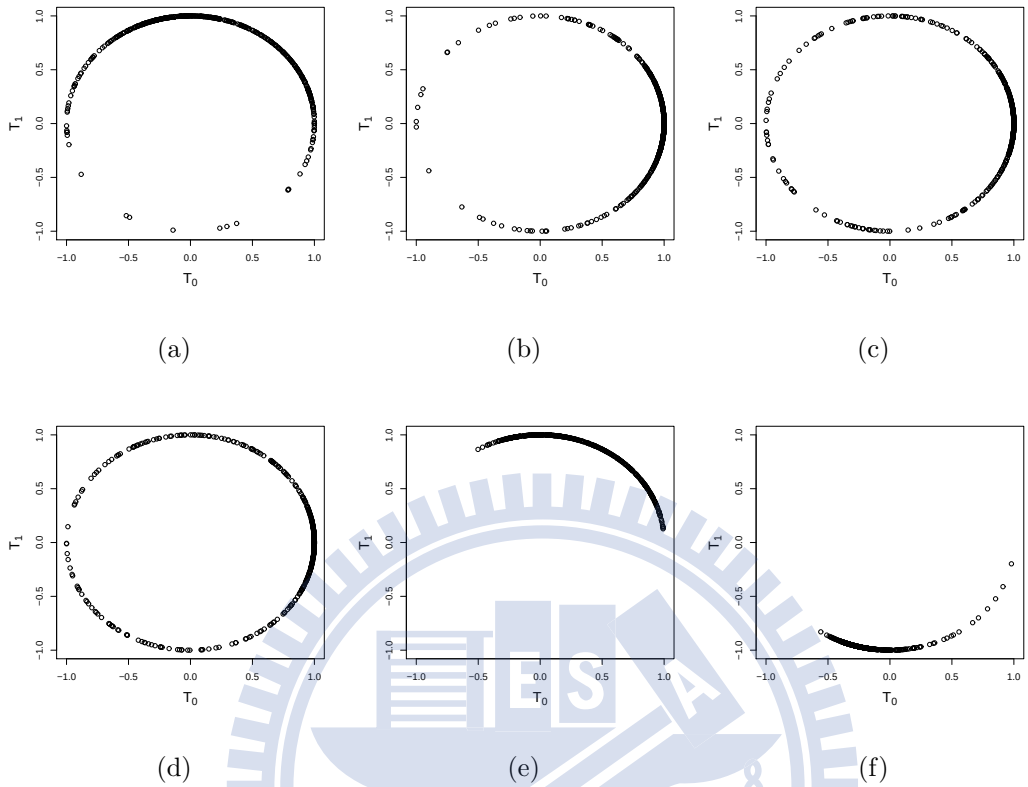

(a) (b) (c)

(d) (e) (f)

Figure 5.2: The scatter plots of the spatial sign vectors of the profiles generated from OC Models (a) - (e).

to the upper side of the unit circle for $\delta > 1$ (see Figure 5.2(e)), or the lower side for $\delta < 1$ (see Figure 5.2(f)). The more concentrated pattern of the spatial signs of the vectors $(T_0^2, T_1^2)'$ within a subgroup leads to a larger values of the Q statistic in the SMSS chart. It should be noticed that, although the Hotelling's T^2 chart was originally developed for the mean change, it has some power for detecting the process dispersion change because the contamination of the reference sample in dispersion also affects the estimation of the variance-covariance matrix. Nevertheless, we consider the Hotelling's T^2 chart in the comparison simply because there is no existing nonparametric monitoring scheme for the variance-covariance matrix of profiles or multivariate data so far.

Table 5.7: The type-I and type-II error rates and their standard errors (in parentheses) of OC Model (5.11) for $\alpha = 0.05$

	p_I					p_{II}				
δ	T^2	S(2)	S(3)	S(4)	S(5)	T^2(mod)	S(2)	S(3)	S(4)	S(5)
0.0	0.248	0.050	0.050	0.050	0.050	-	-	-	-	-
	(.0007)	(.0003)	(.0003)	(.0003)	(.0003)	-	-	-	-	-
0.6	0.2511	0.0505	0.0503	0.0503	0.0496	0.9357	0.9170	0.9236	**0.9164**	0.9235
	(.0008)	(.0003)	(.0003)	(.0003)	(.0003)	(.0011)	(.0013)	(.0013)	(.0013)	(.0012)
1.2	0.2473	0.0510	0.0503	0.0501	0.0505	0.8603	0.4521	0.5286	**0.3869**	0.4763
	(.0008)	(.0003)	(.0003)	(.0003)	(.0003)	(.0017)	(.0052)	(.0040)	(.0034)	(.0034)
1.8	0.2469	0.0495	0.0499	0.0493	0.0492	0.2845	0.0484	0.0374	**0.0119**	0.0188
	(.0007)	(.0003)	(.0003)	(.0003)	(.0003)	(.0058)	(.0037)	(.0016)	(.0005)	(.0008)
2.4	0.2465	0.0498	0.0494	0.0489	0.0489	0.0010	0.0017	0.0013	**0.0010**	0.0003
	(.0007)	(.0003)	(.0003)	(.0003)	(.0003)	(.0001)	(.0003)	(.0007)	(.0008)	(.0001)
3.0	0.2457	0.0488	0.0494	0.0495	0.0495	0.0000	0.0000	0.0000	**0.0000**	0.0000
	(.0007)	(.0003)	(.0003)	(.0003)	(.0003)	(.0000)	(.0000)	(.0000)	(.0000)	(.0000)

Analogous to the CS and CE charts introduced in Section 3.1.2, choosing the number of effective PCs K is also an issue in implementing the SMSS chart. According to the tables of total variation explained (in Appendix A.5), one may choose $K = 3$ for all the five OC models. However, the best choice of K is 2 for OC Models (b) and (d) from the aspect of the type-II error rate. Therefore, we suggest that one should try several candidates of K according to the percentage of the total variation explained. Note that the performance is not necessarily better when a larger K is chosen. If an unnecessary PC is chosen in computing the T_0^2 statistic, the weights of the effective PCs are diluted and hence the power of the SMSS chart degrades. Recall that a similar phenomenon was observed for the CS and CE charts and the same issue was discussed in Section 3.3.2.

To emphasize the ability in detecting outliers with mean shifts, we next consider profiles distributed further depart from the multivariate normal distribution.

Consider the IC profiles of the form:

$$y_{ij} = g_0(x_j) + f_i(x_j) + \varepsilon_{ij},\ i = 1, \ldots, m, j = 1, \ldots, p, \tag{5.11}$$

where $\{x_1, \ldots, x_p\}$ is the set of the design points equally spaced ranging from 0.025 to 0.975 with $p = 20$, $g_0(\cdot)$ is the fixed effect of the profile, $f_i(\cdot)$ is assumed following the multivariate t distribution $t_p(\nu)$ described in Section 4.2 with degrees of freedom $\nu = 3$ (the variance-covariance matrix used is $\mathbf{\Sigma}_{ij} = 0.5^{|i-j|}$) and $\{\varepsilon_{i1}, \ldots, \varepsilon_{ip}\}$ is the i.i.d. random noise from $N(\mathbf{0}, \sigma_\varepsilon^2)$, $\sigma_\varepsilon = 0.3$. This model is used to simulate profiles with the heavy-tailed distribution. Assume that $g_0(x) = 0$ and the OC profiles are generated by shifting the fixed effect to $g_1(x) = \delta \sin(2\pi(x - 0.5))$ where $\delta = 0(0.6)3$. Choose $\alpha = 0.05$. The results are summarized in Table 5.7. Note that the type-I error rates of the Hotelling's T^2 chart are quite stable but much larger than 0.05. As before, we adjust the control limit to control the type-I error rates around 0.05 for fair comparison. From Table 5.7, we observe that the SMSS chart outperforms the T^2 chart in terms of the type-II error rate. It shows that the SMSS chart has a better detecting power than the Hotelling's T^2 chart not only in the dispersion but also in the mean change when the underlying profile distribution is not too close to the normal distribution.

When implementing the SMSS chart, the spatial median and the Tyler's transformation matrix of the vector (T_0^2, T_1^2) need to be estimated numerically. We remark that, when solving equations (5.5) and (5.6), the solutions may not exist when the historical data contain very extreme outliers. Other than that, the SMSS chart is an efficient and powerful tool for monitoring profiles in Phase I applications and very easy to use for practitioners.

5.3.2 Phase II Applications

In this section, we demonstrate the use of the proposed SMSE chart in Phase II applications. The IC profiles are assumed from the simulated aspartame model of the form (3.11) in Section 3.3.1 and the same setting of the parameters in the

model are followed as in the last section. In Phase II analysis, the necessary parameters are assumed known or have been well estimated from the reference sample. In this study, the mean vector $\boldsymbol{\mu} = (\mu_1, \ldots, \mu_p)'$ and variance-covariance matrix $\boldsymbol{\Sigma} = [\sigma_{ij}]_{i,j=1,\ldots,p}$ of the aspartame model can be easily obtained as follows, for $i, j = 1, \ldots, p$,

$$\mu_j = \mu_I + \mu_M e^{\mu_N (x_j - 1)^2 + \frac{\sigma_N^2 (x_j - 1)^4}{2}} \tag{5.12}$$

$$\sigma_{ij} = \sigma_I^2 + \left(\mu_M^2 + \sigma_M^2\right) \left[e^{\mu_N [(x_i-1)^2 + (x_j-1)^2] + \frac{\sigma_N^2}{2} [(x_i-1)^2 + (x_j-1)^2]^2} \right] - \mu_M^2 e^{\mu_N [(x_i-1)^2 + (x_j-1)^2] + \frac{\sigma_N^2}{2} [(x_i-1)^4 + (x_j-1)^4]} + \sigma_\varepsilon^2 \delta_{ij}. \tag{5.13}$$

Note that the variance-covariance matrix is the same as that of the model used in Section 3.3.1, thus the corresponding eigen-values and eigen-vectors are the same as shown in Figure 3.3. Choose the number of the effective PCs $K = 3$ as presented in Section 3.3.3. The spatial median and the Tyler's transformation matrix of the vector $(T_0^2, T_1^2)'$ used in the SMSE chart can be obtained from the IC profiles in the historical data.

For comparison, the MENPC chart introduced in Section 3.3.3 is also considered in this case. Let the IC ARL be 200 and the weight parameter λ used in both EWMA charts be 0.2. Then the control limits for the SMSE chart and MENPC chart are 7.831 and 80.464, respectively. The results for different λ and IC ARL are similar, so we only present the results for $\lambda = 0.2$ and $ARL_0 = 200$. The ARLs reported in what follows are computed from 20,000 replications. In this case, the IC ARL computed by using the SMSE chart and the MENPC chart are 198.712 and 203.407, respectively; and the standard deviations of the run length (SDRL) are 193.036 and 197.295, respectively. Thus both charts show the distribution-free property in terms of the IC ARL.

Next, the ability of quickly detecting the OC condition in the process is evaluated and measured by the OC ARL. The OC profiles are generated from Models (a) - (e) in the last section, and the steady-state ARL is also considered when comparing the performance of the control charts. Recall that the steady-state ARL

Table 5.8: The ARL and SDRL of the SMSE and MENPC charts for Models (a) and (b).

	Model (a)				Model (b)			
	SMSE		MENPC		SMSE		MENPC	
δ	ARL	SDRL	ARL	SDRL	ARL	SDRL	ARL	SDRL
0.375	189.2151	189.7918	114.9635	111.2247	180.3218	181.0382	83.4508	80.2040
0.750	161.3417	160.5739	58.0028	54.7279	108.1268	104.7291	30.9931	26.8459
1.125	91.8636	88.7935	29.3029	25.2197	44.3060	39.1574	14.3316	10.0885
1.500	42.6466	37.4506	16.4312	12.0432	20.0643	14.8101	8.5383	4.8375
1.875	21.2911	16.0736	10.6402	6.4070	11.6113	6.7260	5.9502	2.8908
2.250	13.0676	8.1239	7.5461	3.8377	8.3089	3.7028	4.5815	1.9489
2.625	9.3023	4.6640	5.8841	2.6161	6.7974	2.4478	3.7561	1.4626
3.000	7.4911	3.0190	4.8182	1.9150	6.0389	1.8154	3.1900	1.1701

considers the case that the OC condition occurs only after $(\tau + 1)$th observation and thus any OC signal before τ would be discarded. Choose $\tau = 60$, and the results are summarized in Tables 5.8 - 5.10.

The results show that the MENPC has better performance in the mean shift and the SMSE is more powerful in detecting the dispersion change of the process. Roughly speaking, the charting statistic used in the MENPC chart considers the "smoothed" residual profiles that measures the departure between the incoming profile and the estimated mean profile $g(\cdot)$. Since the SMSE chart considers only the multivariate direction of $(T_0^2, T_1^2)'$, the MENPC is more sensitive in the mean change of the process than the SMSE chart. On the other hand, the charting statistic of the MENPC chart considers only the variance of the profiles at each set point x_j; but ignores the covariance structure of the profile, hence it is not as powerful as the SMSE chart in detecting variance-covariance matrix changes in the process.

Consider the OC Model (e) that simulates the situation that the dispersion of the process is dilated ($\delta > 1$) or shrunk ($\delta < 1$); and the results are tabulated in Table 5.10. For the ability of detecting shifts in dispersion, the SMSE chart

Table 5.9: The ARL and SDRL of the SMSE and MENPC charts for Models (c) and (d).

	Model (c)				Model (d)			
	SMSE		MENPC		SMSE		MENPC	
δ	ARL	SDRL	ARL	SDRL	ARL	SDRL	ARL	SDRL
1.125	183.0544	183.5335	179.2851	177.2393	168.3171	167.2262	156.1793	154.7999
1.250	154.2734	153.5871	157.5040	155.7514	127.7672	125.3543	120.7838	118.6060
1.375	122.4067	119.4684	138.3895	139.8465	91.5064	88.2415	91.3288	89.6974
1.500	93.6533	90.9547	117.1738	114.9733	65.9507	61.2346	70.1929	68.1510
1.625	73.7578	70.8436	102.1484	101.3781	50.8848	45.8203	54.6011	53.9370
1.750	57.8421	52.6144	85.1966	85.2647	40.2904	35.4151	42.2975	40.7447
1.875	47.3645	42.5198	72.0350	70.9165	32.8041	27.7809	34.9871	34.3236
2.000	39.6148	34.2434	60.2192	59.0845	27.4082	22.4492	28.6340	27.5080

is still better than the MENPC chart, especially in the shrinking case. When the dilation of the dispersion happens, the actual dispersion of the OC profiles is larger than the dispersion estimated from the reference sample; thus the values of the charting statistic of OC profiles would be larger than that of the IC profiles, making OC profiles easier to be detected by the MENPC chart. Oppositely, when the dispersion shrinks, OC profiles would be harder to detect. Therefore, the ARL of the MENPC chart becomes larger as the degree of the shrinkage gets larger. However, as described in the last section, both situations of the dispersion dilation and shrinkage lead to the directions of the spatial signs of the statistics T_0^2 and T_1^2 clustering to a certain side of the unit circle. Therefore, the SMSE chart performs better than the MENPC chart.

From the simulation results, the SMSE chart seems to be an omnibus method and any abnormal situations in the process could trigger the SMSE chart and signal an OC alarm. For diagnostic aids, one can observe patterns of the PC or rotated scores introduced in Section 3.2.3 to explore which part of the profiles has been out of control (see the demonstration in Section 3.3.3). It should be pointed out that for the SMSE chart to be effective, the OC condition has to sustained for

Table 5.10: The ARL and SDRL of the SMSE and MENPC charts for Model (e).

$\delta > 1$					$\delta < 1$				
	SMSE		MENPC			SMSE		MENPC	
δ	ARL	SDRL	ARL	SDRL	δ	ARL	SDRL	ARL	SDRL
1.0667	59.6925	53.8713	135.5452	134.3693	0.9375	57.1975	52.5514	286.7925	287.2256
1.1429	19.5107	13.6950	93.5927	92.4735	0.8750	17.0960	11.6072	428.2851	413.7034
1.2308	10.7207	5.4747	61.9159	59.9307	0.8125	9.0943	4.2046	660.2913	563.7220
1.3333	7.8351	2.9708	42.1941	41.1881	0.7500	6.6970	2.2430	931.4656	669.3491
1.4545	6.6311	2.0034	28.8630	27.2735	0.6875	5.8155	1.5481	1227.2587	697.9550
1.6000	6.0891	1.6027	19.8745	18.5785	0.6250	5.4617	1.3275	1485.3408	641.1092
1.7778	5.8423	1.4257	13.5191	12.2218	0.5625	5.2921	1.2512	1676.4782	534.1689
2.0000	5.6890	1.3670	9.3716	8.3404	0.5000	5.2225	1.2262	1795.8508	411.8930

a while such that the spatial sign of the two T^2 statistics would tend to cluster to a certain direction and hence leads to a large value of the charting statistic. The SMSE chart is not designed for detecting the abrupt and short-lived shifts in the process.

5.4 Real Data Application

In this section, we use the etching process in the semiconductor manufacturing to demonstrate our proposed distribution-free monitoring scheme. Lee et al. (2011) illustrated profiles of five sensors variables, denoted by V1-V5, for 364 wafers from 16 lots of an industrial etching process. For the original data, the lengths of profiles are different from wafer to wafer. They interpolated the profiles by using Akima splines (Akima, 1970) to synchronize the design points of the profiles. There are 547 synchronized points for each profile and they are divided into 23 steps. According to Lee et al. (2011), the variables V1-V4 are known to be related to plasma operations and V5 is the chamber temperature. In this dissertation, we analyze the profiles of variable V3 at step 9 with wafer size 363 from 16 lots and

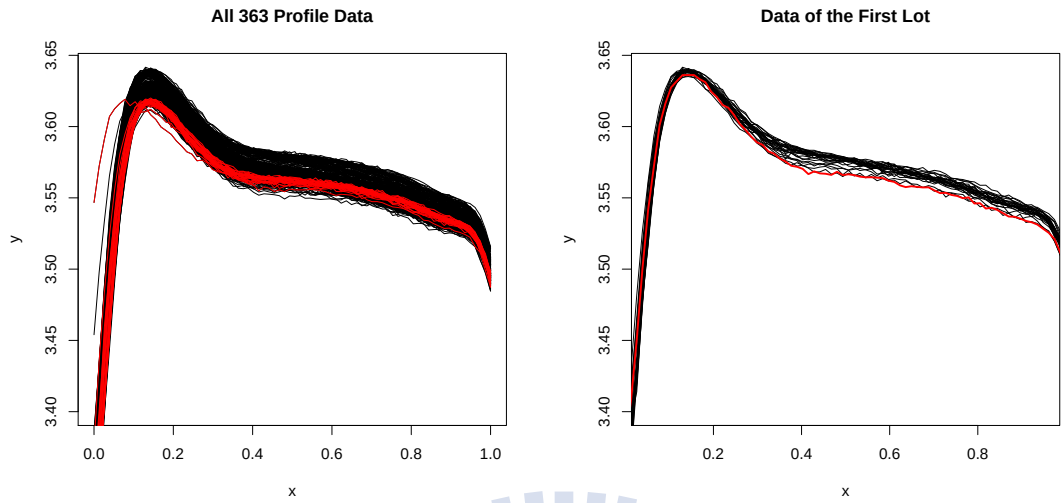

(a) (b)

Figure 5.3: The plots of the profile segments of variable V3 at step 9. (a) To show the long-term aging trend from wafer to wafer (the profiles of the last lot are highlighted in red) (b) To show the short-term first-wafer effect within a lot, the first wafer is highlighted in red.

78 design points. The scatter plot of the profiles is shown in Figure 5.3. Note that these data have been re-scaled to range from 3 to 4. A careful examination of the profiles in time order would reveal two unusual trends among wafers. One is a long-term aging trend that a lot produced at a later time would have lower profiles. Figure 5.3(a) illustrates this by highlighting the profiles of the last lot in red. The other is a short-term trend observed within a lot that the profile of the first wafer is substantially lower than the other wafers and the profiles move up gradually in order within the lot. Figure 5.3(b) plots the profiles of the first lot and highlights the first wafer in red. The peculiar behavior of the first wafer of a lot is the so-call "first-wafer effect". According to the subject-matter experts, both the long- and short-term trends are normal and should not cause alarms.

To eliminate the long-term aging and short-term first-wafer effects, we follow the procedure used in Lee et al. (2011) as follows. Denote $\boldsymbol{y}_i$ the ith profile with

78 design points, Lee et al. (2011) obtained the residual profiles as

$$\boldsymbol{e}_i = \boldsymbol{y}_i - \hat{\boldsymbol{\mu}} - \hat{b}_i \mathbf{1}, \tag{5.14}$$

where

$$\hat{\boldsymbol{\mu}} \equiv (\hat{\mu}_1, \ldots, \hat{\mu}_p)' = \frac{1}{m}\sum_{i=1}^{m} \boldsymbol{y}_i,$$

$$\hat{b}_i = \sum_{j=1}^{p} \hat{w}_{ij}(y_{ij} - \mu_j),$$

$$\hat{w}_{ij} = \frac{1/\hat{\sigma}_j^2}{\sum_{j'=1}^{p} 1/\hat{\sigma}_{j'}^2},$$

$$\hat{\sigma}_j = \frac{1}{d_2 m}\sum_{i=1}^{m}\{|y_{ij} - y_{i-1,j}|\},$$

$\mathbf{1} = (1, \ldots, 1)'$, $d_2 = 1.128$, $p = 78$, m is the size of the reference sample. Note that the level shifts caused by the long- and short-term effects can be captured by $\hat{\boldsymbol{\mu}}$ and $\hat{b}_i$, respectively. Thus, the level shift caused by these unstable effects can be eliminated if we use the residual profiles for monitoring. It should be noticed that the parameter estimators $\hat{\boldsymbol{\mu}}$ and $\hat{b}_i$'s used for future profile monitoring (in Phase II) have to be estimated from the IC profiles obtained from Phase I analysis.

To apply our proposed monitoring scheme, we need to group data in subgroups. Although these data were collected by lots, it is not appropriate to take the observations in a lot as a subgroup for two reasons. One is that the wafer size varies from lot to lot in this data set, a situation our methodology is not yet adapted to. The other is that the variation of the profiles within a lot is significant, which violates the principle of choosing subgroups. To demonstrate our monitoring scheme, we choose a small number of subgroup size, $n = 3$, to alleviate the effect caused by the variation between profiles.

Analogous to Lee et al. (2011), the first 222 profiles are treated as the historical data set in Phase I analysis. The corresponding residual profiles as in (5.14) are shown in Figure 5.4(a). Since the residual profiles look wiggly so we first smooth the data. In this case, we adopt the smoothing spline with the smoothing parameter

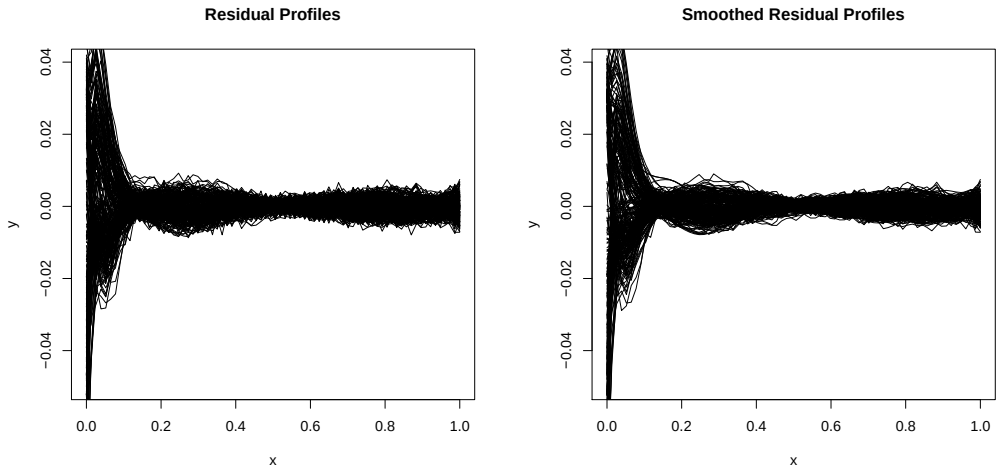

(a) (b)

Figure 5.4: (a) The plots of the first 222 residual profiles and (b) the corresponding smoothed estimates.

for each profile determined by the GCV method. This is easily done by using the R function "smooth.spline" with the default setting. Figure 5.4(b) shows the smoothed estimates of the residual profiles. By taking 3 profiles in a row to be a subgroup, we have 74 subgroups for Phase I analysis.

In this case, the mean vector and the variance-covariance matrix are estimated by equations (5.1) and (5.2). Applying PCA to the sample variance-covariance matrix of the historical data, the eigen-values-vectors and the corresponding PC scores are obtained. Since the first 3 PCs explain 94.51% of the total variation, we choose $K = 3$ to implement the SMSS chart. Let $\alpha = 0.01$. The control limit calculated from simulation is 5.8596 for $n = 3$. As a result, the 6th subgroup, i.e., the 16th, 17th, and 18th profiles, is detected by the proposed SMSS chart. The spatial signs of $(T_0^2, T_1^2)'$ and the values of the charting statistic Q are shown in Figure 5.5. From the figures, it can be observed that a subgroup with consistent multivariate directions for its observations tend to have a large value of the charting statistic. We remove the 6th subgroup and repeat the above steps with the remaining 219 profiles and find that no more subgroup is out of control. We take

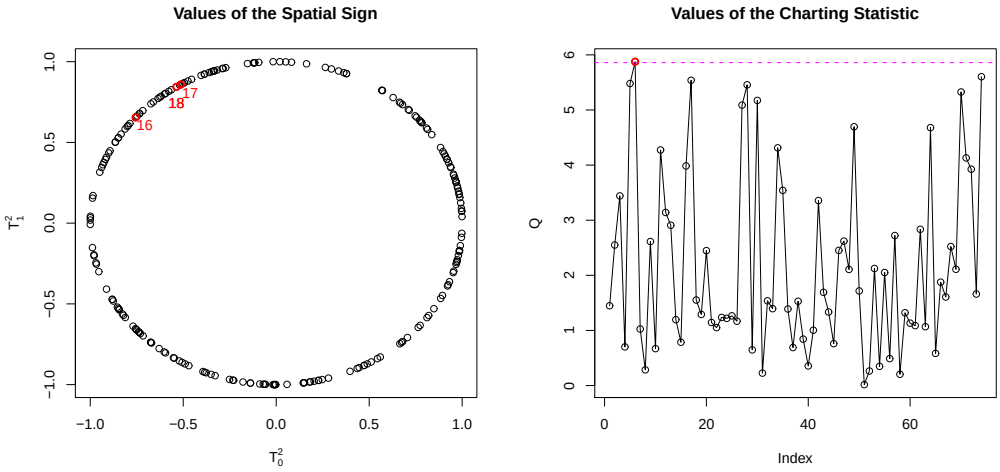

(a) (b)

Figure 5.5: (a) The spatial sign vectors of $(T_0^2, T_1^2)'$ and (b) the values of the charting statistic Q.

these 219 profiles as the reference sample for IC profiles. The first three eigenvectors of the sample variance-covariance matrix explain 94.57% of the total variation and their effect-visualizing plots are shown in Figure 5.6. It can be seen that most of the variation (77.89%) is from the front part of the profiles ($x < 0.2$) and is captured by the first PC. The second PC captures the variation on the interval $0.2 \leq x \leq 0.5$ and explains 12.32% of the total variation. Both the second and third PCs explain the variation for the design points larger than 0.5.

Next, the last 141 wafers are used to demonstrate the Phase II monitoring. The residual profiles obtained by subtracting the long- and short-term effects are monitored instead of the original profiles. Figure 5.7 show the plots of the residual profiles before and after smoothing by smoothing splines. Choosing $K = 3$, $ARL_0 = 370$, and $\lambda = 0.2$, the control limit is then 8.567 (from the table in Appendix A.3). Figure 5.8 shows the values of the charting statistic of the SMSE chart and it can be observed that there are many observations exceeding the control limit and should be regarded as OC cases. The corresponding spatial signs of the detected observations are labeled in red in Figure 5.9(a), and they tend to

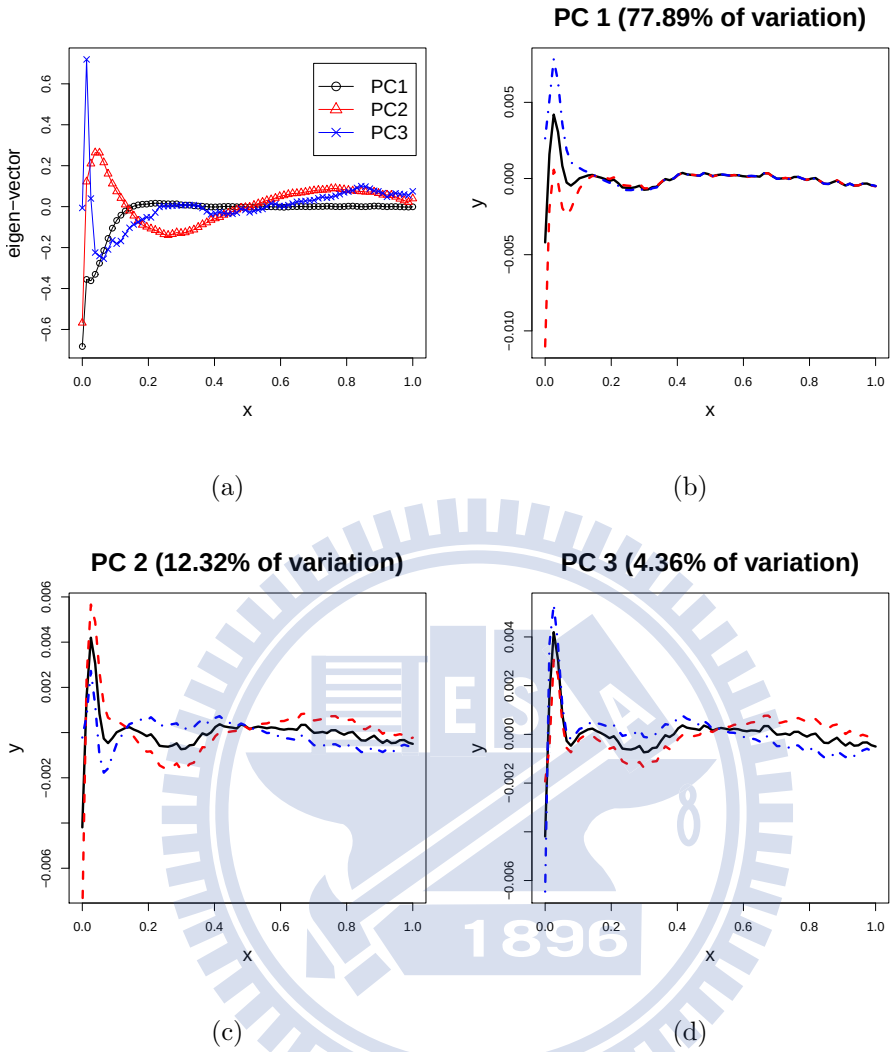

Figure 5.6: (a) The first three PCs and (b)-(d) the corresponding effect-visualizing plots.

concentrate to the upper-right part of the unit circle. Comparing with the reference profiles, 5.9(b) shows the reference and detected profiles colored by black and red, respectively. We can see that the detected profiles have similar patterns with lower values between $0.2 \leq x \leq 0.5$ and higher values at $x > 0.5$. The monitoring scheme we proposed regards the in-control state as profiles that vary randomly but within a normal level. Therefore, the profiles with similar patterns in a row tend to have larger values of charting statistic Q and are signaled by our proposed control chart.

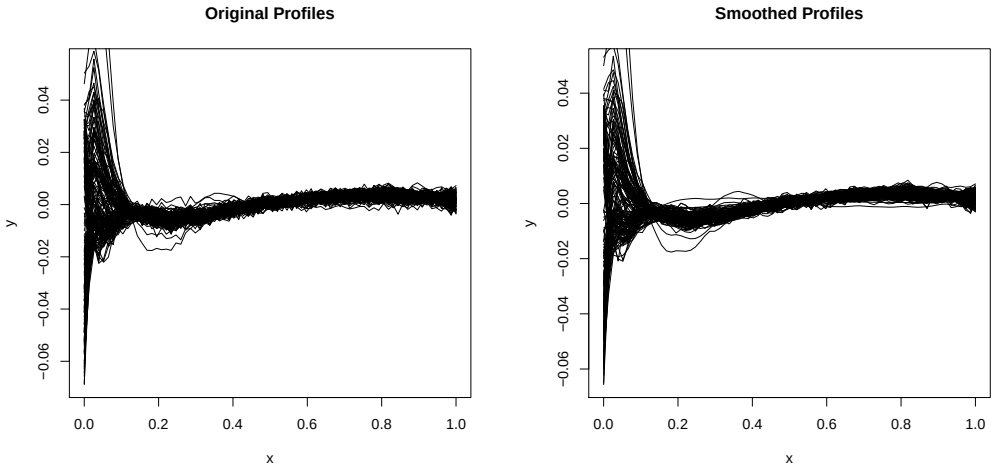

(a) (b)

Figure 5.7: (a) The plots of the 141 residual profiles used in Phase II analysis and (b) the corresponding smoothing estimates.

It should be pointed out that if we use the profiles after smoothing as the reference sample, the estimated scatter matrix may not be full-rank. In this example, the rank of the sample variance-covariance matrix is 58 but there are 78 design points. Thus, we only consider the PCs with positive eigen-values in the computation of T_1^2. Nevertheless, the computed first few eigenvectors can still explain the majority of the variation and then the T^2 statistic calculated based on the corresponding scores still has the ability to detect most changes of a process.

The analysis results of our proposed control charts in Phase I and II are quite different from that in Lee et al. (2011). The authors mentioned that, by taking the sum of square of the scaled residual profiles as the monitoring statistic, the 58th wafer in Phase I monitoring and the 287th and 357th wafers in Phase II were detected. However, the random effects of profiles were not considered in their monitoring procedure. In addition, the normality assumption was assumed in their method. However, from the normal Q-Q plots of the residual profiles at the first three design points, shown in Figure 5.10, the normality seems not satisfied for the data, and many of the entries of the variance-covariance matrix of the residual

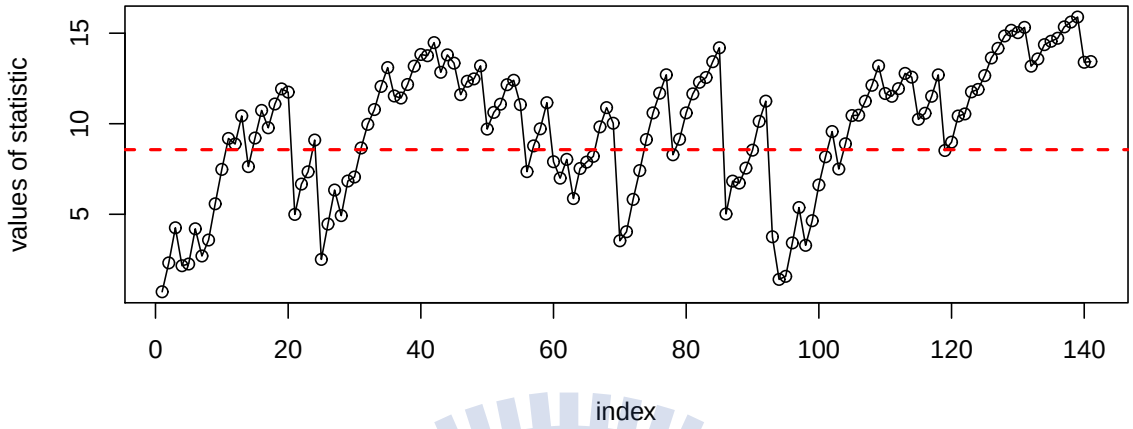

Figure 5.8: The values of the charting statistic of the SMSE chart (the dashed line is the control limit of $ARL_0 = 370$).

profiles (not shown here) are significantly large.

5.5 Conclusions

In this chapter, we propose distribution-free control charts for profile monitoring in the retrospective and prospective analyses. For Phase I, analogous to the last chapter, we consider the data with subgroups and the OAAT detecting procedure is used as well. The proposed SMSS chart is based on the spatial signs of the vector of T^2 statistics, $(T_0^2, T_1^2)'$, which are calculated from the standardized PC scores. Any kind of OC conditions, including location and scatter matrix shifts, lead to a concentration of the spatial signs to a certain direction and then would be detected by the SMSS chart. In addition, not only the dilation but also the shrinkage of the scatter matrix would be alarmed when using the SMSS chart. The simulation studies show that the SMSS chart is also robust to the outliers in the sense that the type-I error rate can be controlled at the specified level. In comparison, the traditional Hotelling's T^2 chart performs better in the case of the location shift

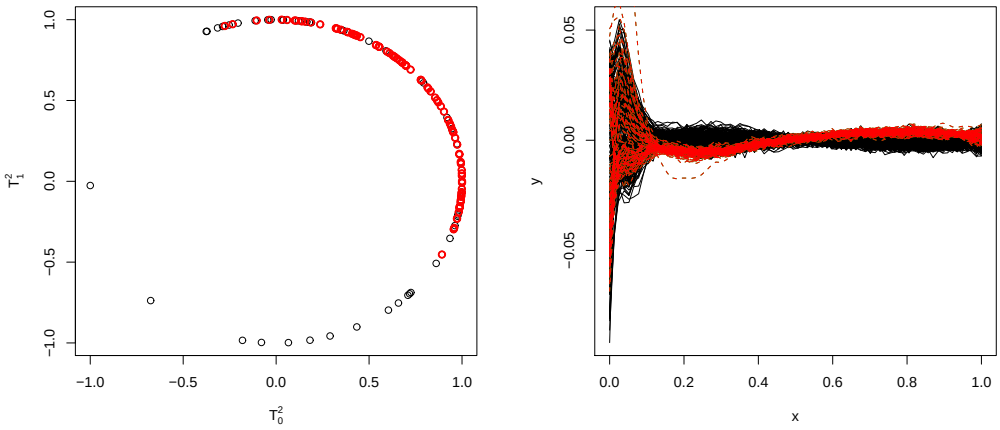

(a) (b)

Figure 5.9: (a) The spatial sign vectors of (T_0^2, T_1^2) (the red circles are the spatial signs detected as OC). (b) The detected OC profiles (red curves) and the reference profiles (black curves).

when the profiles are normally distributed. On the other hand, when the scatter matrix of the profile changes or the normality assumption is violated, the SMSS chart outperforms the Hotelling's T^2 chart.

It is well known that Shewhart-type control charts are not sensitive to small or moderate shifts in the process, so EWMA-type control charts are often considered in Phase II analysis. Similarly, the spatial signs of $(T_0^2, T_1^2)'$ are also considered and then the exponentially weighted sum of the signs are used to construct the control chart called the SMSE chart. In comparison, the MENPC chart, a distribution-free control chart proposed by Zou and Tsung (2011), performs better than the SMSE chart in the case of location shifts since their charting statistic measures the difference between the incoming profile and the target of the process while the SMSE chart considers only the multivariate directions. However, the SMSE chart outperforms the MENPC chart in the cases that the scatter matrix dilates and shrinks since both cases change the spatial sign vectors of $(T_0^2, T_1^2)'$ and hence provide the detecting power. We also perform a real case study in Phase I and II

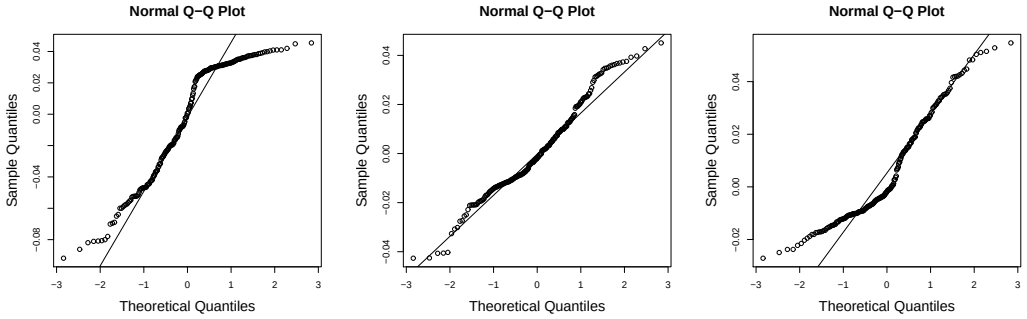

(a) (b) (c)

Figure 5.10: The Q-Q plots of the residual profiles at the first three design points.

monitoring to demonstrate the use of our proposed control charts.

Finally, in the use of our proposed sign-based control chart, the OC conditions occurring in the process are assumed to be the same within a subgroup in Phase I, and have to sustain for a period of time in Phase II applications. The detecting ability of the sign-based method relies on the cumulative effect of the signs of the observations concentrated to a certain part of the multi-dimensional unit circle when an OC condition occurs in the process. In Phase I application, if the observations within a subgroup are separately affected by different OC conditions, the directions of the corresponding spatial signs may not cluster on the unit circle and then the sign-based control chart might fail to detect them in this case. In Phase II monitoring, if a similar situation happens to the incoming observations, the sign-based EWMA chart might also fail to detect this kind of OC conditions.

Chapter 6

Conclusions and Future Works

In this dissertation, we have studied three topics for process monitoring. One is on the nonparametric control charting schemes of Phase I and II for profile data under the normality assumption. The second topic is on the distribution-free process monitoring methodology for multivariate data with rational subgroups in Phase I applications. Finally, the third topic is on the distribution-free profile monitoring methods for Phase I and II applications.

In Chapter 3, two control charts based on the PC scores of the profiles are developed for monitoring changes in the process. By choosing proper number of effective PCs, the profiles are projected onto the space spanned by the effective PCs and the corresponding complementary space, then the two T^2 statistics are used to summarize the information of a profile in these two spaces, respectively. A profile with a large value of any of the T^2 statistics could be regarded as an OC case. In Phase I analysis, a combined Shewhart-type control chart is constructed to detect the OC profiles in the historical data set and check the stability of the process. In Phase II process monitoring, the EWMA-type chart is more recommended than the Shewhart-type chart to enhance the ability of detecting small or moderate changes in the process. An combined EWMA-type chart is constructed for Phase II profile monitoring. Compared with the Hotelling's T^2 chart in Phase I and the MEWMA chart in Phase II that put an equal weight on each of the design points,

our methods emphasize more on the primary space and would be more efficient in detecting shifts in the primary space. Simulation studies show that our proposed control charting schemes are efficient and outperform some existing methods in detecting OC conditions, especially in the variance-covariance matrix. A real data set is used to demonstrate our methods. In addition, the PC scores or the rotated PC scores can help diagnose the OC conditions.

In Chapter 4, to obtain a distribution-free control chart, a charting statistic based on the spatial sign of a multivariate observation is utilized. By using the spatial sign function, multivariate observations are transformed to locate on the multi-dimensional unit circle and hence only the multivariate directions are preserved. Consider the data with subgroups, the subgroup with its observations clustering toward the same direction tends to have a large value of the charting statistic to trigger the OC alarm. It is shown by simulations that the sign-based control chart is robust to the distribution of the observations and the outlying subgroups in the historical data set. In addition, it is also very powerful in detecting outliers, especially when the data distribution is far from normal. Moreover, the OAAT detecting procedure is shown to be useful to control the type-I error rate at a specified level and is recommended for all Phase-I analysis.

In Chapter 5, we combine the ideas of spatial-sign-based methodology and the T^2 control chart to develop distribution-free schemes for profile monitoring. The two T^2 statistics based on the PC scores are computed as in Chapter 3. The distribution-free control chart for Phase I analysis is constructed by treating these T^2 statistics as two-dimensional vectors and then applying the sign-based control chart developed in Chapter 4 to the subgroups of the T^2 vectors directly. The proposed SMSS chart also shows the robustness property to the distribution of profiles and to the magnitude of shifts of the OC conditions. Moreover, it has ability detecting the outliers caused by not only the mean but also the dispersion shifts in the historical data set. In Phase II, we construct an EWMA chart for monitoring individual profiles (in contrast to the grouped profiles for the SMSS

chart in Phase I) based on the spatial sign of the two T^2 statistics. Comparing with some existing methods, the sign-based control chart is competitive in detecting mean shifts and much better in detecting dispersion changes. Since both the dilation and shrinkage of the dispersion will change the multivariate directions of the T^2 statistics, the sign-based control charts performs well in detecting the OC conditions caused by the dispersion increases or decreases.

Two issues arise in implementing the control charts proposed in this dissertation. One is the selection of the number of the effective PCs K. From the simulation studies (see Sections 3.3 and 5.3), we can observe that the charts are not necessary to perform better with a larger K. Practitioners can still choose a reasonable K with the help from experts. Nevertheless, it would be helpful to have an objective method to decide how many effective PCs one should use. Perhaps, one may construct a monitoring scheme by combining the information from the control charts with various numbers of the effective PCs. The other issue is on how many design points should be chosen when smoothing profiles. It is obvious that some features of the profile may lose if we choose too few design points. On the other hand, too many design points would lead to poor estimation of the variance-covariance matrix of the smoothed profiles with the limited amount of sample profiles. We would consider these two issues in our future studies.

There are limitations in the use of our proposed control charts. First, in the distribution-free monitoring schemes for multivariate data and profile data, the sample has to be collected in the manner of the rational subgroups. The process change is assumed to occur between the subgroups rather than within a subgroup. However, data in the form of rational subgroups are not always available, or it is sometimes hard to ensure that shifts only occur between the subgroups in real applications. Therefore, developing a distribution-free chart for individual multivariate data or profile data in Phase I analysis is regarded as one of our future works. Second, there is an inherent drawback of the sign-based control chart that it is not particularly sensitive to very large shifts since the magnitude of the shift

does not reflect on the sign vector fully. Thus, when extreme cases occur in the process, the sign-based chart is inferior to the Hotelling's T^2 chart, which utilizes the magnitude of the shift in the observations. It is worth to develop a distribution-free scheme that can overcome this drawback for profile data, which would be our immediate future study.

Appendix A

Tables

A.1 The Proportion of the Total Variation Explained by the CS Chart in Section 4.2

Table A.1: The proportion of the total variation explained by the CS chart for OC Model (a)

$\delta_2 = 0$					$\delta_1 = 0$				
δ_1	$K=1$	$K=2$	$K=3$	$K=4$	δ_2	$K=1$	$K=2$	$K=3$	$K=4$
0.625	0.7528	0.9468	0.9737	0.9818	0.875	0.7580	0.9483	0.9755	0.9831
1.250	0.7523	0.9489	0.9748	0.9826	1.750	0.7650	0.9508	0.9772	0.9843
1.875	0.7560	0.9521	0.9764	0.9837	2.625	0.7722	0.9530	0.9787	0.9853
2.500	0.7621	0.9561	0.9784	0.9851	3.500	0.7821	0.9556	0.9801	0.9863
3.125	0.7736	0.9603	0.9804	0.9865	4.375	0.7904	0.9578	0.9814	0.9872
3.750	0.7879	0.9645	0.9825	0.9879	5.250	0.7978	0.9595	0.9823	0.9878
4.375	0.8040	0.9685	0.9845	0.9893	6.125	0.8061	0.9614	0.9833	0.9884
5.000	0.8224	0.9720	0.9863	0.9905	7.000	0.8131	0.9631	0.9841	0.9890

Table A.2: The proportion of the total variation explained by the CS chart for OC Model (b)

$\delta_2 = 0$					$\delta_1 = 0$				
δ_1	$K = 1$	$K = 2$	$K = 3$	$K = 4$	δ_2	$K = 1$	$K = 2$	$K = 3$	$K = 4$
0.625	0.7519	0.9453	0.9727	0.9816	0.875	0.7507	0.9441	0.9716	0.9815
1.250	0.7502	0.9433	0.9706	0.9814	1.750	0.7495	0.9422	0.9697	0.9813
1.875	0.7470	0.9395	0.9671	0.9813	2.625	0.7483	0.9407	0.9682	0.9814
2.500	0.7431	0.9343	0.9626	0.9813	3.500	0.7460	0.9387	0.9665	0.9813
3.125	0.7372	0.9279	0.9585	0.9814	4.375	0.7450	0.9370	0.9649	0.9813
3.750	0.7311	0.9204	0.9570	0.9816	5.250	0.7443	0.9354	0.9635	0.9814
4.375	0.7246	0.9116	0.9569	0.9818	6.125	0.7431	0.9335	0.9621	0.9814
5.000	0.7168	0.9017	0.9571	0.9820	7.000	0.7406	0.9315	0.9607	0.9814

Table A.3: The proportion of the total variation explained by the CS chart for OC Model (c)

$\delta_2 = 0$					$\delta_1 = 0$				
δ_1	$K = 1$	$K = 2$	$K = 3$	$K = 4$	δ_2	$K = 1$	$K = 2$	$K = 3$	$K = 4$
0.625	0.7579	0.9468	0.9735	0.9820	0.875	0.7675	0.9484	0.9740	0.9827
1.250	0.7745	0.9495	0.9743	0.9832	1.750	0.7790	0.9504	0.9746	0.9836
1.875	0.7982	0.9537	0.9758	0.9850	2.625	0.7903	0.9522	0.9753	0.9844
2.500	0.8227	0.9585	0.9778	0.9870	3.500	0.8010	0.9543	0.9761	0.9853
3.125	0.8473	0.9635	0.9801	0.9888	4.375	0.8102	0.9560	0.9768	0.9860
3.750	0.8697	0.9683	0.9825	0.9905	5.250	0.8182	0.9576	0.9775	0.9866
4.375	0.8887	0.9727	0.9847	0.9919	6.125	0.8272	0.9594	0.9782	0.9873
5.000	0.9051	0.9764	0.9867	0.9931	7.000	0.8334	0.9607	0.9788	0.9877

A.2 Tables of Control Limits of the Multivariate Sign Shewhart Chart

Table A.4: The control limits of the MSS chart under various type-I error rate α and dimension p for subgroup size $n = 5$ and 10

	$n = 5$				$n = 10$			
$p \setminus \alpha$	0.1	0.05	0.025	0.01	0.1	0.05	0.025	0.01
2	4.5389	5.7682	6.7792	7.7785	4.5715	5.8551	7.0586	8.5575
3	6.0667	7.3357	8.5102	9.7727	6.1737	7.6045	8.9379	10.5843
4	7.5077	8.8700	10.0660	11.5485	7.6566	9.1953	10.6565	12.4936
5	8.8922	10.3998	11.6049	13.0823	9.0830	10.7347	12.2848	14.2150
6	10.2713	11.7759	13.2359	14.8293	10.4537	12.2223	13.8789	15.9152
7	11.5540	13.2178	14.7163	16.3313	11.8151	13.6604	15.3782	17.4833
8	12.8584	14.5475	16.0664	17.9817	13.1033	15.0439	16.8603	19.0399
9	14.1725	15.8923	17.5245	19.3744	14.4277	16.4375	18.2856	20.5399
10	15.4006	17.2440	18.9378	20.8904	15.7302	17.8252	19.7704	22.1752
11	16.6419	18.5921	20.3916	22.4674	16.9885	19.1807	21.1643	23.6199
12	17.9034	19.8679	21.5413	23.7267	18.2477	20.4850	22.5448	25.0914
13	19.1541	21.1886	22.9394	25.2508	19.4842	21.8235	23.9474	26.5164
14	20.3148	22.4179	24.3059	26.5638	20.7035	23.0850	25.2360	27.8857
15	21.5662	23.6894	25.6323	27.8837	21.9343	24.3785	26.5912	29.3195
16	22.8057	25.0329	27.0073	29.4227	23.1556	25.6759	27.9395	30.6781
17	23.9828	26.2942	28.3212	30.8493	24.3848	26.9657	29.3021	32.1036
18	25.0949	27.4015	29.3765	31.8791	25.6196	28.2124	30.6244	33.5328
19	26.2793	28.6728	30.8581	33.3985	26.7922	29.4739	31.9594	34.8218
20	27.4470	29.8996	32.0873	34.7946	27.9576	30.6992	33.1977	36.2590
25	33.3205	36.0910	38.4579	41.5408	33.9202	36.8936	39.6033	42.9360
30	39.1625	42.0398	44.6561	47.8261	39.7118	42.9243	45.8312	49.3391

Table A.5: The control limits of the MSS chart under various type-I error rate α and dimension p for subgroup size $n = 15$ and 20

	$n = 15$				$n = 20$			
$p \setminus \alpha$	0.1	0.05	0.025	0.01	0.1	0.05	0.025	0.01
2	4.5948	5.8987	7.1748	8.8162	4.5749	5.9201	7.2021	8.8511
3	6.1961	7.6485	9.0442	10.8323	6.2061	7.7120	9.1500	11.0124
4	7.6904	9.2785	10.7962	12.6838	7.7131	9.3499	10.8945	12.8687
5	9.1237	10.8420	12.4617	14.5048	9.1686	10.9125	12.5810	14.6331
6	10.5325	12.3693	14.0671	16.1757	10.5595	12.4142	14.1588	16.3678
7	11.8915	13.8148	15.5928	17.7889	11.9041	13.8440	15.6789	17.9441
8	13.2105	15.2424	17.1085	19.4374	13.2336	15.2844	17.1981	19.6085
9	14.4891	16.5736	18.4977	20.9268	14.5462	16.6549	18.6058	21.1165
10	15.8339	17.9918	19.9934	22.4393	15.8702	18.0531	20.1194	22.6562
11	17.0645	19.3292	21.4278	23.9792	17.1307	19.4354	21.5705	24.1854
12	18.3266	20.6495	22.7847	25.4407	18.3880	20.7335	22.9135	25.6144
13	19.5746	21.9864	24.1762	26.8358	19.6605	22.1047	24.3477	27.1126
14	20.8375	23.2869	25.5302	28.3439	20.8902	23.3543	25.6411	28.4310
15	22.0739	24.5764	26.8830	29.7576	22.0950	24.6778	27.0605	29.9846
16	23.2740	25.8547	28.2195	31.1366	23.3689	26.0200	28.4325	31.3664
17	24.4967	27.1260	29.5482	32.4618	24.6034	27.2845	29.7590	32.7777
18	25.7506	28.4538	30.9518	33.9521	25.8153	28.5557	31.0746	34.1523
19	26.9336	29.6845	32.2148	35.3386	27.0267	29.8468	32.3885	35.5418
20	28.1275	30.9316	33.4771	36.6063	28.1868	31.0855	33.6976	36.9528
25	34.0688	37.1609	40.0127	43.3410	34.1323	37.2538	40.0952	43.5510
30	39.8844	43.1692	46.1795	49.8073	39.9551	43.3526	46.4096	50.1125

Table A.6: The control limits of the MSS chart under various type-I error rate α and dimension p for subgroup size $n = 25$ and 30

	$n = 25$				$n = 30$			
$p \setminus \alpha$	0.1	0.05	0.025	0.01	0.1	0.05	0.025	0.01
2	4.5969	5.9323	7.2532	9.0101	4.5758	5.9259	7.2485	9.0051
3	6.2078	7.7049	9.1790	11.0241	6.2331	7.7519	9.2297	11.1513
4	7.7203	9.3569	10.9231	12.8965	7.7342	9.3907	10.9716	13.0132
5	9.1614	10.9274	12.6019	14.7518	9.1799	10.9619	12.6337	14.7992
6	10.5650	12.4407	14.2176	16.4556	10.5954	12.5019	14.2797	16.5167
7	11.9317	13.9013	15.7464	18.0505	11.9504	13.9441	15.8339	18.1980
8	13.2761	15.3493	17.2716	19.6415	13.2920	15.3580	17.2825	19.7480
9	14.5949	16.7419	18.7153	21.1827	14.5837	16.7397	18.7789	21.3008
10	15.8750	18.1014	20.2147	22.8614	15.9003	18.1677	20.2380	22.8513
11	17.1554	19.4623	21.5732	24.2315	17.1565	19.5131	21.6699	24.3546
12	18.4181	20.8187	23.0376	25.8133	18.4289	20.8098	23.0430	25.8060
13	19.7097	22.1626	24.4559	27.2530	19.7085	22.1698	24.4997	27.2885
14	20.8986	23.4305	25.7247	28.6052	20.9408	23.4863	25.8037	28.7288
15	22.1728	24.7444	27.1174	30.1143	22.1892	24.7839	27.1377	30.1685
16	23.3560	26.0232	28.4791	31.4578	23.3953	26.0618	28.5017	31.4997
17	24.6418	27.3516	29.8263	32.8996	24.6458	27.3835	29.8989	32.9755
18	25.8307	28.5542	31.1184	34.2296	25.8474	28.6315	31.2225	34.3444
19	27.0128	29.8253	32.4208	35.5711	27.0559	29.9278	32.5072	35.7386
20	28.2325	31.1411	33.7572	36.9613	28.2953	31.2305	33.8721	37.1395
25	34.1595	37.3272	40.2456	43.6676	34.2010	37.3909	40.2615	43.7520
30	40.0298	43.4266	46.5425	50.3403	40.0452	43.5088	46.6283	50.3244

A.3 Table of Control Limits of the Multivariate Sign EWMA Chart

Table A.7: The control limits of the multivariate sign EWMA chart for $p = 2$

$\lambda \setminus ARL_0$	200	370	500
0.4	6.009	6.276	6.390
0.2	7.831	8.576	8.904
0.1	8.043	9.183	9.716
0.05	7.225	8.605	9.265
0.025	5.895	7.399	8.126

A.4 The Results of the Type-I and Type-II Error Study of the Wine Data

Table A.8: The type-I and type-II error rates for size 20

Level 6	p_I			p_{II}		
index	MSS	T^2	T^2(mod)	MSS	T^2	T^2(mod)
1	0.0000	0.2818	0.0182	0.50	0.10	0.75
2	0.0091	0.3273	0.0091	0.60	0.15	0.80
3	0.0091	0.2727	0.0091	0.65	0.25	0.95
4	0.0000	0.3000	0.0182	0.50	0.00	0.75
5	0.0000	0.3091	0.0182	0.60	0.10	0.60
6	0.0000	0.3000	0.0182	0.60	0.00	0.75
7	0.0000	0.3000	0.0091	0.15	0.00	0.10
8	0.0000	0.2818	0.0091	0.65	0.05	0.75
9	0.0000	0.3000	0.0182	0.65	0.05	0.60
Level 5	p_I			p_{II}		
1	0.0000	0.3000	0.0182	0.50	0.00	0.50
2	0.0000	0.3000	0.0182	0.45	0.00	0.55
3	0.0000	0.3000	0.0182	0.40	0.00	0.20
4	0.0000	0.3000	0.0091	0.65	0.00	0.60
5	0.0000	0.3000	0.0091	0.65	0.05	0.70
6	0.0000	0.3273	0.0182	0.70	0.25	0.85
7	0.0000	0.3000	0.0182	0.40	0.00	0.70
8	0.0000	0.3000	0.0182	0.40	0.00	0.65
9	0.0000	0.3000	0.0091	0.15	0.00	0.50

A.5 The Proportion of the Total Variation Explained by the SMSS Chart of Simulations in Section 5.3.1

Table A.9: The proportion of the total variation explained by the SMSS chart for OC Model (a) and (b)

	Model (a)				Model (b)			
δ	$K=2$	$K=3$	$K=4$	$K=5$	$K=2$	$K=3$	$K=4$	$K=5$
0.6	0.9504	0.9800	0.9879	0.9936	0.9516	0.9803	0.9881	0.9937
1.2	0.9491	0.9802	0.9880	0.9936	0.9537	0.9811	0.9886	0.9939
1.8	0.9468	0.9804	0.9881	0.9937	0.9566	0.9823	0.9893	0.9943
2.4	0.9439	0.9806	0.9882	0.9938	0.9600	0.9837	0.9902	0.9948
3.0	0.9405	0.9810	0.9885	0.9939	0.9638	0.9852	0.9911	0.9953

Table A.10: The proportion of the total variation explained by the SMSS chart for OC Model (c) and (d)

	Model (c)				Model (d)			
δ	$K=2$	$K=3$	$K=4$	$K=5$	$K=2$	$K=3$	$K=4$	$K=5$
1.4	0.9495	0.9801	0.9880	0.9936	0.9528	0.9808	0.9884	0.9938
1.8	0.9479	0.9803	0.9880	0.9937	0.9552	0.9817	0.9889	0.9941
2.2	0.9457	0.9805	0.9882	0.9937	0.9578	0.9828	0.9896	0.9945
2.6	0.9432	0.9807	0.9883	0.9938	0.9604	0.9839	0.9902	0.9948
3.0	0.9407	0.9809	0.9884	0.9939	0.9634	0.9851	0.9909	0.9952

Table A.11: The proportion of the total variation explained by the SMSS chart for OC Model (e)

$\delta > 0$					$\delta < 0$				
δ	$K=2$	$K=3$	$K=4$	$K=5$	δ	$K=2$	$K=3$	$K=4$	$K=5$
1.143	0.9509	0.9800	0.9879	0.9936	0.875	0.9509	0.9800	0.9879	0.9936
1.333	0.9510	0.9800	0.9879	0.9936	0.750	0.9510	0.9800	0.9879	0.9936
1.600	0.9509	0.9800	0.9879	0.9936	0.625	0.9509	0.9800	0.9879	0.9936
2.000	0.9508	0.9800	0.9879	0.9936	0.500	0.9508	0.9800	0.9879	0.9936

Appendix B

B.1 ARL Calculation of The Combined EWMA Chart

An approximation of the ARL of the CE chart can be obtained via approximating the properties of the continuous-state two-dimensional Markov chain $\{(W_{0,i}, W_{1,i}, i = 0, 1, \cdots)\}$ by a two-dimensional Markov chain with discrete-state space. By the independency of the T_0^2 and T_1^2 statistics as well as the $W_{0,i}$ and $W_{1,i}$, the two-dimensional chain can be described by two one-dimensional chains, one for each individual EWMA chart. Following Morais and Pacheco (2000) and others, the Markovian ARL approximation is introduced as follows.

First, dividing the in-control interval $C_l = (0, L_l)$ into $v - 1$ subintervals with equal range, $l = 0, 1$, where L_0 and L_1 are defined in equations (3.9) and (3.10), respectively. That is, for each subinterval $E_j = (e_j, e_{j+1})$, where $e_j = L_l(j-1)/(v-1)$, $j = 1, \ldots, v$. Define the absorbing state of each chain as $(-\infty, 0) \cup (L_l, \infty)$ for each l. Then an approximation of the probability transition matrix of each individual Markov chain is

$$\boldsymbol{P}_l(\boldsymbol{\delta}) = \begin{pmatrix} \boldsymbol{Q}_l(\boldsymbol{\delta}) & [\boldsymbol{I}_{v-1} - \boldsymbol{Q}_i(\boldsymbol{\delta})] \times \mathbf{1}_{v-1} \\ \mathbf{0}'_{v-1} & 1 \end{pmatrix},$$

where $\mathbf{1}_{v-1}$ and $\mathbf{0}_{v-1}$ are vectors of ones and zeros with dimension $v-1$, respectively, $\boldsymbol{I}_{v-1}$ is the identity matrix with rank $v-1$, $\boldsymbol{\delta}$ is the vector of mean difference between IC and OC cases, and the matrix $\boldsymbol{Q}_l(\boldsymbol{\delta})$ has entries given by

$$q_{l,jk} = P\left\{W_{l,i} \in E_j \middle| W_{l,i-1} = \frac{e_k + e_{k+1}}{2}, \boldsymbol{\delta}\right\}.$$

Under the normality assumption, the T_0^2 and T_1^2 follow the non-central χ^2 distribution with degrees of freedom K and $n-K$ and the non-centrality parameters $\boldsymbol{\delta}'\boldsymbol{P}_0\boldsymbol{\Lambda}_0^{-1}\boldsymbol{P}_0'\boldsymbol{\delta}$ and $\boldsymbol{\delta}'\boldsymbol{P}_1\boldsymbol{\Lambda}_1^{-1}\boldsymbol{P}_1'\boldsymbol{\delta}$, respectively, where $\boldsymbol{P}_0$, $\boldsymbol{P}_1$, $\boldsymbol{\Lambda}_0$, and $\boldsymbol{\Lambda}_1$ are given in Section 3.2. Therefore, the entries of $\boldsymbol{Q}_l(\boldsymbol{\delta})$ are of the form

$$q_{l,jk} = F_d(a_{j,k+1}) - F_d(a_{j,k}),$$

where

$$a_{j,k} = \frac{L_l}{\lambda(v-1)}\big((k-1) - (1-\lambda)(j-0.5)\big), \qquad j,k = 1,\ldots,v-1,$$

and F_d is the distribution function of χ^2 distribution with degrees of freedom d, and $d = K$ if $l = 0$, $n-K$ if $l = 1$.

Let $RL_0^{\alpha}(\boldsymbol{\delta})$, $RL_1^{\beta}(\boldsymbol{\delta})$, and $RL_{CE}^{\alpha,\beta}(\boldsymbol{\delta})$ denote the run length of the T_0^2, T_1^2, and CE charts, respectively, conditional on $\boldsymbol{\delta}$ and the initial values of $W_{0,0}$ and $W_{1,0}$, which belong to the transient states E_α and E_β, respectively. Define $\boldsymbol{p}_\alpha$ to be a vector with one at the position α and zeros at the rest, and $\boldsymbol{p}_\beta$ similarly. Then the survival function of RL_0^{α}, RL_1^{β}, and $RL_{CE}^{\alpha,\beta}$ can be approximated by

$$\begin{aligned} F_{RL_0^{\alpha}(\boldsymbol{\delta})}(s) &= P\big[RL_0^{\alpha}(\boldsymbol{\delta}) > s\big] \\ &= \begin{cases} 1, & \text{if } s < 1 \\ \boldsymbol{p}_\alpha' \times \big[\boldsymbol{Q}_0(\boldsymbol{\delta})\big]^{[s]} \times \mathbf{1}_{v-1}, & \text{if } s \geq 1 \end{cases} \end{aligned}$$

$$\begin{aligned} F_{RL_1^{\beta}(\boldsymbol{\delta})}(s) &= P\big[RL_1^{\beta}(\boldsymbol{\delta}) > s\big] \\ &= \begin{cases} 1, & \text{if } s < 1 \\ \boldsymbol{p}_\beta' \times \big[\boldsymbol{Q}_1(\boldsymbol{\delta})\big]^{[s]} \times \mathbf{1}_{v-1}, & \text{if } s \geq 1 \end{cases} \end{aligned}$$

$$
\begin{aligned}
F_{RL_{CE}^{\alpha,\beta}(\boldsymbol{\delta})}(s) &= P\big[RL_{CE}^{\alpha,\beta}(\boldsymbol{\delta}) > s\big] \\
&= P\big[\min\{RL_0^{\alpha}(\boldsymbol{\delta}), RL_1^{\beta}(\boldsymbol{\delta})\} > s\big] \\
&= F_{RL_0^{\alpha}(\boldsymbol{\delta})}(s) \times F_{RL_1^{\beta}(\boldsymbol{\delta})}(s) \text{ for } -\infty < s < \infty,
\end{aligned}
$$

where $[s]$ denotes the integer part of s. Finally, the approximations of the ARLs of the T_0^2, T_1^2, and CE charts are given by

$$
\begin{aligned}
ARL_{T_0^2}(\boldsymbol{\delta}) &= \sum_{s=0}^{\infty} F_{RL_0^{\alpha}(\boldsymbol{\delta})}(s) \\
&= \boldsymbol{p}_{\alpha}' \times \big[\boldsymbol{I}_{v-1} - \boldsymbol{Q}_0(\boldsymbol{\delta})\big]^{-1} \times \mathbf{1}_{v-1}, \\
ARL_{T_1^2}(\boldsymbol{\delta}) &= \sum_{s=0}^{\infty} F_{RL_1^{\beta}(\boldsymbol{\delta})}(s) \\
&= \boldsymbol{p}_{\beta}' \times \big[\boldsymbol{I}_{v-1} - \boldsymbol{Q}_1(\boldsymbol{\delta})\big]^{-1} \times \mathbf{1}_{v-1}, \\
ARL_{CE}(\boldsymbol{\delta}) &= \sum_{s=0}^{\infty} F_{RL_0^{\alpha}(\boldsymbol{\delta})}(s) \times F_{RL_1^{\beta}(\boldsymbol{\delta})}(s).
\end{aligned}
$$

Note that the number of partition of the in-control interval, $v-1$, should be odd. Moreover, one should choose a larger v for the wider range of the in-control interval. In our simulations and real case studies, v is chosen to be 52 for the T_0^2 part of the CE chart, and 102 for the T_1^2 part.

Bibliography

Akima, H. (1970), "A New Method of Interpolation and Smooth Curve Fitting Based on Local Procedures," *Journal of the Association for Computing Machinery*, 17, 589–602.

Alt, F. A. (1984), "Multivariate Quality Control," *The Encyclopedia of Statistical Science*, 6, 110–122.

Anderson, T. W. (2003), *An Introduction to Multivariate Statistical Analysis (3rd ed.)*, Wiley.

Boone, J. M. and Chakraborti, S. (2012), "Two Simple Shewhart-type Multivariate Nonparametric Control Charts," *Applied Stochastic Models in Business and Industry*, 28, 130–140.

Chakraborty, B., Chaudhuri, P., and Oja, H. (1998), "Operating Transformation Retransformation on Spatial Median and Angle Test," *Statistica Sinica*, 8, 767–784.

Champ, C. W. and Jones, L. A. (2004), "Designing Phasi I $\bar{X}$ Charts with Small Sizes," *Quality Reliability Engineering International*, 20, 497–510.

Cheng, C.-Y. (2009), "Pfofile Monitoring via Simplicial Data Depth," Master's thesis, National Chiao Tung University.

Chicken, E., Pignatiello, JR., J. J., and Simpson, J. R. (2009), "Statistical Process Monitoring of Nonlinear Profiles Using Wavelets," *Journal of Quality Technology*, 41, 198–212.

Colosimo, B. M., Semeraro, Q., and Pacella, M. (2008), "Statistical Process Control for Geometric Specifications: On the Monitoring of Roundness Profiles," *Journal of Quality Technology*, 40, 1–18.

Cortez, P., Cerdeira, A., Almeida, F., Matos, T., and Reis, J. (2009), "Modeling Wine Preferences by Data Mining from Physicochemical Properties," *Decision Support Systems*, 47, 547–553.

Craven, P. and Wahba, G. (1979), "Smoothing Noisy Data with SplineFunctions: Estimating the Correct Degree of Smoothing by the Method of Generalized Crossvalidation," *Numerische Mathematik*, 31, 377–403.

Crosier, R. B. (1988), "Multivariate Generalizations of Cumulative Sum Quality-Control Schemes," *Technometrics*, 30, 291–303.

Cuevas, A., Febrero, M., and Fraiman, R. (2006), "On The Use of Bootstrap for Estimating Functions with Functional Data," *Computational Statistics and Data Analysis*, 51, 1063–1074.

— (2007), "Robust Estimation and Classification for Functional Data via Projection-Based Depth Notions," *Computational Statistics*, 22, 481–496.

Ding, Y., Zeng, L., and Zhou, S. (2006), "Phase I Analysis for Monitoring Nonlinear Profiles in Manufacturing Processes," *Journal of Quality Technology*, 38, 199–216.

Eyvazian, M., Noorossan, R., Saghaei, A., and Amiri, A. (2011), "Phase II Monitoring of Multivariate Multiple Linear Regression Profiles," *Quality and Reliability Engineering International*, 27, 281–296.

Fan, J. and Gijbels, I. (1996), *Local Polynomial Modelling and Its Applications*, Chapman & Hall.

Fan, J., Zhang, C., and Zhang, J. (2001), "Generalized Likelihood Ratio Statistics and Wilks Phenomenon," *The Annals of Statistics*, 29, 153–193.

Febrero, M., Galeano, P., and González-Manteiga, W. (2008), "Outlier Detection in Functional Data by Depth Measures, with Application to Identify Abnormal NOx Levels," *Environmetrics*, 19, 331–345.

Fraiman, R. and Muniz, G. (2001), "Trimmed Means for Functional Data," *Test*, 10, 419–440.

Gu, C. (2002), *Smoothing Spline ANOVA Models*, Springer.

Hamurkaroğlu, C., Mert, M., and Saykan, Y. (2004), "Nonparametric Control Charts Based on Mahalanobis Depth," *Hacettepe Journal of Mathematics and Statistics*, 33, 57–67.

Hawkins, D. M. and Maboudou-Tchao, E. M. (2007), "Self-Starting Multivariate Exponentially Weighted Moving Average Control Charting," *Technometrics*, 49, 199–209.

— (2008), "Multivariate Exponentially Weighted Moving Covariance Matrix," *Technometrics*, 50, 155–166.

Hawkins, D. M. and Olwell, D. H. (1998), *Cumulative Sum Charts and Charting for Quality Improvement*, Springer.

Hettmansperger, T. P. and Randles, R. H. (2002), "A Practical Affine Equivariant Multivariate Median," *Biometrika*, 89, 851–860.

Huwang, L., Yeh, A. B., and Wu, C.-W. (2007), "Monitoring Multivariate Process Variability for Individual Observations," *Journal of Quality Technology*, 39, 258–278.

Hyvärinen, A., Karhunen, J., and Oja, E. (2001), *Independent Component Analysis*, Wiley.

Jensen, W. A. and Birch, J. B. (2009), "Profile Monitoring via Nonlinear Mixed Models," *Journal of Quality Technology*, 41, 18–34.

Jensen, W. A., Birch, J. B., and Woodall, W. H. (2007), "High Breakdown Estimation Methods for Phase I Multivariate Control Charts," *Quality and Reliability Engineering International*, 23, 615–629.

— (2008), "Monitoring Correlation Within Linear Profiles Using Mixed Models," *Journal of Quality Technology*, 40, 167–183.

Jeong, M. K., Lu, J.-C., and Wang, N. (2006), "Wavelet-Based SPC Procedure for Complicated Functional Data," *International Journal of Production Research*, 44, 729–744.

Jin, J. and Shi, J. (2001), "Automatic Feature Extraction of Waveform Signals for In-Process Diagnostic Performance Improvement," *Journal of Intelligent Manufacturing*, 12, 257–268.

Jones-Farmer, L. A. and Champ, C. W. (2010), "A Distribution-Free Phase I Control Chart for Subgroup Scale," *Journal of Quality Technology*, 42, 373–387.

Jones-Farmer, L. A., Jordan, V., and Champ, C. W. (2009), "Distribution-Free Phase I Control Charts for Subgroup Location," *Journal of Quality Technology*, 41, 304–316.

Kang, L. and Albin, S. L. (2000), "On-line Monitoring When the Process Yields a Linear Profile," *Journal of Quality Technology*, 32, 418–426.

Kazemzadeh, R. B., Noorossana, R., and Amiri, A. (2008), "Phase I Monitoring of Polynomial Profiles," *Communications in Statistics-Theory and Methods*, 37, 1671–1686.

— (2009), "Monitoring Polynomial Profiles in Quality Control Applications," *The International Journal of Advanced Manufacturing Technology*, 42, 703–712.

Kim, K., Mahmoud, M. A., and Woodall, W. H. (2003), "On the Monitoring of Linear Profiles," *Journal of Quality Technology*, 35, 317–328.

Lada, E. K., Lu, J.-C., and Wilson, J. R. (2002), "A Wavelet-Based Procedure for Process Fault Detection," *IEEE Transations on Semiconductor Manufacturing*, 15, 79–90.

Lee, S.-P., Chao, A.-K., Tsung, F., Wang, D. S. H., Tseng, S.-T., and Jang, S.-S. (2011), "Monitoring Batch Processes with Multiple On-Off Steps in Semiconductor Manufacturing," *Journal of Quality Technology*, 43, 142–157.

Liu, R. Y. (1990), "On a Notion of Data Depth Based on Random Simplices," *The Annals of Statistics*, 18, 405–414.

— (1995), "Control Charts for Multivariate Processes," *Journal of the American Statistical Association*, 90, 1380–1387.

Liu, R. Y., Singh, K., and Teng, J. H. (2004), "DDMA-Charts: Nonparametric Multivariate Moving Average Control Charts Based on Data Depth." *Allgemeines Statistisches Archiv*, 88, 235–258.

Lopuhaa, H. P. and Rousseeuw, P. J. (1991), "Breakdown Points of Affine Equivariant Estimators of Multivariate Location and Covariance Matrices," *The Annals of Statistics*, 19, 229–248.

Lowry, C. A., Woodall, W. H., Champ, C. W., and Rigdon, S. E. (1992), "A Multivariate Exponentially Weighted Moving Average Control Chart," *Technometrics*, 34, 46–53.

Maboudou-Tchao, E. M. and Hawkins, D. M. (2011), "Self-Starting Multivariate Control Charts for Location and Scale," *Journal of Quality Technology*, 43, 113–126.

Mahalanobis, P. C. (1936), "On the Generalized Distance in Statistics," *Proceedings of the National Academy India*, 12, 49–55.

Mahmoud, M. A. (2008), "Phase I Analysis of Multiple Linear Regression Profiles," *Communications in Statistics: Simulation and Computation*, 37, 2106–2130.

Mahmoud, M. A., Parker, P. A., Woodall, W. H., and Hawkins, D. M. (2007), "A Change Point Method for Linear Profile Data," *Quality and Relibility Engineering International*, 23, 247–268.

Mahmoud, M. A. and Woodall, W. H. (2004), "Phase I Analysis of Linear Profiles with Calibration Applications," *Technometrics*, 46, 380–391.

Mardia, K. V. (1970), "Measures of Multivariate Skewness and Kurtosis with Applications," *Biometrika*, 57, 519–530.

Mason, R. L., Chou, Y.-M., Sullivan, J. H., Stoumbos, Z. G., and Young, J. C. (2003), "Systematic Patterns in T^2 Charts," *Journal of Quality Technology*, 35, 47–58.

Milasevic, P. and Ducharme, G. R. (1987), "Uniqueness of the Spatial Median," *The Annals of Statistics*, 15, 1332–1333.

Montgomery, D. G. (2009), *Statistical Quality Control: A Modern Introduction (6th ed.)*, Wiley.

Morais, M. C. and Pacheco, A. (2000), "On the Performance of Combined EWMA Schemes for μ and σ: a Markovian Approach," *Communications in Statistics - Simulation and Computation*, 29, 153–174.

Noorossana, R., Eyvazian, M., Amiri, A., and Mahmoud, M. A. (2010), "Statistical Monitoring of Multivariate Multiple Linear Regression Profiles in Phase I with Calibration Application," *Quality and Reliability Engineering International*, 26, 291–303.

Oja, H. (2010), *Multivariate Nonparametric Methods with R*, Springer.

Qiu, P. (2008), "Distribution-Free Multivariate Process Control Based on Log-Linear Modeling," *IIE Transactions*, 40, 664–677.

Qiu, P. and Hawkins, D. (2001), "A Rank-Based Multivariate CUSUM Procedure," *Technometrics*, 43, 120–132.

— (2003), "A Nonparametric Multivariate Cumulative Sum Procedure for Detecting Shifts in All Directions," *Journal of the Royal Statistical Society, Series D (The Statistician)*, 52, 151–164.

Qiu, P. and Zou, C. (2010), "Control Chart for Monitoring Nonparametric Profiles with Arbitrary Design," *Statistica Sinica*, 20, 1655–1682.

Qiu, P., Zou, C., and Wang, Z. (2010), "Nonparametric Profile Monitoring by Mixed Effects Modeling," *Technometrics*, 52, 265–277.

Ramsay, J. and Silverman, B. W. (2005), *Functional Data Analysis (2nd ed.)*, Springer.

Randles, R. H. (2000), "A Simple, Affine-Invariant, Multivariate, Distribution-Free Sign Test," *Journal of the American Statistical Association*, 95, 1263–1268.

Reynolds, JR., M. R. and Cho, G.-Y. (2006), "Multivariate Control Charts for Monitoring the Mean Vector and Covariance Matrix," *Journal of Quality Technology*, 38, 230–253.

Rousseeuw, P. J. (1984), "Least Median of Squares Regression," *Journal of the American Statistical Association*, 79, 871–880.

Rousseeuw, P. J. and Leroy, A. M. (1987), *Robust Regression and Outlier Detection*, Wiley.

Rousseeuw, P. J. and van Driessen, K. (1999), "A Fast Algorithm for the Minimum Covariance Determinant Estimator," *Technometrics*, 41, 212–223.

Saghaei, A., Mehrjoo, M., and Amiri, A. (2009), "A CUSUM-Based Method for Monitoring Simple Linear Profiles," *The International Journal of Advanced Manufacturing Technology*, 45, 1252–1260.

Shiau, J.-J. H., Huang, H.-L., Lin, S.-H., and Tsai, M.-Y. (2009), "Monitoring Nonlinear Profiles with Random Effects by Nonparametric Regression," *Communications in Statistics - Theory and Methods*, 38, 1664–1679.

Shiau, J.-J. H. and Sun, J.-H. (2010), "A New Strategy for Phase I Analysis in SPC," *Quality Reliability Engineering International*, 26, 475–486.

Stoumbos, Z. G. and Sullivan, J. H. (2002), "Robustness to Non-normality of the Multivariate EWMA Control Chart," *Journal of Quality Technology*, 34, 260–276.

Sullivan, J. H. and Woodall, W. H. (1996), "A Comparison of Multivariate Control Charts for Individual Observations," *Journal of Quality Technology*, 28, 398–408.

Testik, M. C., Runger, G. C., and Borror, C. M. (2003), "Robustness Properties of Multivariate EWMA Control Charts," *Quality Reliability Engineering International*, 19, 31–38.

Tracy, N. D., Young, J. C., and Mason, R. I. (1992), "Multivariate Control Charts for Individual Observations," *Journal of Quality Technology*, 24, 88–95.

Tyler, D. E. (1987), "A Distribution-Free M-Estimator of Multivariate Scatter," *The Annals of Statistics*, 15, 234–251.

Vaghefi, A., Tajbakhsh, S. D., and Noorossana, R. (2009), "Phase II Monitoring of Nonlinear Profiles," *Communications in Statistics - Theory and Methods*, 38, 1834–1851.

Vardi, Y. and Zhang, C.-H. (2000), "The multivariate L_1-median and associated data depth," *PNAS*, 97, 1423–1426.

Vargas, J. A. (2003), "Robust Estimation in Multivariate Control Charts for Individual Observations," *Journal of Quality Technology*, 35, 367–376.

Walker, E. and Wright, S. P. (2002), "Comparing Curves Using Additive Models," *Journal of Quality Technology*, 34, 118–129.

Wang, S.-H. (2009), "Profile Monitoring via Oja Data Depth," Master's thesis, National Chiao Tung University.

Weiszfeld, E. (1937), "Sur le point pour lequel la somme des distances de n points donnés est minimum," *Tôhoku Mathematical Journal*, 43, 355–386.

Weiszfeld, E. and Plastria, F. (2009), "On The Point for which the Sum of the Distances to n Given Points is Minimum," *Annals of Operations Research*, 167, 7–41.

Williams, J. D., Woodall, W. H., and Birch, J. B. (2007a), "Statistical Monitoring of Nonlinear Product and Process Quality Profiles," *Quality and Relibility Engineering International*, 23, 925–941.

Williams, J. D., Woodall, W. H., Birch, J. B., and Ferry, N. M. (2007b), "Statistical Monitoring of Heteroscedastic Dose-Response Profiles from High-Throughput Screening," *Journal of Agricultural, Biological, and Environmental Statistics*, 12, 216–235.

Williams, J. D., Woodall, W. H., Birch, J. B., and Sullivan, J. H. (2006), "Distribution of Hotelling's T^2 Statistic Based on the Successive Differences Estimator," *Journal of Quality Technology*, 38, 217–229.

Yeh, A. B., Huwang, L., and Wu, C.-W. (2005), "A Multivariate EWMA Control Chart for Monitoring Process Variability with Individual Observations," *IIE Transactions*, 37, 1023–1035.

Yeh, A. B., Huwang, L., and Wu, Y.-F. (2004), "A Likelihood-Ratio-Based EWMA Control Chart for Monitoring Variability of Multivariate Normal Processes," *IIE Transactions*, 36, 865–879.

Yen, C.-L. and Shiau, J.-J. H. (2010), "A Multivariate Control Chart for Detecting Increasing in Process Dispersion," *Statistica Sinica*, 20, 1683–1707.

Yen, C.-L., Shiau, J.-J. H., and Yeh, A. B. (2012), "Effective Control Charts for Monitoring Multivariate Process Dispersion," *Quality Reliability Engineering International*, 28, 409–426.

Zamba, K. D. and Hawkins, D. M. (2006), "A Multivariate Change-Point Model for Statistical Process Control," *Technometrics*, 48, 539–549.

Zhang, H. and Albin, S. L. (2009), "Detecting Outliers in Complex Profiles Using a χ^2 Control Chart Method," *IIE Transactions*, 41, 335–345.

Zhang, J., Li, Z., and Wang, Z. (2009), "Control Chart Based on Likelihood Ratio for Monitoring Linear Profiles," *Computational Statistics and Data Analysis*, 53, 1440–1448.

Zou, C., Ning, X., and Tsung, F. (2012a), "LASSO-Based Multivariate Linear Profile Monitoring," *Annals of Operations Research*, 192, 3–19.

Zou, C. and Qiu, P. (2009), "Multivariate Statistical Process Control Using LASSO," *Technometrics*, 104, 1586–1596.

Zou, C., Qiu, P., and Hawkins, D. (2009), "Nonparametric Control Chart for Monitoring Profiles Using Change Point Formulation and Adaptive Smoothing," *Statistica Sinica*, 19, 1337–1357.

Zou, C. and Tsung, F. (2011), "A Multivariate Sign EWMA Control Chart," *Technometrics*, 53, 84–97.

Zou, C., Tsung, F., and Wang, Z. (2007a), "Monitoring General Linear Profiles Using Multivariate Exponentially Weighted Moving Average Schemes," *Technometrics*, 49, 395–408.

— (2008), "Monitoring Profiles Based on Nonparametric Regression Methods," *Technometrics*, 50, 512–526.

Zou, C., Wang, Z., and Tsung, F. (2012b), "A Spatial Rank-Based Multivariate EWMA Control Chart," *Naval Research Logistics*, 59, 91–110.

Zou, C., Zhang, Y., and Wang, Z. (2006), "A Control Chart Based on a Change-point Model for Monitoring Linear Profiles," *IIE Transactions*, 38, 1093–1103.

Zou, C., Zhou, C., Wang, Z., and Tsung, F. (2007b), "A Self-Staring Control Chart for Linear Profiles," *Journal of Quality Technology*, 39, 364–375.

Zou, Y. and Serfling, R. (2000), "General Notations of Statistical Depth Function," *The Annals of Statistics*, 28, 461–482.